universität wien

DISSERTATION

Titel der Dissertation

“Competing Light Induced Molecular Torsions: Molecular Symmetry, Quantum Chemistry and Dynamical Simulations”

Verfasserin

Rana Obaid

angestrebter akademischer Grad

Doktorin der Naturwissenschaften (Dr. rer. nat.)

Wien, 2014

Studienkennzahl lt. Studienblatt:	A 796 605 419
Dissertationsgebiet lt. Studienblatt:	Chemie
Betreuerin:	Univ.-Prof. Dr. Leticia González

Abstract

This thesis investigates the torsional dynamics of nuclear spin isomers (NSIs). The final goal is to discriminate different NSIs by exploiting their excited-state dynamics. The investigation was done for 2-[4-(cyclopenta-2,4-dien-1-ylidene)cyclohexa-2,5-dien-1-ylidene]-2H-1,3-dioxole, abbreviated as CCD. This molecule serves as an ABC-system consisting of three non-identical segments A, B and C with a C_2-symmetry axis around which each of these segments can rotate independently. For this class of molecules, two independent torsions A vs. B, denoted as Φ_1, and C vs. B, denoted as Φ_2, are possible. These two torsional angles are the two degrees of freedom that have been used in our simulations.

We used molecular symmetry group to label these NSIs. We found that this class of molecules has the Abelian group G_{16}^A and we constructed its character table. G_{16}^A represents 16 feasible permutations and permutation inversions, from which eight permutations constitute the permutation subgroup, so CCD has at most eight different NSIs. It was also shown that only four of them "survive" in the T $\rightarrow$ 0 K limit, analogous to the dominance of para-hydrogen in the T $\rightarrow$ 0 K limit.

We calculated the potential energy surfaces (PESs) for the lowest singlet electronic states along the two torsional degrees of freedom Φ_1 and Φ_2 using the state-averaged complete active space multi-configuration method (SA-CASSCF). From the ground state PES, two-dimensional torsional wavefunctions were calculated to be used as initial wavefunctions for quantum dynamical simulations on the electronic excited states.

We simulated ultra-short laser pulses to trigger the excited state dynamics. We found that an isomer discrimination can be seen in the expectation value of the directed angular momentum operator and the dispersion of the torsional wave packet. Finally, we showed that one can use ultra-short laser pulses in a pump-dump sequence to modify the ratio of the different NSIs, which makes it possible to separate different NSIs.

Zusammenfassung

Diese Arbeit untersucht die Torsionsdynamik von Kernspinisomeren (NSI). Ziel ist die Unterscheidung verschiedener NSI durch Ausnutzung der Unterschiede in der Dynamik angeregter Zustände. Die Untersuchung wurde für das Molekül 2-[4-(cyclopenta-2,4-dien-1-ylidene)cyclohexa-2,5-dien-1-ylidene]-2H-1,3-dioxole (abgekürzt als CCD) durchgeführt, welches als Modell für ein ABC-System dient. Bei diesem Modell können 3 nicht-identische Segmente A, B und C entlang einer C_2-Symmetrie-Achse unabhängig voneinander rotieren. Für diese Klasse von Molekülen sind daher zwei unabhängige Torsionen möglich: A vs. B, mit Φ_1 bezeichnet, und C vs. B, mit Φ_2 bezeichnet. In den Simulationen wurden diese beiden Freiheitsgrade benutzt.

Mittels Molekülsymmetriegruppen wurden die verschiedenen NSI klassifiziert. Die untersuchte Klasse von Molekülen gehört zur Abelschen Gruppe G_{16}^A. Die zugehörige Charaktertafel wurde konstruiert. G_{16}^A enthält 16 mögliche Permutationen und Permutationsinversionen, von denen 8 die Permutationssubgruppe bilden. Daher hat CCD hat 8 unterschiedliche NSI. Bei sehr niedrigen Temperaturen (T $\rightarrow$ 0 K) liegen, analog zur Dominanz von para-Wasserstoff bei niedrigen Temperaturen, nur 4 dieser NSI vor.

Mittels der "complete active space self consistent field" Methode (CASSCF) wurden die Potentialenergieflächen (PES) der niedrigsten elektronisch angeregten Zustände entlang der beiden Freiheitsgrade Φ_1 und Φ_2 berechnet.

Die zweidimensionalen Torsionswellenfunktionen der Grundzustands-PES wurden als Ausgangswellenfunktionen für quantendynamische Simulationen in den elektronisch angeregten Zuständen verwendet, wobei mittels ultrakurzer Laserpulse die Dynamik in den angeregten Zuständen gestartet wurde. Es zeigte sich, dass eine Unterscheidung der Isomere anhand des Erwartungswertes des Drehmomentoperators und der Dispersion der Torsionswellenpakete möglich ist. Schließlich wurde gezeigt, dass mittels ultrakurzer Laserpulse ein pump-dump Szenario realisiert werden kann, das es ermöglicht die verschiedenen NSI zu separieren.

Contents

List of Figures

List of Tables

Acronyms

TDSE time-dependent Schrödinger equation

TISE time-independent Schrödinger equation

BOA Born-Oppenheimer approximation

NACTs non-adiabatic coupling terms

HF Hartree-Fock

CSFs configuration state functions

CI configuration interaction

FCI full configuration interaction

FFT Fast Fourier Transformation

MCSCF multi-configurational-self-consistent field

CASSCF complete-active-space-self-consistent field

PES potential energy surface

CI conical intersection

FT Fourier transform

IREPs Irreducible representations

Notation

B	Rotational constant of a linear molecule
C_0	Coefficient of Hartree-Fock wavefunction
$C_{\mathrm{S/D/T}}$	Coefficients of singlet/doublet/triplet configuration state functions (CSFs)
$C_{\mathrm{A/B/C}}$	Coefficient of the torsional angle $\Phi_{\mathrm{A/B/C}}$
$\mathcal{D}_a$	Distance of the nucleus a to the C_2-torsional axis
d_i	Eigenvalue of the symmetry projection operator of the ith IREP
$d_{ii/ij}$	Permanent/transition dipoles
E_e	Electronic energy
E_i	Energy of orbital i
E_N	Nuclear energy
$E(\bar{R})$	Potential energy
E_{rot}	Rotational energy
$E(t)$	Envelope function of laser pulse
E_{tot}	Total energy
$\mathcal{E}$	Identity
$\mathcal{E}^*$	Inversion
e	Electronic charge
F_0	Field amplitude
$\hat{f}$	Fock operator
G_{16}^A	Abelian molecular symmetry (MS) group of the ABC-systems
G^{MS}	MS-group
G^{PISMS}	Permutation inversion subgroup of G_{16}^A
G^{PSMS}	Permutation subgroup of G_{16}^A

$\hat{H}^{(1)}$	One-fragment Hamiltonian
$\hat{H}^{(2)}$	Two-fragment Hamiltonian
$H_{ii/ij}$	Diagonal and off-diagonal matrix elements of the Hamiltonian
$\hat{H}_{\mathrm{e}}$	Electronic Hamiltonian
$\hat{H}(t)$	Time-dependent Hamiltonian
$\hat{H}_{\mathrm{tot}}$	Total Hamiltonian
h	Order of the G^{MS}
$h_{\mathcal{S}_\mathcal{N}}$	Order of $\mathcal{S}_\mathcal{N}$
$I_{1/2}$	Reduced moment of inertia between segments A and B/B and C
$I_{\mathfrak{S}}$	Moment of inertia of segment $\mathfrak{S}$
$\mathcal{I}$	Interference term for the localized wavefunctions
J	Rotational quantum number
$\hat{L}_{\mathfrak{S}}$	Internal angular momentum for the rotation of the segment $\mathfrak{S}$ about the C_2-axis
$\mathcal{L}$	Total nuclear spin
l_{Γ_i}	Dimension of the irreducible representation (IREP) Γ_i
M_a	Nuclear mass of atom a
M_{iK}	Nuclear mass of nucleus K in fragment i
$\mathcal{M}_\mathcal{L}$	The component of the total nuclear spin along a defined axis
m	Number of active orbitals
m_{e}	Electronic mass
N	Number of nuclei
$\mathcal{N}_i$	Normalization constant
$\mathcal{N}$	Number of grid points
n	Number of electrons
$\hat{\vec{\mathcal{P}}}_{iK}$	Momentum of nucleus K in fragment i
$\mathcal{P}$	Feasible permutation
$\mathcal{P}^*$	Feasible permutation-inversion
$\hat{P}^{\Gamma_i}$	Symmetry projection operator of the IREP Γ_i

$\mathcal{R}$	MS-operation
$\vec{R}$	Nuclear coordinates vector
$\vec{R}_{iK}$	Nuclear coordinate of nucleus i in fragment K
$\vec{r}$	Electronic coordinates vector
$\vec{r}_i$	Electronic coordinate of electron i
S_0	Electronic ground state
$S_{1/2/3}$	First/second/third electronic excited state
$\mathcal{S}$	Subgroup of the G^{MS}
$\mathcal{S}'$	Subgroup of the G^{MS}
$\mathcal{S}_\mathcal{N}$	Permutation subgroup of the number of identical fragments $\mathcal{N}$
$\mathfrak{S}$	Molecular segment
$T^{(1)/(2)}$	First/second derivative of the electronic wavefunction with respect to nuclear coordinates
$\hat{T}$	Kinetic energy operator
$\hat{T}_\mathrm{e}$	Electronic kinetic energy operator
$\hat{T}_\mathrm{N}$	Nuclear kinetic energy operator
t	Time
t_p	Pulse duration
u	Number of spin orbitals
V_{ii}	Ab initio potential energy surface of state i
V_{ij}	General coupling term, within this thesis it is laser coupling
$\hat{V}_\mathrm{ee}$	Sum of the electrons Coulomb interactions
$\hat{V}_\mathrm{eN}$	Sum of the electron nuclear Coulomb interactions
$\hat{V}_\mathrm{NN}$	Sum of the nuclear Coulomb interactions
$v^{HF}(i)$	Average potential experienced by the ith electron due to the presence of the other electrons
$\mathcal{X}^{\Gamma_i}(\mathcal{R})$	Character of the symmetry operation $\mathcal{R}$ in the IREP Γ_i
$Z_{a/b}$	Nuclear charge of nucleus a/b
Z_{iK}	Nuclear charge of nucleus K in fragment i

Γ_i	ith IREP
γ_{ij}	Polarizability element
$\epsilon(t)$	Electric field
$\vec{\epsilon}_{xyz}$	Polarization vector
ε	Inversion subgroup
ζ_{ij}	Hyperpolarizability element
λ	Wavelength of the laser pulse
Φ_1	Relative torsional angle between the segments A and B
Φ_2	Relative torsional angle between the segments B and C
$\Phi_{\mathrm{A/B/C}}$	Internal rotational angle, i.e. torsion of the segment A/B/C
$\chi_k(i)$	ith electron moving in the kth one-electron wavefunction, which is called spin orbital
Ψ_{CI}	Configuration interaction wavefunction
Ψ_{e}	Electronic wavefunction
Ψ_{HF}	Hartree-Fock wavefunction
Ψ_l	Localized wavefunction in a single potential well
Ψ_{N}	Nuclear wavefunction
$\Psi_{\mathrm{S/D/T}}$	CSFs with single/double/triple excitations
Ψ^k_{tor}	Torsional wavefunction in the kth electronic state
Ψ_{tot}	Total wavefunction
Ψ^{Γ_i}	Symmetry-adapted eigenfunction that transforms according to the IREP Γ_i
ω	Frequency of the laser pulse
$\hbar$	Planck's reduced constant
∇^2_a	Laplace operator, it is the sum of the second partial derivatives of the ath nucleus coordinates in three dimensions
∇^2_i	Laplace operator, it is the sum of the second partial derivatives of the ith electron coordinates in three dimensions

1. Introduction

The purpose of this thesis is to investigate and finally discriminate the nuclear spin isomers of a derivative of quinodimethane through their torsional dynamics. This discrimination could be used in a femto-second experiment to separate these nuclear spin isomers. We will explain the concept of nuclear spin isomers in Section 1.1. The model system that is utilized for this purpose is illustrated in Section 1.2. For the investigation of the torsional dynamics of the nuclear spin isomers of this model system, we need a symmetry tool to label them, which is demonstrated in Section 1.3. An overview of all of this thesis is given in Section 1.4.

1.1. The concept of nuclear spin isomers

The notion of nuclear spin isomers was introduced independently by Heisenberg [1] and Hund [2]. As an example, they considered molecular hydrogen and hypothesized that H_2 should exist in form of two nuclear spin isomers, ortho-hydrogen and para-hydrogen, see Figure 1.1. The figure also shows the corresponding nuclear spins. Ortho-hydrogen has a parallel spin, indicated by the arrows in Figure 1.1, while para-hydrogen has an anti-parallel spin.

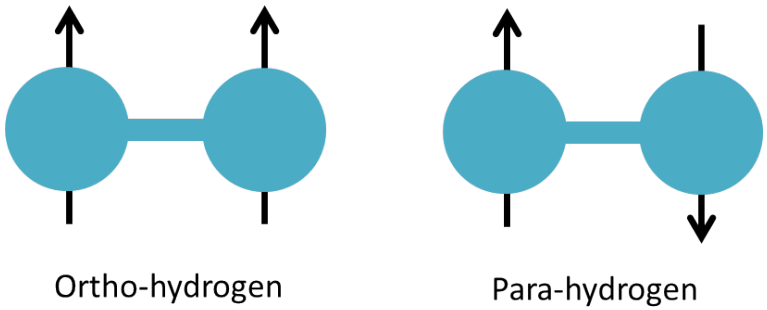

Figure 1.1.: The nuclear spin isomers of molecular hydrogen, ortho-hydrogen and para-hydrogen with their parallel and anti-parallel nuclear spins indicated by arrows.

Ortho-hydrogen has three nuclear spin states of the same energy, and is thus called a triplet state. The corresponding nuclear spin wavefunctions (in Dirac

notation) are:

$$\mid \Psi_{\mathrm{N,ortho}}\rangle = \begin{cases} |\uparrow\uparrow\rangle \\ \frac{1}{\sqrt{2}}(|\uparrow\downarrow\rangle + |\downarrow\uparrow\rangle) \\ |\downarrow\downarrow\rangle \end{cases} . \tag{1.1}$$

Para-hydrogen has only one nuclear spin state, and is called a singlet state. Its nuclear spin wavefunction is:

$$\mid \Psi_{\mathrm{N,para}}\rangle = \frac{1}{\sqrt{2}}(|\uparrow\downarrow\rangle - |\downarrow\uparrow\rangle). \tag{1.2}$$

Molecular hydrogen consists of approximately 75% ortho-hydrogen and 25% para-hydrogen at room temperature and thermal equilibrium [3].

The parallel and the anti-parallel spins of the hydrogen nuclei cause symmetric and anti-symmetric nuclear spin wavefunctions with respect to permutation of the corresponding atoms. The total wavefunction of H_2 is assumed to be the product of the electronic and the nuclear wavefunctions. The electronic ground state wavefunction of H_2 is symmetric with respect to permutation of the two nuclei. Since the total wavefunction should be anti-symmetric with respect to the exchange of the two fermionic nuclei, the complete nuclear wavefunction of H_2 must be anti-symmetric.

The nuclear wavefunction of H_2 is assumed to be the product of the rotational, the vibrational and the previously mentioned nuclear spin wavefunctions:

$$\Psi_{\mathrm{N}} \approx \Psi_{\mathrm{rot}} \cdot \Psi_{\mathrm{vib}} \cdot \Psi_{\mathrm{nu.sp.}}. \tag{1.3}$$

Within this thesis, the approximations in the above equation are considered to be small and therefore we assume the relation in this equation to be equal. Considering only the symmetric vibrational ground state, for ortho-hydrogen, the rotational wavefunctions should be anti-symmetric (odd rotational quantum numbers J), which has a symmetric nuclear spin wavefunction and symmetric (even rotational quantum numbers J) for para-hydrogen, which has an anti-symmetric nuclear spin wavefunction [3]. Figure 1.2 shows the rotational energies (E_{rot}) for para- and ortho-hydrogen with their even and odd J, respectively. Since the rotational energy is calculated as:

$$E_{\mathrm{rot}} = \mathrm{J}(\mathrm{J}+1)B. \tag{1.4}$$

where B is the rotational constant, ortho- and para-hydrogen have different rotational spectra. The intensity alternations in the rotational spectra had first been reported by Mecke [4] and explained theoretically by Heisenberg and Hund [1, 2].

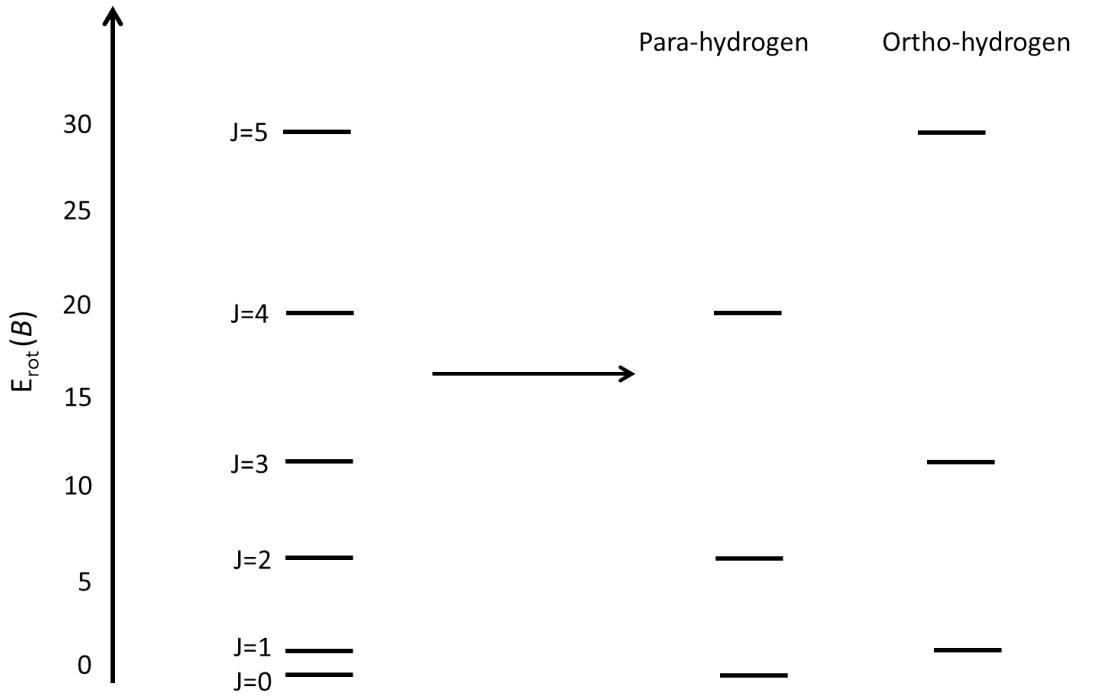

Figure 1.2.: The rotational energy (E_{rot}) of para- and ortho-hydrogen with their even and odd rotational quantum numbers J, respectively.

This concept of Heisenberg and Hund implies enormous further consequences: Essentially, different nuclear spin isomers have different properties, hence they appear as different species, at least on time scales shorter than nuclear spin conversion. For example, they have different temperature dependencies of their concentrations or populations, of the internal energies and, as a consequence, of the heat capacities [5, 6]. The experimental verification of this prediction by Bonhoeffer and Harteck [7] marks one of the great successes of quantum theory. At the same time, the quantum theory of Heisenberg and Hund could explain the anomalous specific heat capacity of normal hydrogen (first measured by Eucken [8]), which means that the specific heat capacity of H_2 unaccountably departs from that of a diatomic gas below room temperature. This is owing to the wide-spaced rotational energy levels that exist in H_2 but not in homodiatomic gases composed of heavier atoms [9].

On the theoretical side, the historic success of Heisenberg, Hund, Bonhoeffer

and Harteck supported the symmetrization postulate for identical and therefore indistinguishable particles [10], one of the keys to successful quantum evaluations of chemical properties [5, 6].

Nowadays, nuclear spin isomer selectivity is an important topic in broad areas of chemistry and physics [11]. This selectivity in the different properties of hydrogen (specific heat, heat of vaporization and boiling point [10, 12]) cannot be easily detected for heavier diatomic molecules, as it has a negligible effect due to missing large gap between the rotational energy levels which exists only in H_2. Thus, the separation of the nuclear spin isomers of heavy molecules requires a special technique. This is a nontrivial problem because nuclear spin isomers have identical masses and similar physical and chemical properties. Nevertheless, separation methods are under development.

One of the most recent general breakthroughs in this field is the discovery of nuclear spin selective coherent quantum dynamics [13–15]. The results are spectacular: Different nuclear spin isomers show different transient alignment after excitation with femtosecond laser pulses, opening new avenues to laser separations of nuclear spin isomers. Moreover, nuclear spin isomers have different periods of torsion in electronically excited states [16].

The purpose of the present thesis is to extend previous quantum mechanical investigations of nuclear spin isomers, from polyatomic molecules with a single torsional degree of freedom [16–20] to molecules with two torsional degrees of freedom. Ultimately, we aim at nuclear spin isomer selective control of these molecular torsions.

1.2. The model system under study

We are interested throughout this work in the investigation of the selectivity of the nuclear spin isomers (i.e. their different torsional dynamics) of molecules, which are characterized by two criteria:

(i) Their structures at the minima of the potential energy surface of the electronic ground state ("minimum structures") have a C_2 symmetry axis.

(ii) The molecules have three non-identical "torsional" segments which can rotate independently around that C_2-axis, possibly in the electronic ground state or in electronic excited states. Those three rotations correspond to two torsional degrees of freedom for the torsions of two neighboring segments with respect to each other, plus the overall rotation of the entire molecule around the C_2-axis.

Precise evaluations of the quantum dynamics of molecules which belong to this class, in full dimensionality are all technically too demanding. To simplify this task, we assumed that the C_2 symmetry axis has been pre-oriented parallel to the laboratory fixed Z-axis.

The approach of the investigation of the torsional selectivity of the nuclear spin isomers will be demonstrated for a model system, specifically the quinodimethane derivative 2-[4-(cyclopenta-2,4-dien-1-ylidene)cyclohexa-2,5-dien-1-ylidene]-2H-1,3-dioxole, abbreviated as CCD, see Figure 1.3. This figure shows the CCD molecule with only two of its hydrogen atoms shown out of ten (for simplicity), together with their nuclear spin orientations indicated by arrows. Since the carbon and oxygen nuclei of CCD are assumed to be only those of the isotopes ^{12}C and ^{16}O for simplicity, its nuclear spin isomers depend exclusively on the spins of the ten protons. The different combinations of different orientations of the spins of these ten protons give rise to different nuclear spin isomers. The relative two torsional angles between the dioxole and the middle ring (described by Φ_1) and between the middle and the cyclopentadienyl ring (described by Φ_2), (see Figure 1.3) will be the two degrees of freedom for our simulations throughout this work.

The investigation of the nuclear spin isomer selectivity of CCD, as a representative of the present class of molecules, will proceed in three steps: First, we will calculate the potential energy surfaces (PESs) of the singlet electronic ground and the lowest excited states. Second, we shall identify the nuclear spin isomers of CCD in the electronic ground state. Third, we will demonstrate that electronic excitations of different nuclear spin isomers induce different time evolutions of the torsional wavepackets in electronic excited states.

For the second step, which is the identification of the nuclear spin isomers of CCD in the electronic ground state, we shall show that (in the limit of the present two dimensional model) the nuclear spin isomers can be identified by different torsional states. This step recalls the pioneering work of Heisenberg [1] and Hund [2], who had shown that the nuclear spin isomers of H_2 are associated with different rotational states, this analogy is valid irrespective of the fact that Heisenberg and Hund had to deal with the exchange of just two protons, whereas the present torsions of CCD involve exchanges of ten protons. Thus for H_2, there are $2^2 = 4$ nuclear spin wavefunctions which can be separated into two sets with 1 and 3 nuclear spin wavefunctions that can be assigned to para-hydrogen and to ortho-hydrogen, as in equations (1.2) and (1.1), respectively. In contrast, CCD supports $2^{10} = 1024$ nuclear spin wavefunctions. One of the challenges of this thesis is to determine how these functions should be separated into corresponding sets for nuclear spin isomers, and even more fundamentally to discover the number and the characteristics of those nuclear spin isomers.

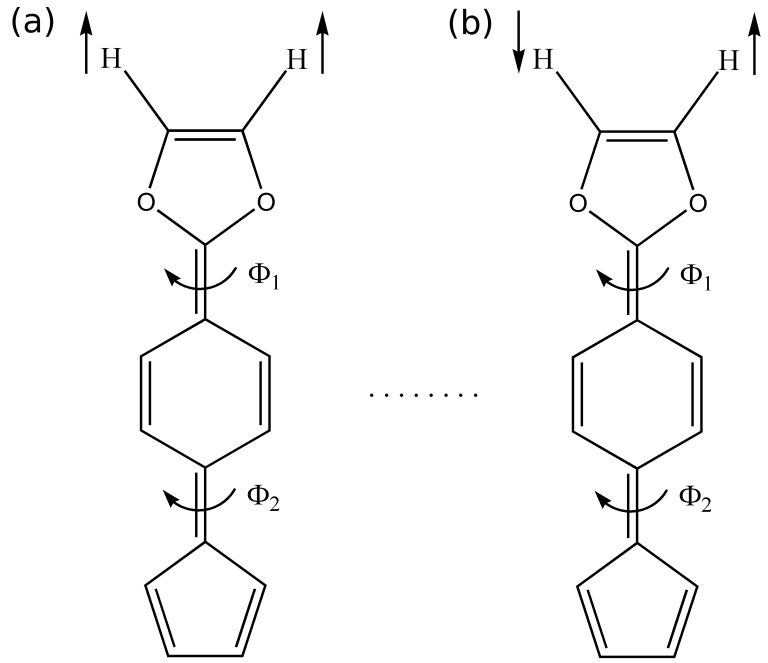

Figure 1.3.: The structure of 2-[4-(cyclopenta-2,4-dien-1-ylidene)cyclohexa-2,5-dien-1-ylidene]-2H-1,3-dioxole (CCD). Two hydrogen atoms of CCD out of ten (for simplicity) are shown together with their nuclear spin indicated by arrows. The relative torsions between the dioxole and the middle ring and the middle and the cyclopentadienyl ring are decribed by Φ_1 and Φ_2, respectively. (a) and (b) indicate the two possibilities for the orientation of the spin of these two protons of CCD.

Another problem that we shall solve is suggested by the well-known fact that para-hydrogen is the only nuclear spin isomer which "survives" as the temperature approaches the limit of $T \to 0$ [3,4]. By analogy, we shall determine the subset of nuclear spin isomers of CCD which "survive" as $T \to 0$. Obviously, these tasks are much more demanding for the oriented CCD molecule than for H_2, calling for a symmetry tool that enables labelling these nuclear spin isomers as will be explained in the next section.

1.3. Molecular symmetry

In order to investigate the nuclear spin isomers of the present class of molecules (characterized by the criteria (i) and (ii) mentioned in Section 1.2) and to classify their symmetries, we shall employ a symmetry concept which is based on the permutations of identical nuclei that may be achieved by observable torsions. The ubiquitous molecular point groups are not sufficient for this task: They are tailored to "local" molecular properties which are located at, or close to stationary points on

the potential energy surface, e.g. they provide the symmetry properties of normal modes, i.e. vibrations with small amplitudes around the minimum structures [21]. In contrast, the present class of molecules allows for large amplitude motions after photo-excitation, i.e. torsions which cover domains on the potential energy surface even far away from the "local" minimum structures. As it was shown by Longuet-Higgins [22] on the basis of preliminary works of Hougen [23, 24] it is, however, possible to define a concept which can be used for the classification of the molecular states for molecules allowing for internal large amplitude motions: the molecular symmetry group [25].

The molecular symmetry group is a group that contains all the so-called "feasible" permutations and permutation-inversions of identical nuclei. From an experimental point of view, the term "feasible" means, qualitatively speaking, that the permutations and permutation-inversions are observable on the time scale which is associated with the resolution of the experiment. From the perspective of a quantum dynamicist, the permutations and permutation-inversions are feasible if they can be simulated by time-dependent wavepackets, within the time scales of the process which is investigated. For the present class of molecules, with CCD as a model representative, those wavepackets are torsional wavepackets.

The main three "feasible" permutations of CCD resemble the torsion of its torsional rings, which are defined as segments A, B and C, as in Figure 1.4. This figure shows CCD with its three torsional segments labeled A, B and C. Rotations around 180° of these segments around the C_2 symmetry axis, denoted with Φ_{A}, Φ_{B} and Φ_{C}, interchange equivalent fragments (1) and (2), (3) and (4) and (5) and (6), respectively, where equivalent fragments are sets composed of the same number, type and arrangement of nuclei. Another set labeled (0), contains the nuclei on the C_2 symmetry axis and it is not included in these three main feasible permutations.

We shall show that the molecular symmetry group for this class of molecules is G_{16}^{A}. To the best of our knowledge, this Abelian molecular symmetry group has not been applied previously to any other molecule. In any case, it is different from the non-Abelian group G_{16} which has been employed in References [26, 27] for the description of the molecular symmetry of ethylene-like molecules with just one feasible torsion. In order to distinguish the two molecular symmetry groups, we shall call the present Abelian group G_{16}^{A} , with superscript "A" representing "Abelian". Since G_{16}^{A} is a new group, we also will report various important properties, e.g. the irreducible presentations (IREPs), to facilitate the task of finding the nuclear spin isomers of the model CCD, as a representative of the present class of molecules.

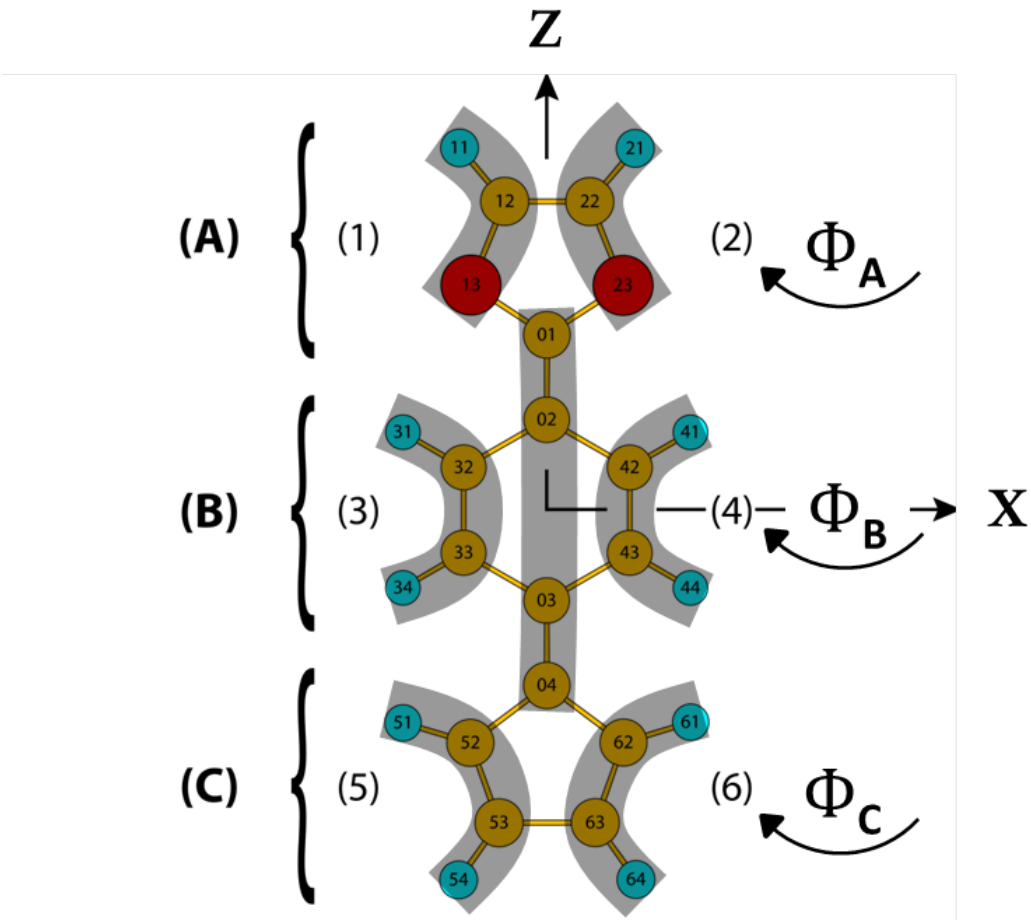

Figure 1.4.: The structure of 2-[4-(cyclopenta-2,4-dien-1- ylidene)cyclohexa-2,5-dien-1-ylidene]-2H-1,3-dioxole (CCD). The local symmetry is C_{2v}, with the C_2 symmetry axis oriented along the laboratory-fixed Z-axis, and with the planar molecule in the X/Z plane. The molecule has three torsional segments labeled (A), (B) and (C), their torsions are abbreviated as Φ_A, Φ_B and Φ_C. These torsional segments contain equivalent fragments (1) and (2), (3) and (4), as well as (5) and (6), respectively, marked in shaded gray. The set of nuclei which are located on the C_2 symmetry axis is called fragment (0). The nuclei are labeled by double indices iK where i denotes the fragment, and K specifies the nucleus within the fragment, e.g. fragments (1) and (2) have hydrogen (light blue), carbon (orange) and oxygen (red) nuclei labeled 11, 12, 13 and 21, 22, 23, with the same labels K = 1, 2, 3 for equivalent nuclei in these fragments.

1.4. Structure of this thesis

This thesis consists of the following chapters: After the Introduction, chapter 2 summarizes the fundamental quantum mechanical concepts needed for calculating the PESs of the low-lying electronic states, as well as some of their one-electron properties (like the transition dipole moment). In this chapter fundamental concepts as the Born-Oppenheimer approximation and the methods used for solving the electronic time-independent Schrödinger equation are revised. Moreover, some theoretical concepts needed for solving the nuclear time-independent (eigenfunctions) and time-dependent Schrödinger equations (in the absence and presence of a laser field), will be described.

In Chapter 3, the molecular symmetry group of the ABC-systems characterized by criteria (i) and (ii) will be determined, together with its properties like its multiplication, character and product tables. In addition, the molecular symmetry group will be used to label the nuclear spin isomers of CCD.

Chapter 4 presents the quantum chemical calculations of the PESs of the electronic four lowest singlet states and associated one-electron properties of CCD, as well as quantum dynamics simulations. The later includes the expectation values of selected operators and pump-dump simulations aimed at discriminating nuclear spin isomers.

Finally, in Chapter 5 the work is summarized by drawing conclusions and a brief outlook is given.

2. Theory

Within this chapter, the underlying theoretical concepts that are used in this thesis will be briefly introduced. In Section 2.1, the quantum chemical methods utilized for solving the electronic time-independent Schrödinger equation within the Born-Oppenheimer approximation are summarized. Non-Born-Oppenheimer effects are discussed in Section 2.2. Setting up the nuclear time-dependent Schrödinger equation in the absence and presence of an electric field is demonstrated in Sections 2.3 and 2.5, respectively. Deriving the Hamiltonian for CCD, as a representative of the ABC-systems, is illustrated in Section 2.4. Theoretical methods needed for solving the nuclear time-dependent Schrödinger equation and time-independent Schrödinger equation are discussed in Sections 2.6 and 2.7, respectively.

2.1. Quantum chemistry

The goal of this section is to provide a brief description for the quantum chemical methods based on different approximations used in this thesis to solve the electronic time-independent Schrödinger equation (TISE). Detailed description of the quantum chemical methods can be found in references [28–30].

In the following, we use $\vec{r}$ for the electronic coordinates, $\vec{R}$ for the nuclear coordinates, n for the number of electrons and N for the number of nuclei. The indices i and j are used for electrons, while the indices a and b are used for nuclei. M_a is used for the mass of nucleus a. Atomic units are used throughout this work, i.e. the mass of the electron m_e, the reduced Planck constant $\hbar$ and the electronic charge e are set to one and M_a is expressed in multiples of the electron mass.

The main theoretical concepts used to solve the non-relativistic TISE are highlighted here. The TISE is given as:

$$\hat{H}_{\mathrm{tot}}\Psi_{\mathrm{tot}}(\vec{r},\vec{R}) = E_{\mathrm{tot}}\Psi_{\mathrm{tot}}(\vec{r},\vec{R}). \tag{2.1}$$

$\hat{H}_{\mathrm{tot}}$ describes all the interactions involved within the molecule i.e. the interactions between all the n electrons and the N nuclei of the molecule. The total Hamiltonian can be expressed as:

$$\hat{H}_{\mathrm{tot}} = \hat{T}_{\mathrm{e}} + \hat{T}_{\mathrm{N}} + \hat{V}_{\mathrm{ee}} + \hat{V}_{\mathrm{eN}} + \hat{V}_{\mathrm{NN}}. \tag{2.2}$$

Here, $\hat{T}_\mathrm{e}$ and $\hat{T}_\mathrm{N}$ are the sum of the kinetic energy operators of all the electrons n and the nuclei N of the system. $\hat{V}_\mathrm{ee}, \hat{V}_\mathrm{eN}, \hat{V}_\mathrm{NN}$ are the sum of the Coulomb interactions between the electrons themselves, between the electrons and the nuclei and between the nuclei. The solution of the TISE (2.1) gives the total wavefunction (Ψ_tot) with the corresponding total energy of the system (E_tot).

The electronic and the nuclear kinetic energy operators $\hat{T}_\mathrm{e}$ and $\hat{T}_\mathrm{N}$ can be written as:

$$\hat{T}_\mathrm{e} = -\sum_{i=1}^{n} \frac{\nabla_i^2}{2}, \tag{2.3}$$

$$\hat{T}_\mathrm{N} = -\sum_{a=1}^{N} \frac{\nabla_a^2}{2M_a}, \tag{2.4}$$

where i runs over all electrons, a runs over all nuclei with mass M_a and ∇^2 is the Laplace operator. The operators of the potential energy are:

$$\hat{V}_\mathrm{ee} = \frac{1}{2}\sum_{i=1}^{n}\sum_{j=1}^{n} \frac{1}{|\vec{r}_i - \vec{r}_j|}, \tag{2.5}$$

$$\hat{V}_\mathrm{eN} = -\sum_{a=1}^{N}\sum_{i=1}^{n} \frac{Z_a}{|\vec{R}_a - \vec{r}_i|}, \tag{2.6}$$

$$\hat{V}_\mathrm{NN} = \frac{1}{2}\sum_{a=1}^{N}\sum_{b=1}^{N} \frac{Z_a Z_b}{|\vec{R}_a - \vec{R}_b|}, \tag{2.7}$$

where Z_a and Z_b are the charges of nucleus a and nucleus b, $|\vec{r}_i - \vec{r}_j|$ is the distance between electrons i and j, $|\vec{R}_a - \vec{r}_i|$ is the distance between nuclei a and electron i and $|\vec{R}_a - \vec{R}_b|$ is the distance between nucleus a and b. For $\hat{V}_\mathrm{ee}$, i and j run over all the electrons. In equation (2.6) a and i run over all nuclei and electrons, and in equation (2.7), a and b run over all nuclei.

The TISE cannot be solved analytically for systems with a total number of particles $(N + n) > 2$. To circumvent this problem several approximations have to be made. One usually starts with the Born-Oppenheimer approximation [31], which will be explained in subsection 2.1.1. Different methods to solve the electronic TISE will be explained in subsection 2.1.2.

2.1.1. Born-Oppenheimer approximation

The Born-Oppenheimer approximation implies the separation of the electronic motion from the nuclear motion. This is possible due to the large mass of the

nuclei compared to that of the electrons, so that the nuclei can be considered stationary on the time scale of electronic motion. Accordingly, electrons move in a field of fixed nuclei, while nuclei move in an averaged field of the electrons. As a consequence, the total wavefunction $\Psi_{\mathrm{tot}}(\vec{r},\vec{R})$ is written as an approximated product of a nuclear wavefunction (Ψ_{N}) and an electronic wavefunction (Ψ_{e});

$$\Psi_{\mathrm{tot}}(\vec{r},\vec{R}) \approx \Psi_{\mathrm{N}}(\vec{R})\Psi_{\mathrm{e}}(\vec{r},\bar{R}). \tag{2.8}$$

The nuclear wavefunction $\Psi_{\mathrm{N}}(\vec{R})$ depends only on the nuclear coordinates $\vec{R}$, while the electronic wavefunction depends on the electronic coordinates $\vec{r}$ and parametrically on the nuclear coordinates $\bar{R}$.

Putting (2.8) into (2.1), one can split the total TISE into two equations describing the nuclear and electronic motion separately. The resulting electronic TISE is given as:

$$\hat{H}_{\mathrm{e}}\Psi_{\mathrm{e}} = (\hat{T}_{\mathrm{e}} + \hat{V}_{\mathrm{ee}} + \hat{V}_{\mathrm{eN}})\Psi_{\mathrm{e}} = E_{\mathrm{e}}\Psi_{\mathrm{e}}. \tag{2.9}$$

Solving (2.9) gives the electronic eigenstate Ψ_e and its eigenenergy E_{e} for a certain nuclear geometry. Adding the electronic eigenenergy E_{e} to the nuclear potential $\hat{V}_{\mathrm{NN}}$ (which is constant with respect to the electronic movement) gives the potential energy $E(\bar{R})$,

$$E(\bar{R}) = E_{\mathrm{e}} + \hat{V}_{\mathrm{NN}}. \tag{2.10}$$

Both of the electronic energy E_e and the nuclear potential $\hat{V}_{\mathrm{NN}}$ depend parametrically on the nuclear coordinates $\bar{R}$. Thus, $E(\bar{R})$ is a function of $\bar{R}$ which represents the potential energy along the nuclear coordinates. Therefore, the energy $E(\bar{R})$ is calculated for several different nuclear geometries to yield an adiabatic PES along the corresponding nuclear degree of freedom.

Substituting equations (2.8) and (2.2) in equation (2.1) and using equations (2.9) and (2.10) lead to

$$\hat{T}_{\mathrm{N}}\Psi_{\mathrm{N}}\Psi_{\mathrm{e}} + E(\bar{R})\Psi_{\mathrm{N}}\Psi_{\mathrm{e}} = E_{\mathrm{tot}}\Psi_{\mathrm{N}}\Psi_{\mathrm{e}}. \tag{2.11}$$

Since the nuclear kinetic energy operator is a differential operator with respect to nuclear coordinates which is applied on a product of nuclear and electronic

wavefunctions, the following coupling terms results:

$$\begin{aligned}\hat{T}_{\mathrm{N}}\Psi_{\mathrm{e}}\Psi_{\mathrm{N}} &= \sum_{a}^{N}\frac{-\nabla_a^2}{2M_a}(\Psi_{\mathrm{e}}\Psi_{\mathrm{N}}) \\ &= -\frac{1}{2}\sum_{a}^{N}\frac{1}{M_a}(\nabla_a^2\Psi_{\mathrm{e}}\Psi_{\mathrm{N}} + 2\nabla_a\Psi_{\mathrm{e}}\nabla_a\Psi_{\mathrm{N}} + \Psi_{\mathrm{e}}\nabla_a^2\Psi_{\mathrm{N}}) \\ &= -\frac{1}{2}\sum_{a}^{N}\frac{1}{M_a}(T^{(2)}\Psi_{\mathrm{N}} + 2T^{(1)}\nabla_a\Psi_{\mathrm{N}} + \Psi_{\mathrm{e}}\nabla_a^2\Psi_{\mathrm{N}}). \end{aligned} \tag{2.12}$$

The first and the second derivative of the electronic wavefunction with respect to the nuclear coordinates, $T^{(1)} = \nabla_a\Psi_{\mathrm{e}}$ and $T^{(2)} = \nabla_a^2\Psi_{\mathrm{e}}$, are known as the non-adiabatic coupling terms (NACTs) of first and second order, respectively. The Born-Oppenheimer approximation assumes these NACTs to be very small and thus can be neglected [32]. This is only valid when the electronic states are well separated. In regions of the PESs of near-degeneracy of electronic states, the Born-Oppenheimer approximation breaks down [33] and the NACTs cannot be neglected as will be metioned in section 2.2.

Neglecting the NACTs, the nuclear TISE can be written as:

$$(\hat{T}_{\mathrm{N}} + E(\bar{R}))\Psi_{\mathrm{N}} = E_{\mathrm{N}}\Psi_{\mathrm{N}}, \tag{2.13}$$

providing the nuclear eigenfunctions Ψ_{N} and eigenenergies E_{N}. The solution of the nuclear TISE is explained in section 2.7.

2.1.2. Solving the electronic TISE

The electronic TISE (2.9) is still an n-body problem in $3n$ coordinates and cannot be solved analytically. Nevertheless, various methods based on different approximations are used to solve it. Solving the electronic TISE is the realm of quantum chemistry. In this section, we will briefly summarize two fundamental methods.

Hartree-Fock method

One of the most prominent methods used to handle with this n-body problem is the Hartree-Fock method (HF). The main assumption [34] is the reduction of the n-body problem to n one-body problems,

$$\Psi_{\mathrm{e}} = \chi_1(1)\chi_2(2)\chi_3(3)....\chi_k(n), \tag{2.14}$$

where $\chi_k(i)$ is the ith electron moving in the kth one-electron wavefunction which is called spin orbital.The problem with the wavefunction that results from this reduction is that it does not fulfill the Pauli exclusion principle. This principle dictates that the total wavefunction for a fermionic system has to be anti-symmetric with respect to the exchange of two particles. This problem was solved by Slater [35] by introducing a determinant as a wavefunction ansatz, which obeys Pauli's exclusion principle:

$$\Psi_{\mathrm{e}} = \frac{1}{\sqrt{n!}} \begin{vmatrix} \chi_1(1) & \chi_2(1) & \dots & \chi_k(1) \\ \chi_1(2) & \chi_2(2) & & \chi_k(2) \\ \vdots & & \ddots & \vdots \\ \chi_1(n) & \chi_2(n) & \dots & \chi_k(n) \end{vmatrix}. \tag{2.15}$$

Since the Hamiltonian (2.9) is not explicitly dependent on the electron spin, $\chi_k(1)$ can be written as a product of a spatial function (spatial orbital) and a spin operator eigenfunction, α or β. The unknown spatial orbitals are expressed as linear combinations of basis functions. The energy expectation value of the trial wavefunction, expressed as a Slater-determinant is given as:

$$E = \int_{-\infty}^{\infty} \Psi^* \hat{H} \Psi dv, \tag{2.16}$$

where dv is the volume element. Applying the variational principle i.e. minimizing the energy with respect to the spin orbitals, one can derive the so-called Hartree-Fock equations which are eigenvalue equations of the form [28]

$$\hat{f}\chi_i(1) = E_i\chi_i(1), \tag{2.17}$$

with $\hat{f}$ being the Fock operator, E_i is the orbital energy of orbital i and χ_i is the one-electron wavefunction that minimizes the energy E. The Fock operator is an effective one-electron operator that is given as:

$$\hat{f}(i) = \frac{-\nabla_i^2}{2} - \sum_{a=1}^{M} \frac{Z_a}{|\vec{R}_a - \vec{r}_i|} + v^{\mathrm{HF}}(i) \tag{2.18}$$

$v^{\mathrm{HF}}(i)$ is the average potential experienced by the ith electron due to the presence of the other electrons. The advantage of the Hartree-Fock approximation is that one can replace the complicated n-electron problem by n one-electron problems where the electron-electron repulsion is treated in an average way. The Fock operator depends on its eigenfunctions i.e. the spin orbitals. Thus, the Hartree-Fock equations are non-linear and must be solved using an iterative procedure, which is usually the self-consistent-field (SCF) procedure [28].

Since the HF method treats interactions between the electrons in an averaged way by using only one determinant, it has several limitations. For example, it cannot give a good description either for bond dissociations or for excited states. However, it yields qualitatively satisfying results for closed-shell systems in the electronic ground state.

Multi-configurational method

Since the HF method uses a single determinant and treats the electron-electron repulsion in an averaged way, the electron correlation cannot be described properly. Two types of electron correlation can be defined, the dynamical electron correlation, describing the interaction of the two electrons in the same spatial orbital and the statical electron correlation, describing the interaction of two electrons in different spatial orbitals [36]. The correlation energy is given as the difference between the exact non-relativistic energy and the HF energy in the limit of a complete basis set. Due to this deficiency of the HF method, several methods improving the HF energy have been developed, so-called post-Hartree-Fock methods. The multi-configurational method is one example of these post-Hartree-Fock methods that uses multiple determinants to describe a system, leading to a better description of the electron correlation.

Before describing the multi-configurational methods, the configuration interaction (CI) method should be explained. In the CI method, the wavefunction is written as a linear combination of more than one Slater determinant. The reference determinant is the HF determinant from which different electronic excitations are created, i.e. one or more electrons are promoted from occupied to virtual orbitals, leading to configuration state functions (CSFs) with single (S), double (D), triple (T), etc..., excitations. The CI wavefunction can now be written as a linear combination of all these CSFs:

$$\Psi_{\mathrm{CI}} = \mathrm{C}_0\Psi_{\mathrm{HF}} + \mathrm{C}_{\mathrm{S}}\Psi_{\mathrm{S}} + \mathrm{C}_{\mathrm{D}}\Psi_{\mathrm{D}} + \mathrm{C}_{\mathrm{T}}\Psi_{\mathrm{T}} + ... \tag{2.19}$$

The coefficients in front of the CSFs are variationally optimized to give the lowest possible energy. Note that only the CSF coefficients and not the orbital coefficients within the determinants are optimized.

The number of possible determinants for u spin orbitals with n electrons is given as:

$$\binom{u}{n} = \frac{u!}{n!(u-n)!} \tag{2.20}$$

If all possible determinants are considered then the ansatz is called full configuration interaction (FCI). The FCI method gives the exact energy if a complete basis set is used. However, FCI is computationally too expensive due to the large number of determinants included. It is only practical for small systems. Therefore, truncating the excitation to single and double excitations i.e. CISD is commonly used as a compromise between computational costs and reasonable recovery of the electron correlation.

The CI method gives quite satisfactory results for the electronic ground state but not for electronic excited states. The reason for this is that it uses the HF Slater determinant as a reference, where the optimization is done for the coefficients of the orbitals included in this determinant and also for the coefficient in front of this determinant, while for excited states the orbitals are kept frozen, i.e. not re-optimized after excitation. To solve this problem, the multi-configurational-self-consistent field (MCSCF) method has been developed [37]. The MCSCF method is a truncated CI where both the determinant and the orbital coefficients are optimized in a variational fashion. Thus, a more precise description is gained with the price of increasing computational efforts. An efficient method based on MCSCF is the complete-active-space-self-consistent field (CASSCF) approach [38–41].

The CASSCF method is efficient, as it reduces the number of the CSFs that are involved in this method, compared to those involved in the FCI and MCSCF methods. It relies on an elegant selection of the CSFs based on chemical intuition. The careful investigation of the chemical system of interest determines which CSFs have to be included in the CASSCF calculation. The selection of the CSFs is done by partitioning the molecular orbitals of the system into active, inactive and virtual orbitals, see Figure 2.1. In the CASSCF wavefunction, the inactive orbitals are doubly, and the virtual orbitals are unoccupied. The active orbitals are typically a set of highest occupied and lowest unoccupied molecular orbitals from a HF calculation, and these are the orbitals that are expected to play an important role in the chemical reaction to study.

Within the active orbitals (the so-called active space), a FCI is constructed. The common notation for this method is (n, m)-CASSCF [30], implying that n electrons are distributed in all possible ways in m active orbitals. Performing FCI within the active space is computationally demanding, even for small molecules, if the active space is big. Hence, the key step in the CASSCF procedure is the careful selection of the active space. It should be done in a way that it can balance between having a good description of the chemical process of interest and the computational costs. Therefore, the CASSCF approach is not a black-box procedure like HF and CI. It requires a sensible manual choice of the orbitals and the corresponding electrons to constitute the active space.

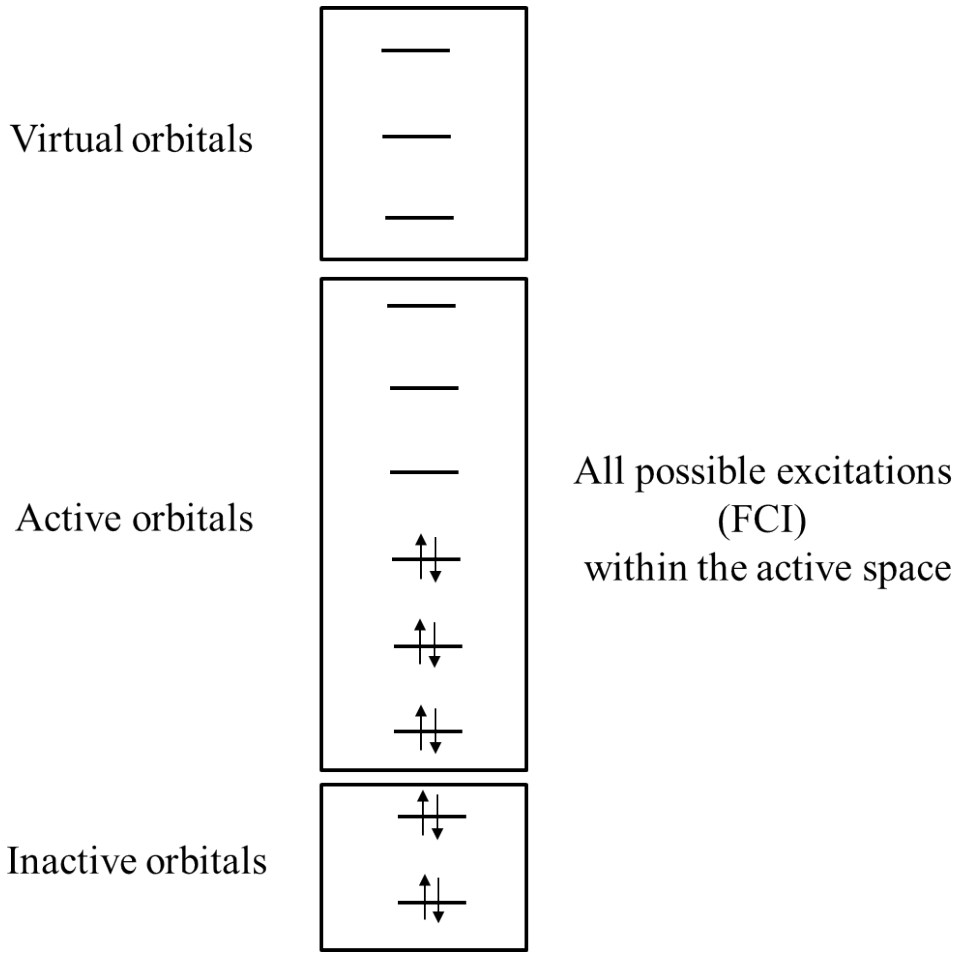

Figure 2.1.: Partitioning of orbitals within a CASSCF calculation. All possible excitations within the active space give rise to the configurations considered in a CASSCF calculation.

For computing excited states properties within the CASSCF approach, the orthogonality of the excited state wavefunctions should be assured, which is not the case if the calculations of the excited states are done separately. The orthogonality can be achieved by using the state averaged CASSCF (SA-CASSCF) method. Within SA-CASSCF, a number of electronic states are optimized simultaneously.

2.2. Beyond Born-Oppenheimer

As mentioned in subsection 2.1.1, the Born-Oppenheimer approximation breaks down when the electronic states get close in energy. This is very common in photochemistry of poly-atomic molecules where there are a large number of energetically close-lying electronic states and many nuclear degrees of freedom, giving rise to conical intersections, which are crossing points of two or more electronic states (e.g. Ψ_{e1} and Ψ_{e2}) with the same spin multiplicity. In the vicinity of a conical intersection the NACTs become very large. As a consequence, the NACTs cannot be neglected anymore, which is the reason for the non-validity of the Born-Oppenheimer approximation in such cases [30]. Conical intersections have important consequences for the nuclear dynamics and they offer pathways for ultra-fast interstate crossings on the femtosecond time scale [42].

The number of internal degrees of freedom for a non-linear molecule with N atoms is $3N-6$. For such molecules, two PESs are allowed to cross in $3N-6-2$ coordinates fulfilling the condition of energetical degeneracy ($E_{e2}-E_{e1}=0$). The two remaining nuclear coordinates make up the so-called branching space [43]. Plotting the considered PESs in the branching space forms a double cone in the region around the degeneracy in which the conical intersection is a single point -the apex of the cone.

Avoided crossing is another case where Born-Oppenheimer approximation breaks down. Avoided crossings results in diatomic molecules. The number of internal degrees of freedom for a linear molecule with N atoms is $3N-5$. Since $3N-5-2=-1$, for a diatomic molecule, a branching space cannot be formed, leading to avoided crossings. This constitutes the non-crossing rule introduced by von Neumann and Wigner [44].

2.3. The nuclear time-dependent Schrödinger equation

For the investigation of the nuclear dynamics, the time-dependent Schrödinger equation (TDSE) for the nuclear wavefunction on each electronic state i, Ψ_N^i, must be solved. In this thesis the nuclear dynamics that we are interested in is the torsional dynamics. The torsional quantum dynamics of a molecular system moving

within k different electronic states can be described as:

$$i\frac{\partial}{\partial t}\begin{pmatrix}\Psi^1_{\text{tor}}(t)\\ \Psi^2_{\text{tor}}(t)\\ \vdots\\ \Psi^k_{\text{tor}}(t)\end{pmatrix} = \begin{pmatrix}H_{11} & H_{12} & \dots & H_{1k}\\ H_{21} & H_{22} & & H_{2k}\\ \vdots & & \ddots & \vdots\\ H_{k1} & H_{k2} & \dots & H_{kk}\end{pmatrix}\begin{pmatrix}\Psi^1_{\text{tor}}(t)\\ \Psi^2_{\text{tor}}(t)\\ \vdots\\ \Psi^k_{\text{tor}}(t)\end{pmatrix} \tag{2.21}$$

where the diagonal H_{ii} and off-diagonal H_{ij} matrix elements of the Hamiltonian are:

$$H_{ii} = T + V_{ii} \quad \text{and} \quad H_{ij} = V_{ij} + T^{(1)}_{ij} + T^{(2)}_{ij}, \tag{2.22}$$

here $T^{(1)}_{ij} + T^{(2)}_{ij}$ are the NACTs, see equation (2.12). Since the non-adiabatic couplings were found to be either zero or very small for our system, see section 4.1, in our simulations we assumed them to be strictly zero, so that

$$T = \begin{pmatrix}T_{11} & & & \\ & T_{22} & & \\ & & \ddots & \\ & & & T_{kk}\end{pmatrix} \quad \text{and} \quad V = \begin{pmatrix}V_{11} & V_{12} & \dots & V_{1k}\\ V_{21} & V_{22} & & V_{2k}\\ \vdots & & \ddots & \\ V_{k1} & V_{k2} & \dots & V_{kk}\end{pmatrix}, \tag{2.23}$$

where $T_{11} = T_{22} = \ldots = T_{kk}$ and this kinetic energy operator T will be explained in the following section. V_{ii} is the ab initio potential energy surface of state i and V_{ij} is a general coupling term and throughout this work it is the laser coupling, which is introduced in the next section.

2.4. Hamiltonian of the ABC-systems

Hamiltonian of the ABC-systems in two torsional degrees of freedom

Within this thesis, we were interested in the investigation of the NSIs of an ABC-system, which is characterized by two coaxial torsions about the C_2 symmetry axis oriented along the laboratory Z-axis (see criteria (i) and (ii) in section 1.3). Therefore, the general full dimensional Hamiltonian, equation (2.13), was reduced to a model Hamiltonian with only these two torsional degrees of freedom using the approach explained in [45], the same type of steps are used here, with the extension of describing two torsional degrees of freedom [11] instead of only one [45]. The approach is explained for CCD as a representative of an ABC-system.

The reduction of the nuclear kinetic energy operator from its full dimensionality form to the two degrees of freedom of interest is explained below. We start from the PES of S_0 and the kinetic energy operator of all nuclei,

$$\hat{T} = \hat{T}_{3N} = \sum_i \sum_K \frac{\hat{\vec{\mathcal{P}}}_{iK}^2}{2M_{iK}} \tag{2.24}$$

with the index $3N = 78$ for CCD that specifies the original total number of nuclear degrees of freedom. $\hat{\vec{\mathcal{P}}}_{iK}$ is the momentum of the nucleus K in fragment i. All $3N$ Cartesian coordinates $\vec{R}_{iK} = (X_{iK}, Y_{iK}, Z_{iK})$ are taken in the laboratory frame, together with the nuclear spin variables, with the nuclear center of mass as origin and with C_2 symmetry axis oriented along the laboratory-fixed Z-axis. The momentum operators are conjugate to these nuclear Cartesian coordinates. The Cartesian coordinates $\vec{R}_{iK}$ of nucleus K in fragment i are replaced by cylindrical coordinates $(\mathcal{R}_{iK}, \Phi_{iK}, Z_{iK})$ using the approach described in [45]. Afterwards, more and more of these coordinates, or suitable linear combinations of these coordinates, are frozen in the equilibrium geometry, in a step-by-step manner, corresponding to systematic freezing of those vibrational and rotational degrees of freedom, which will not be considered in our model. For CCD, all nuclear coordinates are frozen in the equilibrium structure, except the angles $\Phi_\mathrm{A}, \Phi_\mathrm{B}$ and Φ_C, see Figure 1.4, describing the internal rotations i.e. torsions of segments A, B and C about the C_2 symmetry axis, respectively. The nuclear kinetic energy operator describing these torsions is

$$\hat{T}_3 = \frac{\hat{L}_\mathrm{A}^2}{2I_\mathrm{A}} + \frac{\hat{L}_\mathrm{B}^2}{2I_\mathrm{B}} + \frac{\hat{L}_\mathrm{C}^2}{2I_\mathrm{C}}, \tag{2.25}$$

where $\hat{L}_\mathfrak{S} = -i\frac{\partial}{\partial\Phi_\mathfrak{S}}$ is the internal angular momentum for the rotation of the segment $\mathfrak{S} = \mathrm{A}, \mathrm{B}, \mathrm{C}$ around the C_2-axis with the corresponding moment of inertia $I_\mathfrak{S}$, which is determined for the equilibrium structure of CCD by calculating:

$$I_\mathfrak{S} = \sum_{a=1}^{N_\mathfrak{S}} M_a \cdot \mathcal{D}_a^2, \tag{2.26}$$

where M_a is the mass of the moving atom included in segment $\mathfrak{S}$, $\mathcal{D}_a$ is the distance to the C_2-torsional axis and $N_\mathfrak{S}$ is the number of the moving atoms in segment $\mathfrak{S}$.

In the last step, the angles $\Phi_\mathrm{A}, \Phi_\mathrm{B}$ and Φ_C are replaced by the two torsional angles $\Phi_1 = \Phi_\mathrm{B} - \Phi_\mathrm{A}$ and $\Phi_2 = \Phi_\mathrm{C} - \Phi_\mathrm{B}$, and by the angle for overall rotation about the C_2-axis, $\Phi = C_\mathrm{A} \cdot \Phi_\mathrm{A} + C_\mathrm{B} \cdot \Phi_\mathrm{B} + C_\mathrm{C} \cdot \Phi_\mathrm{C}$ with coefficients $C_\mathfrak{S} = \frac{I_\mathfrak{S}}{(I_\mathrm{A}+I_\mathrm{B}+I_\mathrm{C})}$. Separating the overall rotation, the kinetic energy operator is reduced to

$$\hat{T}_2 = \frac{\hat{L}_1^2}{2I_1} + \frac{\hat{L}_1 \cdot \hat{L}_2}{I_\mathrm{B}} + \frac{\hat{L}_2^2}{2I_2}, \tag{2.27}$$

with reduced moments of inertia

$$I_1 = \frac{I_A \cdot I_B}{I_A + I_B} \quad \text{and} \quad I_2 = \frac{I_B \cdot I_C}{I_B + I_C}. \tag{2.28}$$

The first and the last terms of $\hat{T}_2$ describe torsions of the neighboring segments A versus B and B versus C, respectively. The middle term represents the torsional coupling. The derivation of $\hat{T}_2$ from $\hat{T}_3$ is entirely analogous to the derivation of the kinetic energy operator of the Thiele-Wilson Hamiltonian [46] for the coupled vibrations of the bonds AB and BC of a triatomic molecule ABC. Finally, neglecting nonadiabatic and dipole couplings, the two dimensional model Hamiltonian describing adiabatic torsions along Φ_1 and Φ_2 in electronic state k is

$$\hat{H}_{2k}(\Phi_1, \Phi_2) = \hat{T}_2 + V_k(\Phi_1, \Phi_2) \tag{2.29}$$

where the PES (V_k) depends explicitly solely on the two torsional angles Φ_1 and Φ_2, with all other degrees of freedom being frozen in the equilibrium geometry. In summary, the nuclear Hamiltonian derivation started from all nuclear Cartesian coordinates in the laboratory frame, whereas it ends with the expression in terms of the molecule-fixed torsional angles, analogous to [45].

2.5. Laser interaction

The interaction of a system with an external electric field $\epsilon(t)$ can still be described by the nuclear TDSE shown in equation (2.21), but the Hamiltonian now is time-dependent. The off-diagonal matrix elements, V_{ij}, of the Hamiltonian are the couplings between the states i and j induced by the laser. The laser couplings can be given within the dipole field interaction Taylor series as follows:

$$V_{ij} = -d_{ij}\epsilon(t) - \gamma_{ij}\epsilon^2(t) - \zeta_{ij}\epsilon^3(t) - ...., \tag{2.30}$$

here, the d_{ij} are the transition dipoles, γ_{ij} are the polarizability and ζ_{ij} are the hyperpolarizability elements. All these are one-electron properties and can be obtained by solving the electronic TISE (2.9).

In most of the cases, the Taylor series in equation (2.30) is cut after the transition dipole interaction with the laser ($d_{ij}\epsilon(t)$), because this interaction term has the largest contribution. A dipole coupling is caused by the transition dipole moments such that in the presence of a field, $\epsilon(t)$, population transfer between electronic states i and j is induced by that field if it is in resonance.

Throughout this work, we use a dynamic electric field that interacts with the

nuclear wavefunction and can be expressed as a sum of several pulses:

$$\epsilon(t) = \sum_{pulse} (\vec{\epsilon}_{XYZ} F_0 E(t) cos(\omega t)). \tag{2.31}$$

In the previous equation, $\vec{\epsilon}_{XYZ}$ is the polarization vector, F_0 is the field amplitude, the frequency is $\omega = \frac{2\pi}{\lambda}$, with the wavelength λ, and $E(t)$ is the envelope function. In this work, we use a sin-square function, defined as:

$$E(t) = \begin{cases} \sin^2\left(\frac{\pi t}{t_p}\right), & \text{if} \quad t_s < t < t_s + t_p \\ 0, & \text{otherwise} \end{cases} \tag{2.32}$$

where t_p is the pulse duration and t_s is the starting time of the pulse.

2.6. Solving the nuclear TDSE

This section is devoted to solve the nuclear TDSE for the time-dependent Hamiltonian matrix $H(t)$, which includes the interaction with laser, see section 2.5.

The integration of the nuclear TDSE for one state delivers:

$$\int_{\Psi_{\text{tor}}(t_0)}^{\Psi_{\text{tor}}(t)} \frac{d\Psi_{\text{tor}}(t)}{\Psi_{\text{tor}}(t)} = -i \int_{t_0}^{t} \hat{H}(t) dt. \tag{2.33}$$

To solve equation (2.33), we assume that we use a discrete time step Δt short enough so that $\hat{H}(t_0) \approx \hat{H}(t)$, i.e. $cos(\omega t)$ given in equation (2.31) is constant. If this requirement is fulfilled, the Hamiltonian in equation (2.33) becomes time-independent and the integration can be carried out to give:

$$\Psi_{\text{tor}}(t) = e^{-i\hat{H}(t-t_0)} \Psi_{\text{tor}}(t_0), \tag{2.34}$$

i.e.

$$\Psi_{\text{tor}}(t + \Delta t) = e^{-i\hat{H}\Delta t} \Psi_{\text{tor}}(t). \tag{2.35}$$

The obtained operator $e^{-i\hat{H}\Delta t}$ is known as the time-evolution operator or propagator [32].

The propagation of a nuclear wavefunction from time t_0 to t can be described

with the propagator, such that for k states it reads as:

$$\begin{pmatrix} \Psi^1_{\text{tor}}(t+\Delta t) \\ \Psi^2_{\text{tor}}(t+\Delta t) \\ \vdots \\ \Psi^k_{\text{tor}}(t+\Delta t) \end{pmatrix} = e^{-iH\Delta t} \begin{pmatrix} \Psi^1_{\text{tor}}(t) \\ \Psi^2_{\text{tor}}(t) \\ \vdots \\ \Psi^k_{\text{tor}}(t) \end{pmatrix}. \tag{2.36}$$

Several numerical routines can be used to solve equation (2.36) by expressing the propagator, $e^{-iH\Delta t}$, in different ways, e.g. polynomial methods like Chebyshev [47] and short iterative Lanczos propagation [48] or the split operator method [49–52]. In this thesis the split operator method is used and will be briefly introduced below.

Split-operator method

To solve equation (2.36), the propagator, $e^{-iH\Delta t}$, should be calculated. Unfortunately, the propagator cannot be expressed as:

$$e^{-iH\Delta t} = e^{-i(T+V)\Delta t} \neq e^{-iT\Delta t} e^{-iV\Delta t}, \tag{2.37}$$

because the kinetic energy T and the time-dependent potential V operators do not commute. Such split would then produce a large error. To reduce the error caused by this non-commutation, Feit and Fleck introduced the split operator [49–51], splitting either the potential energy operator symmetrically:

$$e^{-iH\Delta t} \approx e^{-i\frac{V}{2}\Delta t} e^{-iT\Delta t} e^{-i\frac{V}{2}\Delta t} + O(\Delta t^3), \tag{2.38}$$

or the kinetic energy operator symmetrically:

$$e^{-iH\Delta t} \approx e^{-i\frac{T}{2}\Delta t} e^{-iV\Delta t} e^{-i\frac{T}{2}\Delta t} + O(\Delta t^3). \tag{2.39}$$

Both splittings involve an error of third order in Δt. In this work the split-operator in equation (2.38) was used.

For the propagation, i.e. solving equation (2.36), the split of the Hamiltonian matrix H involved in the split-operator, see equation (2.38), works effectively when working on grids. The potential, V, acting on $\Psi^i_{\text{tor}}(t)$ is best described on the position grid, while the action of the kinetic energy operator, T, is best described on the momentum space. Consequently, at each time step $\Psi^i_{\text{tor}}(t)$ should be transformed from position to momentum space and back. This is done with a Fast Fourier Transformation (FFT), for further details see [32].

The propagator involves the exponentiation of the kinetic energy T and the potential energy V matrices, which can be calculated only if the matrices, V and T, are diagonal. The kinetic energy matrix is already diagonal, as the NACTs are assumed to be zero. The time-dependent potential matrix, V, should be diagonalized at the beginning of each time step for each grid point.

Using equation (2.38) for the split-operator, first the nuclear wavefunction is propagated in position space and multiplied with $e^{-i\frac{V}{2}\Delta t}$. Afterwards, a forward FFT is done for the nuclear wavefunction, to have it in momentum space, and multiplied with $e^{-iT\Delta t}$, then a backward FFT is applied on the nuclear wavefunction to convert it back into position space. Finally, the nuclear wavefunction is again multiplied by $e^{-i\frac{V}{2}\Delta t}$ to yield the nuclear wavefunction for the next time step $t \to t + \Delta t$. Repeating these steps for several different time steps gives the time-dependent nuclear wavefunction at a final time t_f.

2.7. Relaxation method: propagation in imaginary time

The calculation of the initial nuclear wavefunction at time zero, $\Psi_{\text{tor}}(t = 0)$, i.e. the nuclear eigenfunction for the electronic ground state, was done using the relaxation method [53, 54]. This initial state is prepared in the electronic and torsional ground state by propagating a guess function, step function, in imaginary time. This is called the relaxation method.

Within this method, Δt is replaced by $-i\Delta t$ in the propagation ansatz, see equation (2.35), leading to:

$$\Psi_{\text{tor}}(t + \Delta t) = e^{-\hat{H}\Delta t}\Psi_{\text{tor}}(t). \tag{2.40}$$

The initial state propagated with this method is an arbitrary initial state Ψ_{init}, which can be expanded as follows:

$$\Psi_{\text{init}} = \sum_l c_l \Psi_l \quad \text{with} \quad c_l = \langle \Psi_l \,|\, \Psi_{\text{init}} \rangle \,, \tag{2.41}$$

where Ψ_l are the nuclear eigenfunctions of the electronic ground state and c_l are their corresponding coefficients. Substituting equation (2.41) into equation (2.40) gives:

$$\Psi_{\text{tor}}(t + \Delta t) = \sum_l e^{-\hat{H}\Delta t} c_l \Psi_l = \sum_l e^{-E_l \Delta t} c_l \Psi_l. \tag{2.42}$$

Equation (2.42) is solved iteratively. Thus, the wavefunction with the most negative eigenvalue, E_l, relaxes most slowly, i.e. persists longest. Therefore, propagating an arbitrary initial wavefunction in imaginary time accumulates the ground state

wavefunction. This propagation has been implemented using the split-operator method. However, since the norm of the wavefunction decreases exponentially, the wavefunction has to be normalized after each time step. This prepared initial state is the wave packet that is used in this thesis for the dynamics simulations.

For calculating a certain torsional excited state, all states with energy lower than that excited state must be removed from the initial step. For example, projecting out the torsional ground state, Ψ_0, gives the first torsional excited state Ψ_1:

$$\Psi_{\text{init}} = \sum_l c_l \Psi_l - c_0 \Psi_0 \quad \text{with} \quad c_0 = \langle \Psi_0 \,|\, \Psi_{\text{init}} \rangle \,. \tag{2.43}$$

Substituting equation (2.43) into equation (2.40), as mentioned above, we get the first excited state torsional wavefunction Ψ_1, as it has the largest absolute eigenvalue compared to the rest of the excited states, so it accumulates.

3. Molecular symmetry

Throughout this chapter, molecular symmetry is employed to introduce a compact notation for the total Hamiltonian. The determination of the molecular symmetry group of CCD, as a representative of the ABC-systems, together with its properties like the multiplication table, the character table and the product table are explained in Sections 3.3 and 3.4. The effects of the molecular symmetry operations on molecular configurations are illustrated and finally the nuclear spin isomers of CCD are labelled according to their symmetry properties.

3.1. Hamiltonian of the ABC-systems in full dimensionality

In this section the effect of molecular symmetry on the total Hamiltonian ($\hat{H}_{\text{tot}}$ in equation (2.2)) is studied. Dividing the molecule under study in fragments, as shown in Figure 1.4, simplifies the total Hamiltonian by gathering the terms of the Hamiltonian that belong to a certain fragment, see Appendix A.1.

A compact notation of the Hamiltonian using molecular symmetry properties will be introduced. In the following $\hat{H}_{\text{tot}}$ is simply denoted as $\hat{H}$.

$$\hat{H} = \hat{T}_{\text{e}} + \hat{V}_{\text{ee}} + \hat{H}^{(1)} + \hat{H}^{(2)} \tag{3.1}$$

with

$$\hat{H}^{(1)} = \sum_{i=0}^{6} \hat{H}_i^{(1)} \tag{3.2}$$

and

$$\hat{H}^{(2)} = \sum_{i=0}^{6} \sum_{j=i}^{6} \hat{H}_{ij}^{(2)}. \tag{3.3}$$

Here, $\hat{T}_{\text{e}}$ is the kinetic energy operator of the electrons (as in equation (2.3)). $\hat{V}_{\text{ee}}$ denotes the Coulomb interactions between the electrons (as in equation (2.5)). $\hat{H}^{(1)}$ is a one-fragment Hamiltonian that for each of the seven fragments ($i = 0, \ldots, 6$) contains the kinetic energy of the nuclei of one fragment, the potential energy of the intra-nuclear-nuclear interactions and the potential energy of the intra-

nuclear-electron interactions. $\hat{H}^{(2)}$ is a two-fragment Hamiltonian that describes the inter-nuclear-nuclear potential energy between two nuclei, one of them in fragment $i = 0, \ldots, 6$ and the other one in fragment $j = i, \ldots, 6$. A close inspection of equation (3.1) reveals that it rephrases the Hamiltonian given in equation (2.2) by introducing fragments. Using fragments helps to exclude permutations between identical nuclei within the same fragment. These permutations are excluded because they imply bond breaking and bond formation, which involves passing through an insuperable barrier that causes these permutations to be unfeasible, i.e. they cannot be observed.

3.2. Commutation of the Hamiltonian and the molecular symmetry operations

As it has been already mentioned in the Introduction, a molecular symmetry group (G^{MS}) contains all the feasible permutations and permutation-inversions of identical nuclei. In order to determine the G^{MS} of CCD or any other related ABC molecule that fulfills the criteria (i) and (ii) mentioned in Section 1.2, the feasible permutations and permutation-inversions should be determined. The feasible permutations are those that describe the exchange of all the nuclei $K = 1, \ldots, N_i$ in fragment (i)=(1), (3) or (5) by the equivalent nuclei $K = 1, \ldots, N_j$ in fragment (j)=(2), (4) or (6), respectively, without exchanging any of the nuclei within the fragment itself, see Figure 3.1. This figure shows permutations of the fragments denoted with (12), (34) and (56) to describe the intra-molecular rotations of the segments (A), (B) and (C), recall Figure 1.4. In addition, any combination among any of these three permutations is also included in the G^{MS} like (12)(34), (12)(56), (34)(56) and (12)(34)(56). As a consequence, the permutation subgroup (G^{PSMS}) of the G^{MS} is composed of eight feasible permutations and can be written as:

$$G^{PSMS} = \{\mathcal{E}, (12), (34), (56), (12)(34), (12)(56), (34)(56), (12)(34)(56)\}, \quad (3.4)$$

where $\mathcal{E}$ is the identity. Inversion ($\mathcal{E}^*$) implies the conversion of all of the electronic and the nuclear coordinates of the system to its negative value, see Figure 3.1. Inversion can be followed or preceded by a permutation giving rise to the permutation-inversion. Since the G^{MS} contains eight feasible permutations, there exist eight feasible permutation-inversions. Permutation ($\mathcal{P}$) and inversion commute for the ABC-systems, thus, $\mathcal{P}\mathcal{E}^* \equiv \mathcal{P}^*$.

Since the Hamiltonian of equation (3.1) includes the sum of the kinetic energy of the nuclei and the sum of the nuclear-nuclear Columb interactions, permutation leaves the Hamiltonian invariant. This is due to the fact that summation does not depend on the order of terms. As a consequence,

$$[\hat{H}, \mathcal{P}] = 0 \quad \text{for any} \quad \mathcal{P} \in G^{PSMS}. \quad (3.5)$$

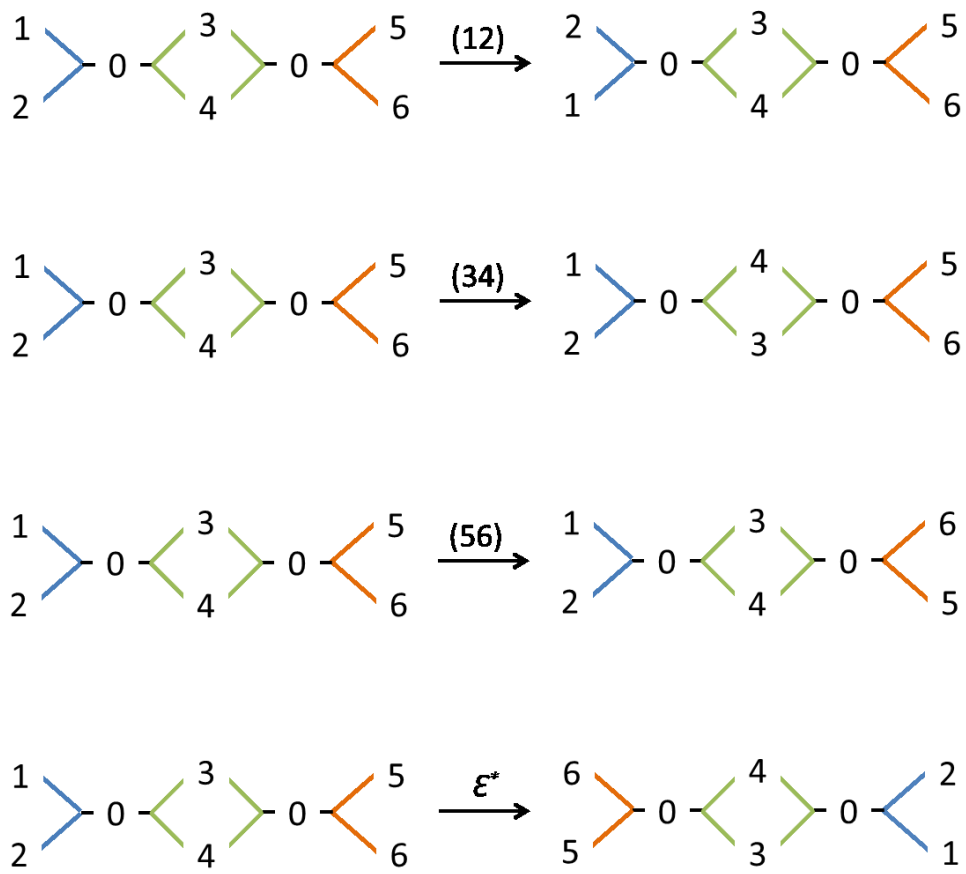

Figure 3.1.: Effects of the symmetry operations (12), (34), (56) and $\mathcal{E}^*$ of the G^{MS} on the fragments of an ABC-system, similar to CCD.

Moreover, $\hat{H}$ commutes with inversion because

$$-\frac{\nabla^2}{2M_{iK}} = -\frac{(-\nabla)^2}{2M_{iK}}, \tag{3.6}$$

for the kinetic energy and

$$\frac{Z_{iK}}{|\,-\vec{R}_{iK}+\vec{r}_i\,|} = \frac{Z_{iK}}{|\,\vec{R}_{iK}-\vec{r}_i\,|}, \tag{3.7}$$

for the Coulomb potential energy. M_{iK} is the nuclear mass of nucleus K in fragment i. Thus,

$$[\hat{H}, \mathcal{P}^*] = 0. \tag{3.8}$$

Consequently, $\hat{H}$ is invariant with respect to the eight feasible permutations contained in equation (3.4) and the eight feasible permutation-inversions. This commutation is of great importance as it enables us to deduce some of the properties

of the eigenstates of the Hamiltonian, without numerically solving the Schrödinger equation. These eigenfunctions may be considered as basis for the IREPs of the G^{MS} to which the molecule belongs [25].

An analogous commutation is also known for the molecular point groups [55], keeping in mind that the molecular point group, in contrast to the G^{MS}, only describes local structures like minima and transition states. Knowing the IREPs of a point group, one can tell a lot about the eigenfunctions of the vibronic Hamiltonian, which is used to label the vibrational and the electronic states of the molecule, without solving the Schrödinger equation. For example, the equilibrium structure of CCD in its electronic ground state belongs to the C_{2v} point group. Accordingly, and with the help of Table 3.1 its eigenfunctions must fall into any of the following categories [55]:

- Those which are totally symmetric (unchanged by all the operators) belong to the A_1 representation.
- Those which are unchanged by C_2 symmetry axis, but which change sign under both of the vertical planes σ_{XZ} and σ_{YZ} belong to the A_2 representation.
- Those which change sign under C_2 and σ_{YZ} but are unchanged by σ_{XZ} belong to the B_1 representation.
- Those which change sign under C_2 and σ_{XZ} but are unchanged by σ_{YZ} belong to the B_2 representation.

Table 3.1.: The character table of C_{2v}.

C_{2v}	$\mathcal{E}$	C_2	σ_{XZ}	σ_{YZ}
A_1	1	1	1	1
A_2	1	1	-1	-1
B_1	1	-1	1	-1
B_2	1	-1	-1	1

In the following section, the G^{MS} will be determined for CCD as a representative of the ABC-systems.

3.3. Molecular symmetry group of ABC-systems

CCD in its electronic ground state can be considered as a rigid molecule, since high potential barriers prevent torsion. To determine the G^{MS} for the rigid CCD molecule, one should keep in mind that the molecular symmetry operations of the G^{MS} should all describe only one version of the molecule. Versions are meant as equivalent equilibrium structures which can be inter-converted to each other by deformation of the molecule across a potential barrier [25]. For the rigid CCD-molecule this interconversion involves a very high barrier and it is thus, unfeasible. As a consequence, the permutations (12), (34) and (56) are unfeasible in the electronic ground state.

The G^{MS} for the rigid CCD-molecule is isomorphic to its point group and reads

$$G^{MS} = \{\mathcal{E}, (12)(34)(56), \mathcal{E}^*, (12)(34)(56)^*\}. \tag{3.9}$$

Two groups are isomorphic to each other if we can make a one-to-one correspondences between the elements of these two groups. Each element in the first group has a corresponding element in the second group. The corresponding elements should be chosen such that, if each element of the first group is replaced in the multiplication table by its corresponding element in the second group, then we obtain the multiplication table of the second group. If these two multiplication tables have the same structure the two groups are isomorphic [25]. It is obvious that isomorphic groups must have the same order, but groups of the same order are not necessarily isomorphic. For example, the rigid CCD-molecule has the point group C_{2v}, which is isomorphic to its G^{MS}. The one-to-one correspondences between these two groups is shown below:

$$\mathcal{E}\widehat{=}\mathcal{E},\ C_2\widehat{=}(12)(34)(56),\ \sigma_{XZ}\widehat{=}\mathcal{E}^*,\ \sigma_{YZ}\widehat{=}(12)(34)(56)^*. \tag{3.10}$$

If we replace each element in the multiplication table of C_{2v} (Table 3.2) by its corresponding element in the G^{MS} for the rigid molecule, then we obtain the multiplication table of the G^{MS}. This is shown in Table 3.3.

Exciting the CCD-molecule electronically, converts it from a rigid to a non-rigid molecule. Non-rigid molecules are molecules where the molecular symmetry operations that describe the conversion from one version to another passes through a low barrier, i.e. these molecular symmetry operations are feasible, in contrary to rigid molecules. Consequently, the permutations (12), (34) and (56) become feasible for the non-rigid CCD-molecule. The G^{MS} for the non-rigid CCD-molecule

Table 3.2.: The multiplication table of C_{2v}.

C_{2v}	$\mathcal{E}$	C_2	σ_{XZ}	σ_{YZ}
$\mathcal{E}$	$\mathcal{E}$	C_2	σ_{XZ}	σ_{YZ}
C_2	C_2	$\mathcal{E}$	σ_{YZ}	σ_{XZ}
σ_{XZ}	σ_{XZ}	σ_{YZ}	$\mathcal{E}$	C_2
σ_{YZ}	σ_{YZ}	σ_{XZ}	C_2	$\mathcal{E}$

Table 3.3.: The multiplication table of the G^{MS} of rigid CCD.

$G^{MS} = C_{2v}(M)$	$\mathcal{E}$	$(12)(34)(56)$	$\mathcal{E}^*$	$(12)(34)(56)^*$
$\mathcal{E}$	$\mathcal{E}$	$(12)(34)(56)$	$\mathcal{E}^*$	$(12)(34)(56)^*$
$(12)(34)(56)$	$(12)(34)(56)$	$\mathcal{E}$	$(12)(34)(56)^*$	$\mathcal{E}^*$
$\mathcal{E}^*$	$\mathcal{E}^*$	$(12)(34)(56)^*$	$\mathcal{E}$	$(12)(34)(56)$
$(12)(34)(56)^*$	$(12)(34)(56)^*$	$\mathcal{E}^*$	$(12)(34)(56)$	$\mathcal{E}$

is:

$$G^{MS} = G^{PSMS} \otimes \{\mathcal{E}, \mathcal{E}^*\}, \tag{3.11}$$

which gives,

$$\begin{aligned} G^{MS} = \{&\mathcal{E}, (12), (34), (56), (12)(34), (12)(56), (34)(56), (12)(34)(56), \mathcal{E}^*, (12)^*, \\ &(34)^*, (56)^*, (12)(34)^*, (12)(56)^*, (34)(56)^*, (12)(34)(56)^*\}. \end{aligned} \tag{3.12}$$

It can be easily verified that the set in equation (3.12) forms a group, see [56]. This group is the G^{MS} of CCD. Since the G^{MS} can be written as:

$$G^{MS} = \{\mathcal{E}, (12)\} \otimes \{\mathcal{E}, (34)\} \otimes \{\mathcal{E}, (56)\} \otimes \{\mathcal{E}, \mathcal{E}^*\}, \tag{3.13}$$

it can be directly deduced from the fundamental theorem of finite Abelian groups that the G^{MS} is Abelian [57].

For a rigid non-linear molecule, the G^{MS} is named by the name of the appropriate point group followed by (M) [25]. For example, the G^{MS} of the rigid CCD-molecule is $C_{2v}(M)$. For non-rigid molecules, the accepted convention for the G^{MS} is G_h, where h is the order of the group. Thus, for the non-rigid CCD-molecule, the G^{MS} is named with G_{16}, as it has eight feasible permutations and eight feasible permutation-inversions, so in total we have a group of order sixteen. The G_h notation is not unique, since there can be more than one non-isomorphic groups of a given order. For example, ethylene has the G_{16} notation, while its G^{MS} is completely different from the G_{16} of CCD. G_{16} for ethylene is a non-Abelian group

and describes only one torsional angle [25–27]. In contrast, G_{16} for CCD is an Abelian group and describes two torsional angles. To avoid any ambiguities of the notations, the G^{MS} of CCD will be called G_{16}^{A}, with superscript A representing Abelian.

3.4. Properties of the molecular symmetry group

3.4.1. Multiplication table

The properties of a group are conveniently summarized in a multiplication table which sets out systematically the products of all h^2 pairs of elements. Each entry in a multiplication table represents the result of first applying the operation at the top of its column and then applying the operation at the beginning of its row [58]. A very important condition for a multiplication table is that each of its rows and columns contains each element of the group once and only once. Thus, multiplication of all the elements of the group by any single element simply reproduces the same collection in a different order, this is called the rearrangement theorem [59].

The multiplication table of the molecular symmetry group G_{16}^{A}, the molecular symmetry group of CCD, is given in Tables 3.4-3.5. Since it is a large table, it is divided into two tables. The molecular symmetry group G_{16}^{A} is an Abelian group, so its multiplication table is symmetric with respect to the diagonal. Nevertheless, checking the off-diagonal molecular symmetry operations, which are supposed to be symmetric in Tables 3.4-3.5, one can see that the order of these molecular symmetry operations is not the same. This is owing to the fact that the molecular symmetry group G_{16}^{A} is an Abelian group, so its molecular symmetry operations commute. Consequently, order does not matter and e.g. (34)(12) is equivalent to (12)(34). Each element of the group is inverse to itself, so the elements in the diagonal are the identity.

Since the molecular symmetry group G_{16}^{A} has a large order equal to sixteen, using the group multiplication table explained above is not the best method to represent the group. There is another easier method that enables us to get the information that we can get from the group multiplication table. This method depends on using generators. Generators are the main molecular symmetry operations in terms of which the other molecular symmetry operations can be written as products and powers of these generators [57].

For the molecular symmetry group G_{16}^{A}, the generators are $(12), (34), (56)$ and $\mathcal{E}^*$. The products of these molecular symmetry operations lead to the other 12 molecular symmetry operations, this is known as the representation of the group. The representation is more compact than the group multiplication table, so we

Table 3.4.: First part of the multiplication table of the molecular symmetry group G_{16}^{A}.

G_{16}^{A}	$\mathcal{E}$	(12)	(34)	(12)(34)	(56)	(12)(56)	(34)(56)	(12)(34)(56)
$\mathcal{E}$	$\mathcal{E}$	(12)	(34)	(12)(34)	(56)	(12)(56)	(34)(56)	(12)(34)(56)
(12)	(12)	$\mathcal{E}$	(12)(34)	(34)	(12)(56)	(56)	(12)(34)(56)	(34)(56)
(34)	(34)	(34)(12)	$\mathcal{E}$	(12)	(34)(56)	(34)(12)(56)	(56)	(12)(56)
(12)(34)	(12)(34)	(34)	(12)	$\mathcal{E}$	(12)(34)(56)	(34)(56)	(12)(56)	(56)
(56)	(56)	(56)(12)	(56)(34)	(56)(12)(34)	$\mathcal{E}$	(12)	(34)	(12)(34)
(12)(56)	(12)(56)	(56)	(12)(56)(34)	(56)(34)	(12)	$\mathcal{E}$	(12)(34)	(34)
(34)(56)	(34)(56)	(34)(56)(12)	(56)	(56)(12)	(34)	(34)(12)	$\mathcal{E}$	(12)
(12)(34)(56)	(12)(34)(56)	(34)(56)	(12)(56)	(56)	(12)(34)	(34)	(12)	$\mathcal{E}$
$\mathcal{E}^*$	$\mathcal{E}^*$	(12)*	(34)*	(12)(34)*	(56)*	(12)(56)*	(34)(56)*	(12)(34)(56)*
(12)*	(12)*	$\mathcal{E}^*$	(12)(34)*	(34)*	(12)(56)*	(56)*	(12)(34)(56)*	(34)(56)*
(34)*	(34)*	(34)(12)*	$\mathcal{E}^*$	(12)*	(34)(56)*	(34)(12)(56)*	(56)*	(12)(56)*
(12)(34)*	(12)(34)*	(34)*	(12)*	$\mathcal{E}^*$	(12)(34)(56)*	(34)(56)*	(12)(56)*	(56)*
(56)*	(56)*	(56)(12)*	(56)(34)*	(56)(12)(34)*	$\mathcal{E}*$	(12)*	(34)*	(12)(34)*
(12)(56)*	(12)(56)*	(56)*	(12)(56)(34)*	(56)(34)*	(12)*	$\mathcal{E}^*$	(12)(34)*	(34)*
(34)(56)*	(34)(56)*	(34)(56)(12)*	(56)*	(56)(12)*	(34)*	(34)(12)*	$\mathcal{E}^*$	(12)*
(12)(34)(56)*	(12)(34)(56)*	(34)(56)*	(12)(56)*	(56)*	(12)(34)*	(34)*	(12)*	$\mathcal{E}^*$

Table 3.5.: Second part of the multiplication table of the molecular symmetry group G_{16}^{A}.

G_{16}^{A}	$\mathcal{E}^*$	$(12)^*$	$(34)^*$	$(12)(34)^*$	$(56)^*$	$(12)(56)^*$	$(34)(56)^*$	$(12)(34)(56)^*$
$\mathcal{E}$	$\mathcal{E}^*$	$(12)^*$	$(34)^*$	$(12)(34)^*$	$(56)^*$	$(12)(56)^*$	$(34)(56)^*$	$(12)(34)(56)^*$
(12)	$(12)^*$	$\mathcal{E}^*$	$(12)(34)^*$	$(34)^*$	$(12)(56)^*$	$(56)^*$	$(12)(34)(56)^*$	$(34)(56)^*$
(34)	$(34)^*$	$(34)(12)^*$	$\mathcal{E}^*$	$(12)^*$	$(34)(56)^*$	$(34)(12)(56)^*$	$(56)^*$	$(12)(56)^*$
$(12)(34)$	$(12)(34)^*$	$(34)^*$	$(12)^*$	$\mathcal{E}^*$	$(12)(34)(56)^*$	$(34)(56)^*$	$(12)(56)^*$	$(56)^*$
(56)	$(56)^*$	$(56)(12)^*$	$(56)(34)^*$	$(56)(12)(34)^*$	$\mathcal{E}*$	$(12)^*$	$(34)^*$	$(12)(34)^*$
$(12)(56)$	$(12)(56)^*$	$(56)^*$	$(12)(56)(34)^*$	$(56)(34)^*$	$(12)^*$	$\mathcal{E}^*$	$(12)(34)^*$	$(34)^*$
$(34)(56)$	$(34)(56)^*$	$(34)(56)(12)^*$	$(56)^*$	$(56)(12)^*$	$(34)^*$	$(34)(12)^*$	$\mathcal{E}^*$	$(12)^*$
$(12)(34)(56)$	$(12)(34)(56)^*$	$(34)(56)^*$	$(12)(56)^*$	$(56)^*$	$(12)(34)^*$	$(34)^*$	$(12)^*$	$\mathcal{E}^*$
$\mathcal{E}^*$	$\mathcal{E}$	(12)	(34)	$(12)(34)$	(56)	$(12)(56)$	$(34)(56)$	$(12)(34)(56)$
$(12)^*$	(12)	$\mathcal{E}$	$(12)(34)$	(34)	$(12)(56)$	(56)	$(12)(34)(56)$	$(34)(56)$
$(34)^*$	(34)	$(34)(12)$	$\mathcal{E}$	(12)	$(34)(56)$	$(34)(12)(56)$	(56)	$(12)(56)$
$(12)(34)^*$	$(12)(34)$	(34)	(12)	$\mathcal{E}$	$(12)(34)(56)$	$(34)(56)$	$(12)(56)$	(56)
$(56)^*$	(56)	$(56)(12)$	$(56)(34)$	$(56)(12)(34)$	$\mathcal{E}$	(12)	(34)	$(12)(34)$
$(12)(56)^*$	$(12)(56)$	(56)	$(12)(56)(34)$	$(56)(34)$	(12)	$\mathcal{E}$	$(12)(34)$	(34)
$(34)(56)^*$	$(34)(56)$	$(34)(56)(12)$	(56)	$(56)(12)$	(34)	$(34)(12)$	$\mathcal{E}$	(12)
$(12)(34)(56)^*$	$(12)(34)(56)$	$(34)(56)$	$(12)(56)$	(56)	$(12)(34)$	(34)	(12)	$\mathcal{E}$

can represent the molecular symmetry group G_{16}^{A} as follows:

$$G_{16}^{A} = \{(12), (34), (56), \mathcal{E}^* \mid (12)^2 = (34)^2 = (56)^2 = (\mathcal{E}^*)^2 = \mathcal{E}\}, \tag{3.14}$$

where $(12)^2$ means (12)(12), etc. and the "|" is used just to separate the generators ((12), (34), (56) and $\mathcal{E}^*$) from the identity ($\mathcal{E} = (12)^2 = (34)^2 = (56)^2 = (\mathcal{E}^*)^2$). Thus, the molecular symmetry group G_{16}^{A} is generated by the four elements (12), (34), (56) and $\mathcal{E}^*$. With the help of equation (3.14) alone, we can generate the complete group G_{16}^{A}. This generation of the molecular symmetry group G_{16}^{A}, will be very helpful for identifying the symmetry-adapted torsional eigenfunctions; this identification will be done in Section 3.7.

3.4.2. Character table

Within a character table the elements of the same class are grouped together, since they have the same character (where the character of a representation is the trace of the matrix of that representation) in each IREP. Only one element in each class is given, but the number of elements in each class is indicated. The number of IREPs is always equal to the number of different classes of symmetry operations. Since G_{16}^{A} is an Abelian group, each symmetry operation forms a class by its own. Accordingly, the IREPs are non-degenerate. The character of the symmetry operation $\mathcal{R}$ in the IREP Γ_i is denoted by $\mathcal{X}^{\Gamma_i}(\mathcal{R})$. For a non-degenerate IREP (Γ_i), for all characters $\mid \mathcal{X}^{\Gamma_i}(\mathcal{R}) \mid = 1$, where $\mathcal{X}^{\Gamma_i}(\mathcal{R}) = +1$ means that the phase of, for example, an orbital is unchanged by the symmetry operations, while $\mathcal{X}^{\Gamma_i}(\mathcal{R}) = -1$ denotes a change of the sign [55].

To deduct information from the molecular symmetry group G_{16}^{A}, we need its character table. For a rigid molecule the abstract character table of G^{MS} is the same as for its point group, because of their isomorphism. Since we are interested in the simulation of nuclear dynamics of electronically excited CCD, i.e. non-rigid CCD-molecule, the character table of G_{16}^{A} is needed, which has an order equal to sixteen, i.e. it has sixteen IREPs. Since there is no point group isomorphic to it, we must construct its character table by ourselves.

To facilitate constructing the character table of the molecular symmetry group G_{16}^{A}, it is decomposed into subgroups, according to equation (3.13). These subgroups are the permutation subgroups of the identical fragments (1) and (2), (3) and (4) and (5) and (6), i.e. $\mathcal{S}_2^{(12)} = \{\mathcal{E}, (12)\}$, $\mathcal{S}_2^{(34)} = \{\mathcal{E}, (34)\}$ and $\mathcal{S}_2^{(56)} = \{\mathcal{E}, (56)\}$ (where the superscript of $\mathcal{S}$ indicates the permuted fragments within this subgroup and its subscript is for its order) and the inversion subgroup $\varepsilon = \{\mathcal{E}, \mathcal{E}^*\}$.

The construction of the character table of the molecular symmetry group G_{16}^{A}

can be done by applying the direct product of the character tables of the three permutation subgroups $\mathcal{S}_2^{(12)}$, $\mathcal{S}_2^{(34)}$ and $\mathcal{S}_2^{(56)}$ of the molecular symmetry group G_{16}^A and the inversion subgroup. The direct product is applied using:

$$\mathcal{X}^{\Gamma_k(\mathcal{S}\cdot\mathcal{S}')}(\mathcal{R}) = \mathcal{X}^{\Gamma_i(\mathcal{S})}(\mathcal{R}) \cdot \mathcal{X}^{\Gamma_j(\mathcal{S}')}(\mathcal{R}). \tag{3.15}$$

where $\mathcal{S}$ and $\mathcal{S}'$ are two different subgroups of G_{16}^A. How to apply the direct product on the character tables of the subgroups to get the character table of the resulting group is explained in [25]. The character tables of $\mathcal{S}_2^{(12)}$, $\mathcal{S}_2^{(34)}$, $\mathcal{S}_2^{(56)}$ and ε are shown below in Table 3.6. Each one of these subgroups is isomorphic to the $\mathcal{C}_2$ point group, so each one of these subgroups has the same abstract character table as $\mathcal{C}_2$ point group. Applying the direct product of these permutation subgroups gives the character table of the molecular symmetry group G_{16}^A, which is listed in Table 3.7. The IREPs of the molecular symmetry group G_{16}^A are labelled with a superscript which is either +, if $\mathcal{X}(\mathcal{E}^*) = 1$, i.e. has even parity, or -, if $\mathcal{X}(\mathcal{E}^*) = -1$, i.e. has odd parity.

Table 3.6.: The Character tables of $\mathcal{S}_2^{(12)}$, $\mathcal{S}_2^{(34)}$, $\mathcal{S}_2^{(56)}$ and ε, respectively.

$\mathcal{S}_2^{(12)}$	$\mathcal{E}$	(12)
A	1	1
B	1	-1

$\mathcal{S}_2^{(34)}$	$\mathcal{E}$	(34)
A	1	1
B	1	-1

$\mathcal{S}_2^{(56)}$	$\mathcal{E}$	(56)
A	1	1
B	1	-1

ε	$\mathcal{E}$	$\mathcal{E}^*$
A^+	1	1
A^-	1	-1

An important application of the character table is the construction of the symmetry projection operators for the (here: sixteen) different IREPs. This will be discussed below.

Table 3.7.: The character table of the molecular symmetry group G_{16}^{A}.

G_{16}^{A}	$\mathcal{E}$	(12)	(34)	(12)(34)	(56)	(12)(56)	(34)(56)	(12)(34)(56)	$\mathcal{E}^*$	(12)*	(34)*	(12)(34)*	(56)*	(12)(56)*	(34)(56)*	(12)(34)(56)*
Γ_1^+	1	1	1	1	1	1	1	1	1	1	1	1	1	1	1	1
Γ_2^+	1	1	1	1	-1	-1	-1	-1	1	1	1	1	-1	-1	-1	-1
Γ_3^+	1	1	-1	-1	1	1	-1	-1	1	1	-1	-1	1	1	-1	-1
Γ_4^+	1	1	-1	-1	-1	-1	1	1	1	1	-1	-1	-1	-1	1	1
Γ_5^+	1	-1	1	-1	1	-1	1	-1	1	-1	1	-1	1	-1	1	-1
Γ_6^+	1	-1	1	-1	-1	1	-1	1	1	-1	1	-1	-1	1	-1	1
Γ_7^+	1	-1	-1	1	1	-1	-1	1	1	-1	-1	1	1	-1	-1	1
Γ_8^+	1	-1	-1	1	-1	1	1	-1	1	-1	-1	1	-1	1	1	-1
Γ_1^-	1	1	1	1	1	1	1	1	-1	-1	-1	-1	-1	-1	-1	-1
Γ_2^-	1	1	1	1	-1	-1	-1	-1	-1	-1	-1	-1	1	1	1	1
Γ_3^-	1	1	-1	-1	1	1	-1	-1	-1	-1	1	1	-1	-1	1	1
Γ_4^-	1	1	-1	-1	-1	-1	1	1	-1	-1	1	1	1	1	-1	-1
Γ_5^-	1	-1	1	-1	1	-1	1	-1	-1	1	-1	1	-1	1	-1	1
Γ_6^-	1	-1	1	-1	-1	1	-1	1	-1	1	-1	1	1	-1	1	-1
Γ_7^-	1	-1	-1	1	1	-1	-1	1	-1	1	1	-1	-1	1	1	-1
Γ_8^-	1	-1	-1	1	-1	1	1	-1	-1	1	1	-1	1	-1	-1	1

$\Gamma_i^{\pm}$: is the ith IREP, where the + and the - signs indicate even and odd parity, respectively.

Symmetry Projection Operator

The molecular symmetry projection operator ($\hat{P}^{\Gamma_i}$) for an IREP Γ_i, is obtained from the characters $\mathcal{X}^{\Gamma_i}(\mathcal{R})$ for the operations $\mathcal{R}$ which are shown in the character table, Table 3.7, as follows:

$$\hat{P}^{\Gamma_i} = \frac{l_{\Gamma_i}}{h} \sum_{\mathcal{R}} \mathcal{X}^{\Gamma_i}(\mathcal{R})\mathcal{R}, \tag{3.16}$$

where h is the order of the group and l_{Γ_i} is the dimension of the IREP Γ_i. For G_{16}^A, $l_{\Gamma_i} = 1$ for all IREPs.

The projection operator $\hat{P}^{\Gamma_i}$ allows to construct so-called symmetry-adapted basis functions (Ψ^{Γ_i}), e.g. symmetry-adapted torsional eigenfunctions, that transform according to the IREP Γ_i. The idempotence property of the $\hat{P}^{\Gamma_i}$ for one-dimensional IREP is defined as follows:

$$\hat{P}^{\Gamma_i}\hat{P}^{\Gamma_i} = \hat{P}^{\Gamma_i}. \tag{3.17}$$

This property is explained for $\hat{P}^{\Gamma_7^+}$ as an example, see Appendix A.2 and it implies that the symmetry projection operator has an eigenvalue (d_i) equal to either 0 or 1, see below:

$$\hat{P}^{\Gamma_i}\Psi^{\Gamma_i} = d_i\Psi^{\Gamma_i} \tag{3.18}$$

$$\begin{aligned} \hat{P}^{\Gamma_i}(\hat{P}^{\Gamma_i}\Psi^{\Gamma_i}) &= \hat{P}^{\Gamma_i}(d_i\Psi^{\Gamma_i}) \\ &= d_i(d_i\Psi^{\Gamma_i}) \\ &= d_i^2\Psi^{\Gamma_i}, \end{aligned} \tag{3.19}$$

by definition,

$$\begin{aligned} \hat{P}^{\Gamma_i}(\hat{P}^{\Gamma_i}\Psi^{\Gamma_i}) &= \hat{P}^{\Gamma_i}\Psi^{\Gamma_i} \\ d_i^2\Psi^{\Gamma_i} &= d_i\Psi^{\Gamma_i}. \end{aligned} \tag{3.20}$$

Hence, $d_i = d_i^2$, see equation (3.20). This can be achieved if and only if $d_i = 1$ or 0. This means that if the function $\Psi = \Psi^{\Gamma_i}$ is an eigenfunction of $\hat{P}^{\Gamma_i}$ with non-zero eigenvalue, i.e. $\hat{P}^{\Gamma_i}\Psi^{\Gamma_i} = \Psi^{\Gamma_i}$, then it is a symmetry-adapted eigenfunction of Γ_i. This property serves to identify the IREP (Γ_i) of any symmetry-adapted basis function Ψ^{Γ_i}.

Another important property of the symmetry projection operators is their orthogonality,

$$\hat{P}^{\Gamma_i}\hat{P}^{\Gamma_j} = 0, \quad \text{for} \quad i \neq j. \tag{3.21}$$

This may serve as a test of self-consistency of the character table, see Appendix A.2. This orthogonality leads to the commutation of the symmetry projection operators of different IREPs [25, 57], i.e.

$$[\hat{P}^{\Gamma_i}, \hat{P}^{\Gamma_j}] = 0, \tag{3.22}$$

because,

$$\hat{P}^{\Gamma_i}\hat{P}^{\Gamma_j} = \hat{P}^{\Gamma_j}\hat{P}^{\Gamma_i} = 0 \quad \text{for} \quad i \neq j. \tag{3.23}$$

Thus, if the symmetry projection operator of an IREP Γ_j is applied to Ψ^{Γ_i} with $i \neq j$, then this gives the zero eigenvalue,

$$\hat{P}^{\Gamma_j}\Psi^{\Gamma_i} = \hat{P}^{\Gamma_j}\hat{P}^{\Gamma_i}\Psi^{\Gamma_i} = 0. \tag{3.24}$$

As a consequence of the orthogonality and the idempotence properties of the $\hat{P}^{\Gamma_i}$, see equations (3.21) and (3.17), the symmetry adapted basis functions can be labelled by one of the sixteen IREPs of the molecular symmetry group G_{16}^A, instead of sixteen eigenvalues of the individual $\hat{P}^{\Gamma_i}, i = 1, \ldots, 16$, i.e. labelled by Ψ^{Γ_i} instead of $\Psi_{0,0,\ldots,1,\ldots,0,0}$, which simplifies the notations for the symmetry adapted basis functions.

Commutation of the Hamiltonian with the $\hat{P}^{\Gamma_i}$

The Hamiltonian, equation (3.1), and the projection operator $\hat{P}^{\Gamma_i}$ commute,

$$[\hat{H}, \hat{P}^{\Gamma_i}] = 0. \tag{3.25}$$

The proof of this commutation is shown below, using the definition of a symmetry projection operator for Abelian groups:

$$\begin{aligned}
\hat{H}\hat{P}^{\Gamma_i} &= \hat{H}\frac{1}{h}\sum_{\mathcal{R}}\chi^{\Gamma_i}(\mathcal{R})\mathcal{R} \\
&= \frac{1}{h}\sum_{\mathcal{R}}\chi^{\Gamma_i}(\mathcal{R})\hat{H}\mathcal{R} \\
&= \frac{1}{h}\sum_{\mathcal{R}}\chi^{\Gamma_i}(\mathcal{R})\mathcal{R}\hat{H} \qquad (\mathcal{R} \text{ commutes with } \hat{H}) \\
&= \hat{P}^{\Gamma_i}\hat{H}. \qquad (3.26)
\end{aligned}$$

(3.27)

This commutation implies that the symmetry adapted torsional eigenfunctions can

be labeled simultaneously with the energy (the eigenvalue of the Hamiltonian) and one of the sixteen IREPs of the the molecular symmetry group G_{16}^{A}.

3.4.3. Permutation subgroup of the molecular symmetry group G_{16}^{A}

As mentioned in the Introduction, CCD exists in form of different nuclear spin isomers. The nuclear spin wavefunctions transform according to the IREPs of the permutation subgroup of the molecule, due to reasons that will be explained in Section 3.7. Thus, for labeling the nuclear spin isomers of CCD, only the G^{PSMS}, see equation (3.4), is needed [60]. The character table of the G^{PSMS} is shown in Table 3.8. It was constructed utilizing the same way used for constructing the character table of the molecular symmetry group G_{16}^{A}. In particular, the character table of the G^{PSMS} was constructed by applying the direct product on only the three permutation subgroups $\mathcal{S}_2^{(12)} = \{\mathcal{E}, (12)\}$, $\mathcal{S}_2^{(34)} = \{\mathcal{E}, (34)\}$ and $\mathcal{S}_2^{(56)} = \{\mathcal{E}, (56)\}$, unlike the construction of the character table of the molecular symmetry group G_{16}^{A}, where the inversion subgroup was also included. The character table of the G^{PSMS} answers one of the questions which have been raised in the Introduction: CCD has at most eight different nuclear spin isomers because the G^{PSMS} has eight IREPs. These nuclear spin isomers are characterized by the IREPs of their nuclear spin wavefunctions. Since the G^{PSMS} is a subgroup of the Abelian group G_{16}^{A}, it is also an Abelian group. It follows that we can utilize its character table for direct construction of the symmetry-adapted torsional and nuclear spin wavefunctions with the help of the projection operator $\hat{P}^{\Gamma_i}$ for the IREP Γ_i. The $\hat{P}^{\Gamma_i}$ for the G^{PSMS}, which have an order equal to eight, are defined as:

$$\hat{P}^{\Gamma_i} = \frac{1}{8} \sum_{\mathcal{R}} \mathcal{X}^{\Gamma_i}(\mathcal{R}) \mathcal{R} \quad \text{with} \quad \mathcal{R} \in G^{PSMS}. \tag{3.28}$$

These $\hat{P}^{\Gamma_i}$ are employed here to generate symmetry adapted torsional wavefunctions of oriented CCD (see section 3.5). To do so, the calculation of a localized wavefunction (Ψ_l) in a single potential well was carried out first. (Ψ_l) is not symmetry adapted yet. Thus, the $\hat{P}^{\Gamma_i}$ is applied - the idempotence (equation (3.17)) implies that $\hat{P}^{\Gamma_i}\Psi_l$ is automatically an eigenfunction of $\hat{P}^{\Gamma_i}$, due to

$$\hat{P}^{\Gamma_i}(\hat{P}^{\Gamma_i}\Psi_l) = \hat{P}^{\Gamma_i}\Psi_l, \tag{3.29}$$

with eigenvalues of 1 or 0 if $\hat{P}^{\Gamma_i}\Psi_l \neq 0$ or $\hat{P}^{\Gamma_i}\Psi_l = 0$, respectively. If $\hat{P}^{\Gamma_i}\Psi_l \neq 0$, then we define the symmetry-adapted torsional wavefunction with IREP Γ_i,

$$\Psi^{\Gamma_i} = \mathcal{N}_i \hat{P}^{\Gamma_i}\Psi_l, \tag{3.30}$$

where $\mathcal{N}_i$ is the normalization constant. These relations explained in this section

are important for the discussion in Section 3.7.

Table 3.8.: The character table of G^{PSMS}, the permutation subgroup of the molecular symmetry group G_{16}^{A}.

G_{16}^{A}	$\mathcal{E}$	(12)	(34)	(12)(34)	(56)	(12)(56)	(34)(56)	(12)(34)(56)
Γ_1	1	1	1	1	1	1	1	1
Γ_2	1	1	1	1	-1	-1	-1	-1
Γ_3	1	1	-1	-1	1	1	-1	-1
Γ_4	1	1	-1	-1	-1	-1	1	1
Γ_5	1	-1	1	-1	1	-1	1	-1
Γ_6	1	-1	1	-1	-1	1	-1	1
Γ_7	1	-1	-1	1	1	-1	-1	1
Γ_8	1	-1	-1	1	-1	1	1	-1

3.4.4. Product table

The product table of the molecular symmetry group G_{16}^{A} is shown in Table 3.9. It is obtained by applying the direct product on the characters of the corresponding IREPs using:

$$\mathcal{X}^{\Gamma_i \otimes \Gamma_j}(\mathcal{R}) = \mathcal{X}^{\Gamma_i}(\mathcal{R}) \mathcal{X}^{\Gamma_j}(\mathcal{R}). \tag{3.31}$$

For example, the characters of the symmetry operations $\mathcal{R}$ that result from applying the direct product on the characters of the two IREPs Γ_2^+ and Γ_6^+, i.e. $\mathcal{X}^{\Gamma_2^+ \otimes \Gamma_6^+}$, are:

	$\mathcal{E}$	(12)		...			...				...				(12)(34)(56)*
$\mathcal{X}^{\Gamma_2^+}(\mathcal{R})$	1	1	1	1	−1	−1	−1	−1	1	1	1	1	−1	−1	−1	−1
$\mathcal{X}^{\Gamma_6^+}(\mathcal{R})$	1	−1	1	−1	−1	1	−1	1	1	−1	1	−1	−1	1	−1	1
$\mathcal{X}^{\Gamma_2^+ \otimes \Gamma_6^+}(\mathcal{R})$	1	−1	1	−1	1	−1	1	−1	1	−1	1	−1	1	−1	1	−1

. (3.32)

The $\mathcal{X}^{\Gamma_2^+ \otimes \Gamma_6^+}$ of equation 3.32 for the sixteen symmetry operations $\mathcal{R} = \mathcal{E}, (12), ..., (12)(34)(56)^*$ (same order as given in the character table of G_{16}^{A}) are the same as those of the $\mathcal{X}^{\Gamma_5^+}$ (as in Table 3.7). Hence, $\Gamma_2^+ \otimes \Gamma_6^+ = \Gamma_5^+$. The other direct product of the IREPs can be determined by analogous multiplication of the characters of the symmetry operations, as shown in the product table of Table 3.9. Since the direct product of any IREP with itself gives the totally symmetric IREP Γ_1^+ (this

is true only for Abelian groups), Γ_1^+ is found along the diagonal in the product table. The product table of the molecular symmetry group G_{16}^A is symmetric with respect to the diagonal, i.e. applying the direct product on the IREPs of the upper-triangular part of the product table yields the lower-triangular part of this table.

Table 3.9.: The product table of the molecular symmetry group G_{16}^{A}.

G_{16}^{A}	Γ_1^+	Γ_2^+	Γ_3^+	Γ_4^+	Γ_5^+	Γ_6^+	Γ_7^+	Γ_8^+	Γ_1^-	Γ_2^-	Γ_3^-	Γ_4^-	Γ_5^-	Γ_6^-	Γ_7^-	Γ_8^-
Γ_1^+	Γ_1^+	Γ_2^+	Γ_3^+	Γ_4^+	Γ_5^+	Γ_6^+	Γ_7^+	Γ_8^+	Γ_1^-	Γ_2^-	Γ_3^-	Γ_4^-	Γ_5^-	Γ_6^-	Γ_7^-	Γ_8^-
Γ_2^+	Γ_2^+	Γ_1^+	Γ_4^+	Γ_3^+	Γ_6^+	Γ_5^+	Γ_8^+	Γ_7^+	Γ_2^-	Γ_1^-	Γ_4^-	Γ_3^-	Γ_6^-	Γ_5^-	Γ_8^-	Γ_7^-
Γ_3^+	Γ_3^+	Γ_4^+	Γ_1^+	Γ_2^+	Γ_7^+	Γ_8^+	Γ_5^+	Γ_6^+	Γ_3^-	Γ_4^-	Γ_1^-	Γ_2^-	Γ_7^-	Γ_8^-	Γ_5^-	Γ_6^-
Γ_4^+	Γ_4^+	Γ_3^+	Γ_2^+	Γ_1^+	Γ_8^+	Γ_7^+	Γ_6^+	Γ_5^+	Γ_4^-	Γ_3^-	Γ_2^-	Γ_1^-	Γ_8^-	Γ_7^-	Γ_6^-	Γ_5^-
Γ_5^+	Γ_5^+	Γ_6^+	Γ_7^+	Γ_8^+	Γ_1^+	Γ_2^+	Γ_3^+	Γ_4^+	Γ_5^-	Γ_6^-	Γ_7^-	Γ_8^-	Γ_1^-	Γ_2^-	Γ_3^-	Γ_4^-
Γ_6^+	Γ_6^+	Γ_5^+	Γ_8^+	Γ_7^+	Γ_2^+	Γ_1^+	Γ_4^+	Γ_3^+	Γ_6^-	Γ_5^-	Γ_8^-	Γ_7^-	Γ_2^-	Γ_1^-	Γ_4^-	Γ_3^-
Γ_7^+	Γ_7^+	Γ_8^+	Γ_5^+	Γ_6^+	Γ_3^+	Γ_4^+	Γ_1^+	Γ_2^+	Γ_7^-	Γ_8^-	Γ_5^-	Γ_6^-	Γ_3^-	Γ_4^-	Γ_1^-	Γ_2^-
Γ_8^+	Γ_8^+	Γ_7^+	Γ_6^+	Γ_5^+	Γ_4^+	Γ_3^+	Γ_2^+	Γ_1^+	Γ_8^-	Γ_7^-	Γ_6^-	Γ_5^-	Γ_4^-	Γ_3^-	Γ_2^-	Γ_1^-
Γ_1^-	Γ_1^-	Γ_2^-	Γ_3^-	Γ_4^-	Γ_5^-	Γ_6^-	Γ_7^-	Γ_8^-	Γ_1^+	Γ_2^+	Γ_3^+	Γ_4^+	Γ_5^+	Γ_6^+	Γ_7^+	Γ_8^+
Γ_2^-	Γ_2^-	Γ_1^-	Γ_4^-	Γ_3^-	Γ_6^-	Γ_5^-	Γ_8^-	Γ_7^-	Γ_2^+	Γ_1^+	Γ_4^+	Γ_3^+	Γ_6^+	Γ_5^+	Γ_8^+	Γ_7^+
Γ_3^-	Γ_3^-	Γ_4^-	Γ_1^-	Γ_2^-	Γ_7^-	Γ_8^-	Γ_5^-	Γ_6^-	Γ_3^+	Γ_4^+	Γ_1^+	Γ_2^+	Γ_7^+	Γ_8^+	Γ_5^+	Γ_6^+
Γ_4^-	Γ_4^-	Γ_3^-	Γ_2^-	Γ_1^-	Γ_8^-	Γ_7^-	Γ_6^-	Γ_5^-	Γ_4^+	Γ_3^+	Γ_2^+	Γ_1^+	Γ_8^+	Γ_7^+	Γ_6^+	Γ_5^+
Γ_5^-	Γ_5^-	Γ_6^-	Γ_7^-	Γ_8^-	Γ_1^-	Γ_2^-	Γ_3^-	Γ_4^-	Γ_5^+	Γ_6^+	Γ_7^+	Γ_8^+	Γ_1^+	Γ_2^+	Γ_3^+	Γ_4^+
Γ_6^-	Γ_6^-	Γ_5^-	Γ_8^-	Γ_7^-	Γ_2^-	Γ_1^-	Γ_4^-	Γ_3^-	Γ_6^+	Γ_5^+	Γ_8^+	Γ_7^+	Γ_2^+	Γ_1^+	Γ_4^+	Γ_3^+
Γ_7^-	Γ_7^-	Γ_8^-	Γ_5^-	Γ_6^-	Γ_3^-	Γ_4^-	Γ_1^-	Γ_2^-	Γ_7^+	Γ_8^+	Γ_5^+	Γ_6^+	Γ_3^+	Γ_4^+	Γ_1^+	Γ_2^+
Γ_8^-	Γ_8^-	Γ_7^-	Γ_6^-	Γ_5^-	Γ_4^-	Γ_3^-	Γ_2^-	Γ_1^-	Γ_8^+	Γ_7^+	Γ_6^+	Γ_5^+	Γ_4^+	Γ_3^+	Γ_2^+	Γ_1^+

3.5. Effect of orientation of CCD on its molecular symmetry group

In this section we discuss the consequences of orienting the CCD molecule on its molecular symmetry group. Within the quantum dynamics simulations, the CCD-molecule is assumed to be oriented, i.e. the molecule-fixed Z-axis is pointing in the same direction as the space-fixed Z-axis. The molecular symmetry group of an isolated molecule is different from the molecular symmetry group of this molecule in a laser field. Watson [61, 62] showed that the molecular symmetry group is, in general, reduced in the presence of an electromagnetic field [25]. Spatial orientation of molecules can be achieved with electric fields [63].

The investigation of the effect of orientation of CCD on its molecular symmetry group G_{16}^{A} was done by T. Grohmann [64]. For molecules to be oriented, they interact via their permanent dipole moment with the laser pulse. The permanent dipole moment is not invariant under inversions [25]. Thus, permutation-inversions are no longer symmetry operations of the Hamiltonian. As a consequence, to classify the electronic and torsional states of an oriented CCD, the permutation subgroup of the molecular symmetry group G^{PSMS} of equation (3.4) should be used, instead of the molecular symmetry group G_{16}^{A}. Its character table is shown in Table 3.8. The eight IREPs of the G^{PSMS} can be used to classify the electronic and torsional states of CCD within the field.

3.6. Effects of the molecular symmetry operations on molecular configurations

The effects of the molecular symmetry operators on the nuclear coordinates of CCD are determined in this section. Figures 3.2 and 3.3 show the effect of the symmetry operations on the configuration of CCD, described by the torsional angles Φ_1 and Φ_2. For example, applying (12) on CCD causes Φ_1 to be rotated to $\pi + \Phi_1$, while Φ_2 remains the same. We notice that the associated radii $\mathcal{R}_1$ and $\mathcal{R}_2$ are not affected by (12). The Cartesian coordinates that are associated to Φ_1 are:

$$X_1 = \mathcal{R}_1 \cos \Phi_1 \tag{3.33}$$

and

$$Y_1 = \mathcal{R}_1 \sin \Phi_1. \tag{3.34}$$

Accordingly, (12) transforms X_1 to $-X_1$ and Y_1 to $-Y_1$ according to:

$$
\begin{aligned}
(12)X_1 &= (12)\mathcal{R}_1 \cos\Phi_1 \\
&= \mathcal{R}_1 \cos(\pi + \Phi_1) \\
&= \mathcal{R}_1(\cos\pi\cos\Phi_1 - \sin\pi\sin\Phi_1) \\
&= -\mathcal{R}_1 \cos\Phi_1 \\
&= -X_1 \qquad (3.35) \\
(12)Y_1 &= (12)\mathcal{R}_1 \sin\Phi_1 \\
&= \mathcal{R}_1 \sin(\pi + \Phi_1) \\
&= \mathcal{R}_1(\sin\pi\cos\Phi_1 + \cos\pi\sin\Phi_1) \\
&= -\mathcal{R}_1 \sin\Phi_1 \\
&= -Y_1 \qquad (3.36)
\end{aligned}
$$

Since Φ_2 is not affected by (12), the associated Cartesian coordinates X_2 and Y_2 remain unchanged (see Table 3.10 and Figure 3.3). Analogous considerations can be done for the other molecular symmetry operations to determine the effect on the associated Cartesian coordinates. The results are summarized in Table 3.10. The effects of all molecular symmetry operations $E, (12), \ldots, (12)(34)(56)^*$ on the polar coordinates $\mathcal{R}_1, \Phi_1, \mathcal{R}_2, \Phi_2$ and on their associated Cartesian coordinates X_1, Y_1, X_2 and Y_2 are listed in the second and the third rows of Table 3.10, respectively. The last row of this table gives graphical illustrations for the effects of these symmetry operations.

These results of the effects of the molecular symmetry operations on the nuclear coordinates of CCD, can be used to label the nuclear and electronic coordinates and their derivatives, as shown in Appendix A.3.

As it can be seen in Figure 3.2 and 3.3, there are always two symmetry operations leading to the same configuration. The reason is that the overall rotation (12)(34)(56) does not result in a different version of the molecule. As a consequence, each molecular configuration (G) exists in form of eight equivalent configurations. In section 4.1.1, this result will be applied in order to generate all equilibrium structures of CCD as well as to construct its PES.

The (electronic and nuclear) eigenstates of CCD can exist only in those IREPs where the pairs of symmetry operations shown in Figures 3.2 and 3.3, have the same character. Comparison with the character table of the molecular symmetry group G_{16}^A (Table 3.7), shows that those are the IREPs $\Gamma_1^{+/-}$, $\Gamma_4^{+/-}$, $\Gamma_6^{+/-}$ and $\Gamma_7^{+/-}$. Therefore, the eigenstates of oriented CCD, which transform according to the G^{PSMS} (Table 3.8) transform only according to Γ_1, Γ_4, Γ_6 and Γ_7.

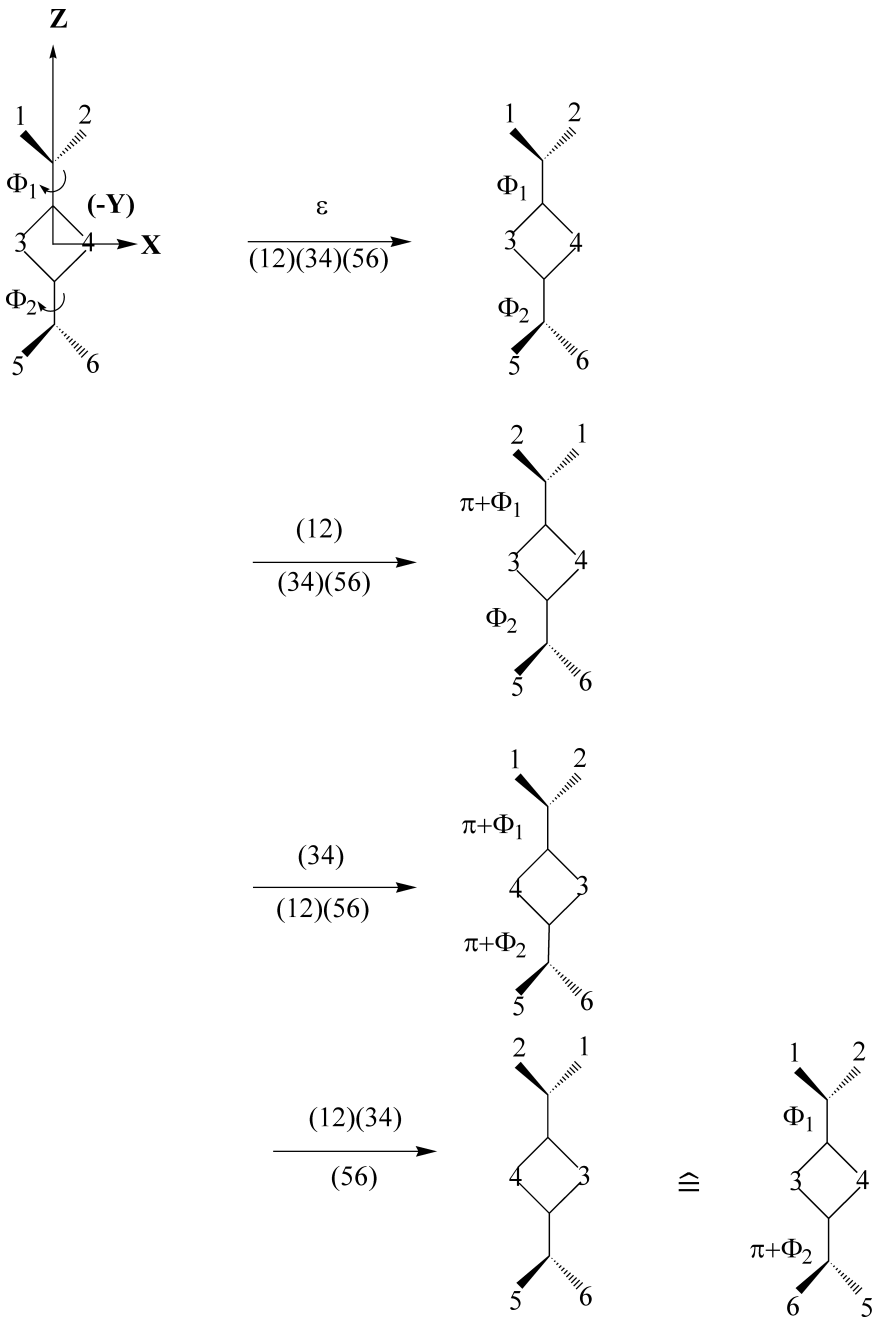

Figure 3.2.: Effects of the permutations of G_{16}^{A} on the polar coordinates of CCD. The right-handed-molecule-fixed-coordinate system is used.

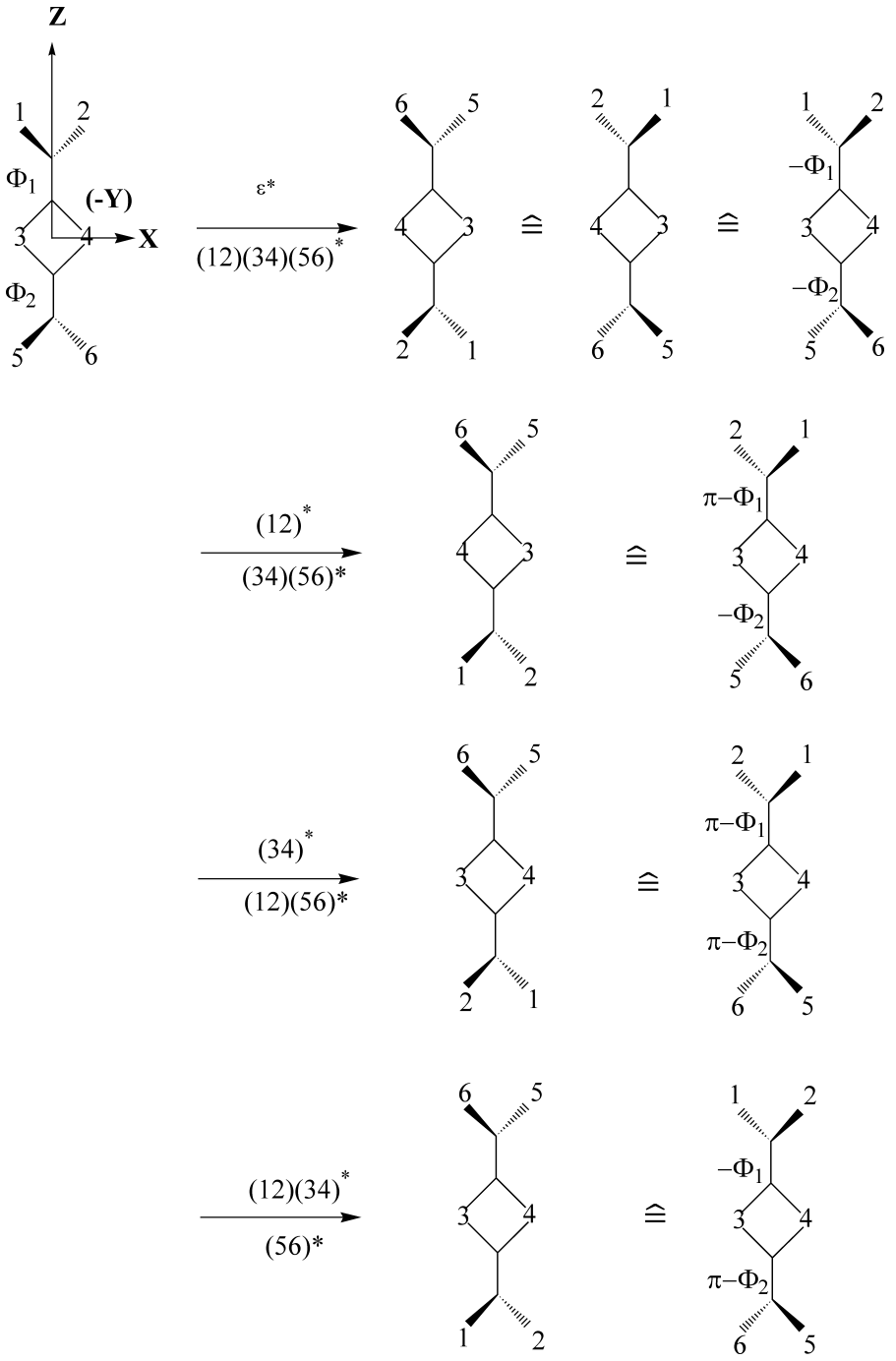

Figure 3.3.: Effects of the inversion and inversion-permutations of G_{16}^{A} on the polar coordinates of CCD. The right-handed-molecule-fixed-coordinate system is used.

Table 3.10.: Effects of the molecular symmetry operators of the molecular symmetry group G_{16}^{A} on the molecular symmetry adapted nuclear coordinates

G_{16}^{A}	$\mathcal{E}$ $(12)(34)(56)$	(12) $(34)(56)$	(34) $(12)(56)$	$(12)(34)$ (56)	$\mathcal{E}^{*}$ $(12)(34)(56)^{*}$	$(12)^{*}$ $(34)(56)^{*}$	$(34)^{*}$ $(12)(56)^{*}$	$(12)(34)^{*}$ $(56)^{*}$
$(\mathcal{R}_1, \Phi_1, \mathcal{R}_2, \Phi_2) \rightarrow$ $\mathcal{R}(\mathcal{R}_1, \Phi_1, \mathcal{R}_2, \Phi_2)$	$(\mathcal{R}_1, \Phi_1, \mathcal{R}_2, \Phi_2)$	$(\mathcal{R}_1, \pi +$ $\Phi_1, \mathcal{R}_2, \Phi_2)$	$(\mathcal{R}_1, \pi + \Phi_1,$ $\mathcal{R}_2, \pi + \Phi_2)$	$(\mathcal{R}_1, \Phi_1, \mathcal{R}_2,$ $\pi + \Phi_2)$	$(\mathcal{R}_1, -\Phi_1,$ $\mathcal{R}_2, -\Phi_2)$	$(\mathcal{R}_1, \pi - \Phi_1,$ $\mathcal{R}_2, -\Phi_2)$	$(\mathcal{R}_1, \pi - \Phi_1,$ $\mathcal{R}_2, \pi - \Phi_2)$	$(\mathcal{R}_1, -\Phi_1, \mathcal{R}_2,$ $\pi - \Phi_2)$
$(X_1, X_2, Y_1, Y_2) \rightarrow$ $\mathcal{R}(X_1, X_2, Y_1, Y_2)$	(X_1, X_2, Y_1, Y_2)	$(-X_1, X_2,$ $-Y_1, Y_2)$	$(-X_1, -X_2,$ $-Y_1, -Y_2)$	$(X_1, -X_2,$ $Y_1, -Y_2)$	$(X_1, X_2,$ $-Y_1, -Y_2)$	$(-X_1, X_2,$ $Y_1, -Y_2)$	$(-X_1, -X_2,$ $Y_1, Y_2)$	$(X_1, -X_2,$ $-Y_1, Y_2)$
symmetry related locations (X_1, Y_1) and (X_2, Y_2)		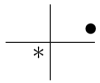	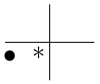	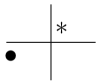		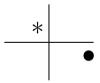	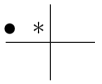	

Effects of the molecular symmetry operators on the polar coordinates and on their associated Cartesian coordinates of CCD are summarized in the second and the third rows of this table, respectively. The last row gives graphical illustrations for the effects of the symmetry operations on the polar coordinates and on their associated Cartesian coordinates of the molecular symmetry adapted nuclear coordinates of CCD.
$* = (X_1, Y_1)$
$\bullet = (X_2, Y_2)$

3.7. Labeling the nuclear spin isomers of CCD

The labelling of the nuclear spin isomers of CCD according to molecular symmetry is done taking into account [11] the symmetrization postulate [65], the permutation subgroup of the molecular symmetry group [25, 66] and the nuclear spin hypothesis [60, 67]. In the following, the molecular IREP (Γ_{mol}) is derived in a way that ensures that every molecular state must fulfill the symmetrization postulate. Subsequently, the symmetry of the nuclear spin states and the torsional states of CCD within the G^{PSMS} are determined.

First, the symmetrization postulate is employed. This states that every state of a quantum system must hold its sign if a pair of identical bosons is exchanged, and must change its sign if a pair of identical fermions is exchanged once. For this theorem to be applied, the spin quantum numbers of the nuclei that are exchanged should be determined. CCD has three types of nuclei, ^{1}H,^{12} C and ^{16}O, which carry the spins 1/2, 0 and 0, respectively. As a consequence, the nuclei ^{12}C and ^{16}O are bosons as they have an integer spin and the nuclei ^{1}H are fermions as they have half-integer spin. The group which is relevant for labeling the nuclear spin isomers of CCD is the permutation subgroup of the molecular symmetry group G^{A}_{16}, i.e. the group G^{PSMS} of equation (3.4), because the symmetrization postulate states nothing about permutation-inversion [60].

For the determination of Γ_{mol}, the transformation properties of the system's wavefunction under only the generators of G^{PSMS} are needed. For CCD these are the operations (12), (34) and (56). Thus,

$\mathcal{R}$	(12)	(34)	(56)
Ψ_{tot}	(-1)·Ψ_{tot}	(+1)·Ψ_{tot}	(+1)·Ψ_{tot}

(3.37)

where Ψ_{tot} was defined in equation (2.8). The transformation properties of Ψ_{tot} shown in equation (3.37), are due to the fact that (12) permutes one pair of fermionic nuclei, while (34) and (56) permute two pairs of fermionic nuclei. From the character table of G^{PSMS}, see Table 3.8, the characters -1, 1 and 1 of the generators (12), (34) and (56) are the ones for the IREP Γ_5, therefore,

$$\Gamma_{\text{mol}} = \Gamma_5, \tag{3.38}$$

for the CCD-molecule.

The next step for the determination of a nuclear spin isomer of a molecule based on the condition shown in equation (3.38), is to apply the nuclear spin hypothesis [67]. This hypothesis implies that the molecular state can be written as:

$$\Psi_{\text{tot}} \approx \Psi_{\text{rve}} \cdot \Psi_{\text{nu.sp.}}, \tag{3.39}$$

where Ψ_{rve} is the rovibronic wavefunction and $\Psi_{\text{nu.sp.}}$ is the nuclear spin wavefunction. The nuclear spin isomers of a system arises from different combinations of wavefunctions Ψ_{rve} and $\Psi_{\text{nu.sp.}}$ with the product of the two transforming according to Γ_{mol}. Clearly, this assumption is an approximation - due to intramolecular interactions of nuclear spins, nuclear spin isomers are not stable species on very long time scales. However, the time-scale of interconversion of nuclear spin isomers is much slower than the torsional dynamics, at least for closed shell systems [12, 65].

The use of molecular symmetry for identifying the symmetry of the nuclear spin states of a molecule is well described in the literature [25]. In order to identify the representation which is spanned by the entity of all nuclear spin states, the number of spin states which are invariant under a given operation of G^{PSMS} should be counted first. With this, the character of the representation $\Gamma_{\text{nu.sp.}}$ for the operation in question is determined. CCD has ten protons, each proton contributes two states, so it has in total $2^{10} = 1024$ spin states. All other nuclei do not posses any nuclear spin. If one applies:

- $\mathcal{E}$ to these states, then all states of all fragments remain unchanged. Thus $2^{10} = 1024$ states are invariant.

- (12) to these states, then all states of fragment 3 to 6 remain unchanged, as well as the $\alpha\alpha$ and $\beta\beta$ states of the dioxole-ring (segment (A)). Only the states $\alpha\beta$ and $\beta\alpha$ are interchanged. Thus, $2 \cdot 2^8 = 2^9 = 512$ states are invariant.

- (34) to these states, then all states of fragments 1, 2, 5 and 6 remain unchanged, in addition to the $\alpha\alpha$ and $\beta\beta$ states of the middle-ring (segment (B)). Consequently, $2 \cdot 2 \cdot 2^6 = 2^8 = 256$ states are invariant.

- (56) to these states, then all states of the fragments 1, 2, 3 and 4 remain unchanged, also the $\alpha\alpha$ and $\beta\beta$ states of the cyclopentadienyl-ring (segment (C)). Therefore, $2 \cdot 2 \cdot 2^6 = 2^8 = 256$ states are invariant.

- (12)(34) to these states, then all states of the fragments 5 and 6 remain unchanged, moreover, the $\alpha\alpha$ and $\beta\beta$ states of the dioxole and middle-rings are also unchanged. As a consequence, $2 \cdot 2 \cdot 2 \cdot 2^4 = 2^7 = 128$ states are invariant.

- (12)(56) to these states, then all states of the fragments 3 and 4 remain unchanged, like the $\alpha\alpha$ and $\beta\beta$ states of the dioxole and cyclopentadienyl-rings. This leads to $2 \cdot 2 \cdot 2 \cdot 2^4 = 2^7 = 128$ invariant states.

- (34)(56) to these states, then all states of the fragments 1 and 2 remain unchanged, also the $\alpha\alpha$ and $\beta\beta$ states of the middle and cyclopentadienyl-rings. This gives rise to $2 \cdot 2 \cdot 2 \cdot 2 \cdot 2^2 = 2^6 = 64$ invariant states.

- (12)(34)(56) to these states, then the $\alpha\alpha$ and $\beta\beta$ states of the three rings of CCD are unchanged, giving rise to $2 \cdot 2 \cdot 2 \cdot 2 \cdot 2 = 2^5 = 32$ invariant states.

The number of invariant spin states under the operations of G^{PSMS} are summarized as follows,

$\mathcal{R}$	$\mathcal{E}$	(12)	(34)	(56)	(12)(34)	(12)(56)	(34)(56)	(12)(34)(56)
$\Gamma_{\text{nu.sp.}}$	1024	512	256	256	128	128	64	32

(3.40)

The reduction of the above $\Gamma_{\text{nu.sp.}}$, by employing the projection operator into its irreducible components gives:

$$\Gamma_{\text{nu.sp.}} = 300 \cdot \Gamma_1 \oplus 180 \cdot \Gamma_2 \oplus 180 \cdot \Gamma_3 \oplus 108 \cdot \Gamma_4 \oplus 100 \cdot \Gamma_5 \oplus 60 \cdot \Gamma_6 \oplus 60 \cdot \Gamma_7 \oplus 36 \cdot \Gamma_8. \tag{3.41}$$

The result shown in equation (3.41) is pivotal, as it answers another question that has been asked in the Introduction, namely that it shows how to separate the 1024 nuclear spin eigenfunctions of CCD into sets that can be assigned to its eight nuclear spin isomers (we have only eight nuclear spin isomers, since we have only eight IREPS $\Gamma_1 - \Gamma_8$ for the G^{PSMS}, that are used for characterizing these nuclear spin isomers). Next, these nuclear spin states have to be combined with the torsional states, which will be explained later in this section, to fulfill equation (3.38).

A few aspects about the rotational and the vibronic states are worth to be mentioned before the torsional states are identified. Since CCD is a rigid molecule in the electronic ground state, the time scales of any contorsional (torsional and inversion) motion are much longer than the time scales on which molecular events typically take place. Therefore, the molecular state in the electronic ground state is assumed to be:

$$\Psi_{\text{tot}} \approx \Psi_{\text{rot}} \cdot \Psi_{\text{tor}} \cdot \Psi_{\text{vib}} \cdot \Psi_{\text{nu.sp.}} \cdot \Psi_e, \tag{3.42}$$

where the torsional motion (Ψ_{tor}) can be manipulated separately from the vibrational motion (Ψ_{vib}) and the rotational motion (Ψ_{rot}). The translational motion of the molecule is separated here from the internal motion. The molecular wavefunction excluding the translational motions is called by some authors the internal wavefunction [25], this discrimination is omitted in this thesis. Throughout this work, the temperature is assumed to be so low ($T \to 0$ K), so that only the lowest non-degenerate rovibronic state is populated. Thus, it transforms as the totally symmetric IREP:

$$\Psi_{\text{rot}} \cdot \Psi_{\text{vib}} \cdot \Psi_{\text{e}} \sim \Gamma_1. \tag{3.43}$$

Based on equation (3.43), different nuclear spin isomers are defined by:

$$\Gamma_{\text{tor}} \otimes \Gamma_{\text{nu.sp.}} = \Gamma_{\text{mol}}, \tag{3.44}$$

Different nuclear spin isomers are represented by different combinations of Γ_{tor} and $\Gamma_{\text{nu.sp.}}$ fulfilling equation (3.44).

What is left for defining the symmetry of the nuclear spin isomers is to find the symmetry of the torsional states. To do so, it is sufficient to find the symmetries of the basis functions $\Psi_{\mathcal{K}_{\Phi_1},\mathcal{K}_{\Phi_2}}(\Phi_1,\Phi_2)$.

$$\begin{aligned}\Psi_{\mathcal{K}_{\Phi_1},\mathcal{K}_{\Phi_2}}(\Phi_1,\Phi_2) &= \Psi_{\mathcal{K}_{\Phi_1}}(\Phi_1)\cdot\Psi_{\mathcal{K}_{\Phi_2}}(\Phi_2)\\ &= \frac{1}{2\pi}e^{(i\mathcal{K}_{\Phi_1}\Phi_1)}e^{(i\mathcal{K}_{\Phi_2}\Phi_2)},\end{aligned} \tag{3.45}$$

where $\mathcal{K}_{\Phi_{1/2}}$ is an integer, which is a multiplicative of π, i.e. $\mathcal{K}_{\Phi_{1/2}} = k\cdot\pi$ and $k\in\mathbb{Z}$. This is due to two facts: first, the true eigenfunctions can always be written as linear combinations of basis functions of the type of equation (3.45) and second, exact eigenfunctions can be composed exclusively of basis functions of the same symmetry [68]. Once the transformation properties of the angles Φ_1 and Φ_2 under the generators (12), (34) and (56) are known, the symmetry of the functions, shown in equation (3.45), in the group G^{PSMS} can be found. The transformations of the angles Φ_1 and Φ_2 under these operations are:

$\mathcal{R}$	(12)	(34)	(56)
Φ_1	$\pi+\Phi_1$	$\pi+\Phi_1$	Φ_1
Φ_2	Φ_2	$\pi+\Phi_2$	$\pi+\Phi_2$

(3.46)

and hence

$\mathcal{R}$	(12)	(34)	(56)
$\Psi_{\mathcal{K}_{\Phi_1}}$	$(-1)^{\mathcal{K}_{\Phi_1}}\cdot\Psi_{\mathcal{K}_{\Phi_1}}$	$(-1)^{\mathcal{K}_{\Phi_1}}\cdot\Psi_{\mathcal{K}_{\Phi_1}}$	$\Psi_{\mathcal{K}_{\Phi_1}}$
$\Psi_{\mathcal{K}_{\Phi_2}}$	$\Psi_{\mathcal{K}_{\Phi_2}}$	$(-1)^{\mathcal{K}_{\Phi_2}}\cdot\Psi_{\mathcal{K}_{\Phi_2}}$	$(-1)^{\mathcal{K}_{\Phi_2}}\cdot\Psi_{\mathcal{K}_{\Phi_2}}$

. (3.47)

Then, it is concluded that, for example, if $\mathcal{K}_{\Phi_1}$ and $\mathcal{K}_{\Phi_2}$ are even then the basis function $\Psi_{\mathcal{K}_{\Phi_1},\mathcal{K}_{\Phi_2}}(\Phi_1,\Phi_2)$ will have the characters $+1$, $+1$ and $+1$ under the generators (12), (34) and (56), respectively, according to equation 3.47. This is only fulfilled for the IREP Γ_1, as shown in Table 3.8. All the other possibilities for $\mathcal{K}_{\Phi_1}$ and $\mathcal{K}_{\Phi_2}$ are summarized in equation 3.48. Depending on these different possibilities, the effect on the character of the associated basis function under the generators (12),

(34) and (56) is determined. By comparing these resulting characters for the basis functions with the characters of the eight IREPs shown in the character table of the G^{PSMS}, one can determine the IREP for each basis function, as summarized in the equation below,

$$\Psi_{\mathcal{K}_{\Phi_1},\mathcal{K}_{\Phi_2}}(\Phi_1,\Phi_2) \sim \begin{cases} \Gamma_1 & \text{if } \mathcal{K}_{\Phi_1} \text{ even} & \text{and } \mathcal{K}_{\Phi_2} \text{ even} \\ \Gamma_4 & \text{if } \mathcal{K}_{\Phi_1} \text{ even} & \text{and } \mathcal{K}_{\Phi_2} \text{ odd} \\ \Gamma_7 & \text{if } \mathcal{K}_{\Phi_1} \text{ odd} & \text{and } \mathcal{K}_{\Phi_2} \text{ even} \\ \Gamma_6 & \text{if } \mathcal{K}_{\Phi_1} \text{ odd} & \text{and } \mathcal{K}_{\Phi_2} \text{ odd} \end{cases} . \tag{3.48}$$

Equation (3.48) proves that only four ($\Gamma_1, \Gamma_4, \Gamma_6$ and Γ_7) out of eight ($\Gamma_1 - \Gamma_8$) nuclear spin isomers "survive" as T $\rightarrow$ 0 K. A sketch of the sign pattern for these four torsional eigenfunctions is shown in Figure 3.4. In Figure 3.4 the characters of the torsional eigenfunctions, labelled with $\Gamma_1, \Gamma_4, \Gamma_6$ and Γ_7, under the generators (12), (34) and (56) are shown. This brings to mind Heisenberg's and Hund's example of molecular hydrogen, where just one out of two nuclear spin isomers of hydrogen, para-hydrogen, "survives" as T$\rightarrow$ 0 K.

For identifying the symmetry of the nuclear spin isomers of CCD, the last needed step is to combine the torsional eigenstates with the IREPs $\Gamma_1, \Gamma_4, \Gamma_6, \Gamma_7$, equation (3.48), with the nuclear spin states, equation (3.41), to fulfill equation (3.37). With the help of the direct product table of G^{PSMS}, which is obtained from the 8×8 entries in the top left of Table 3.9, without the labels "+", the correct combinations of torsional and nuclear spin states can be easily found. For CCD the combinations $\Gamma_{\text{tor}}[\Gamma_{\text{nu.sp.}}]$ give rise to the four nuclear spin isomers,

$$\begin{array}{ll} \Gamma_1[\Gamma_5] & \text{(100 nuclear spin states)} \\ \Gamma_4[\Gamma_8] & \text{(36 nuclear spin states)} \\ \Gamma_6[\Gamma_2] & \text{(180 nuclear spin states)} \\ \Gamma_7[\Gamma_3] & \text{(180 nuclear spin states)} \end{array} , \tag{3.49}$$

where the number of spin states seen in equation (3.49), are obtained from equation (3.41).

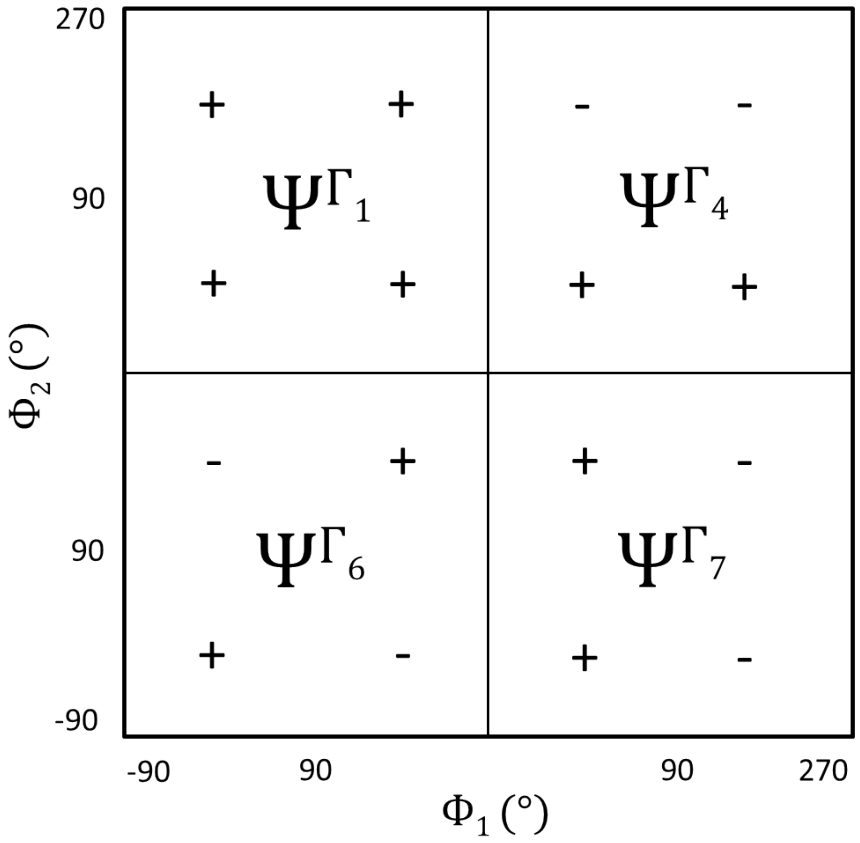

Figure 3.4.: A sketch of the sign pattern for the four lowest torsional eigenfunctions with their irreducible representations $\Gamma_1, \Gamma_4, \Gamma_6$ and Γ_7.

4. Quantum chemistry and quantum dynamics

In this chapter, we present the results of the quantum chemical calculations that deliver the PESs of the low-lying electronic states. On these calculated PESs, quantum dynamics simulations are performed, allowing for the investigation of the torsional dynamics of the four different nuclear spin isomers of CCD, see Section 4.2. These nuclear spin isomers are expected to be discriminated through their torsional dynamics, due to the different sign patterns involved in each, recall Figure 3.4. The reason behind using the quantum dynamics method is that it can describe quantum effects, in particular constructive and/or destructive interferences.

Since the propagation of the wavepackets requires PES, this chapter starts with the quantum chemistry part that involves the calculation of the lowest low-lying singlet electronic states along the two torsional angles Φ_1 and Φ_2, with an explanation of the level of theory, the active space and the basis set that are employed for these calculations (Section 4.1). In the same section, the one-electron properties, like the non-adiabatic coupling terms (NACTs), the transition d_{ij} and the permanent d_{ii} dipole moments are presented.

Section 4.2 demonstrates how the torsional dynamics of the nuclear spin isomers differs and particular differences in the expectation values of some operators are suggested to be used experimentally to discriminate these nuclear spin isomers.

4.1. Quantum chemistry

To calculate the PESs along the two torsional degrees of freedom Φ_1 and Φ_2 for the singlet electronic ground and the lowest excited states of $\pi\pi^*$ character, we used the state-averaged complete active space self consistent field (SA-CASSCF) level of theory. The reason for choosing the CASSCF level of theory is that this is a multi-configurational method that allows for the description of biradicals and zwitter-ionic structures, which are included in the electronic states of CCD (as it will be shown below). The basis set employed is the Dunning type correlation corrected double zeta basis set cc-pVDZ [69].

To calculate the PESs of CCD along the two torsional angles Φ_1 and Φ_2, we need first to calculate the "first" equilibrium structure of the S_0 state, which was done by our partners in Israel [70]. This equilibrium structure is considered as the "first" equilibrium structure becuase we have other equilibrium structures which were created by applying molecular symmetry generators on this equilibrium structure, as will be explained in subsection 4.1.1.

We need first to define the active space for the CASSCF method. To do so, chemical intuition should be employed. Within this work, we were interested in the investigation of the torsional dynamics of the nuclear spin isomers using the two degrees of freedom Φ_1 and Φ_2. Thus, our simulations involve rotating around the two exocyclic double bonds that connect the middle ring to the other two rings. Consequently, only π-orbitals should be included in the active space. For CCD, we have 16 atoms, each with a P_Z-orbital, so it has 16 π- and π^*-orbitals. Thus, CCD has 18 electrons as each P_Z-orbital on a carbon contributes one electron, while each P_Z-orbital on an oxygen contributes two electrons. This means that we need 18 electrons in 16 orbitals to include the full π-space of CCD. Since this active space is computationally demanding, smaller active spaces were tested: (16,14), (14,12) and (12,10) that exclude one, two and three pair/s of π and the corresponding π^* orbitals, respectively. The excluded π^*-orbitals are those which are not included in the description of the excitation of any of the two exocyclic double bonds.

In Table 4.1, the vertical excitation energies of CCD calculated with the above mentioned active spaces (12,10), (14,12) and (16,14), with the SA5-CASSCF(n, m)/cc-pVDZ level of theory, where n is the number of electrons distributed in m molecular orbitals is presented. The relative energies, E_{rel}, (compared to S_0) together with the squared coefficients of the main configuration state functions (CSFs), labeled according to their corresponding molecular orbitals, which are shown in Figure 4.1, are listed.

As it can be seen any of the three active spaces (12,10), (14,12) and (16,14), provides almost the same relative energy for each state. The associated CSFs that describe each state are also the same. Therefore, the active space (12,10) is selected, as it is found to be the most efficient for the reduction of the computational costs while still having a precise description of CCD.

Being the active space decided, we need to determine the number of states that should be included in the SA-CASSCF calculations. This issue was investigated by doing several calculations with different number of states, i.e. three, four and five states were considered. Table 4.2 collects the vertical excitation energies of CCD calculated with different number of states, $\mathcal{N} = 3$, 4 and 5, with SA$\mathcal{N}$-CASSCF(12,10)/cc-pVDZ level of theory. For the SA4-CASSCF(12,10) level of theory, the oscillator strengths f are calculated.

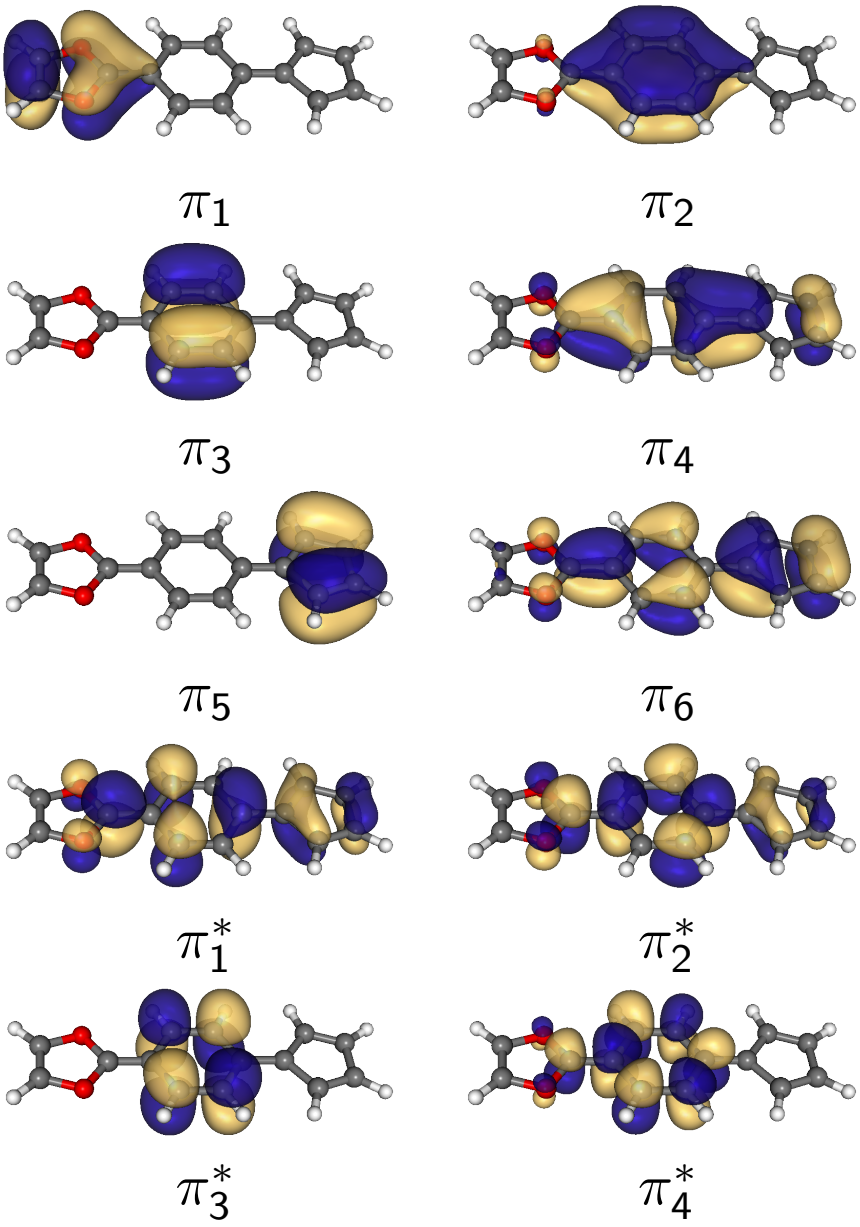

Figure 4.1.: The orbitals of the active space using the SA4-CASSCF(12,10)/cc-pVDZ level of theory for CCD. All of these orbitals are of either π or π^* character.

Table 4.1.: Vertical excitation energies of CCD calculated at SA5-CASSCF(n,m) /cc-pVDZ level of theory, where n is the number of electrons distributed in m molecular orbitals. The relative energies, E_{rel}, (compared to S_0) are shown for the electronic states S_0, S_1, S_2, S_3 and S_4 together with the squared coefficients of the main configuration state functions, C_i^2 (labeled according to their corresponding molecular orbitals, see Figure 4.1).

	CASSCF(12,10)		CASSCF(14,12)		CASSCF(16,14)	
State	E_{rel} (eV)	C_i^2	E_{rel} (eV)	C_i^2	E_{rel} (eV)	C_i^2
S_0	0.00	0.67 $(\pi_6)^2$	0.00	0.64 $(\pi_6)^2$	0.00	0.59 $(\pi_6)^2$
		0.17 $(\pi_6)^1(\pi_1^*)^1$		0.16 $(\pi_6)^1(\pi_1^*)^1$		0.18 $(\pi_6)^1(\pi_1^*)^1$
S_1	3.40	0.73 $(\pi_5)^1(\pi_1^*)^1$	3.40	0.70 $(\pi_5)^1(\pi_1^*)^1$	3.41	0.64 $(\pi_5)^1(\pi_1^*)^1$
S_2	4.42	0.32 $(\pi_6)^0(\pi_1^*)^2$	4.43	0.30 $(\pi_6)^0(\pi_1^*)^2$	4.42	0.26 $(\pi_6)^0(\pi_1^*)^2$
		0.19 $(\pi_6)^1(\pi_2^*)^1$		0.19 $(\pi_6)^1(\pi_2^*)^1$		0.18 $(\pi_6)^1(\pi_2^*)^1$
		0.18 $(\pi_4)^1(\pi_1^*)^1$		0.17 $(\pi_4)^1(\pi_1^*)^1$		0.16 $(\pi_4)^1(\pi_1^*)^1$
S_3	4.87	0.58 $(\pi_6)^1(\pi_1^*)^1$	4.92	0.55 $(\pi_6)^1(\pi_1^*)^1$	4.97	0.47 $(\pi_6)^1(\pi_1^*)^1$
		0.17 $(\pi_6)^2$		0.17 $(\pi_6)^2$		0.18 $(\pi_6)^2$
S_4	5.18	0.36 $(\pi_6)^1(\pi_3^*)^1$	5.18	0.34 $(\pi_6)^1(\pi_3^*)^1$	5.16	0.37 $(\pi_6)^1(\pi_3^*)^1$

Table 4.2.: Vertical excitation energies of CCD calculated at SA$\mathcal{N}$-CASSCF(12,10) /cc-pVDZ level of theory, where $\mathcal{N}$ is the number of states included in the state averaging. The relative energies, E_{rel}, (compared to S_0) are shown for the electronic states S_0, S_1, S_2, S_3 and S_4 together with the squared coefficients of the main configuration state functions C_i^2 (labeled according to their corresponding molecular orbitals, see Figure 4.1).The oscillator strengths f are calculated for the SA4-CASSCF(12,10) level of theory.

	SA3-CASSCF		SA4-CASSCF			SA5-CASSCF	
State	E_{rel} (eV)	C_i^2	E_{rel} (eV)	C_i^2	f	E_{rel} (eV)	C_i^2
S_0	0.00	0.75 $(\pi_6)^2$	0.00	0.64 $(\pi_6)^2$		0.00	0.67 $(\pi_6)^2$
				0.21 $(\pi_6)^1(\pi_1^*)^1$			0.17 $(\pi_6)^1(\pi_1^*)^1$
S_1	3.24	0.74 $(\pi_5)^1(\pi_1^*)^1$	3.35	0.80 $(\pi_5)^1(\pi_1^*)^1$	0.002	3.40	0.73 $(\pi_5)^1(\pi_1^*)^1$
S_2	4.42	0.36 $(\pi_6)^0(\pi_1^*)^2$	4.45	0.36 $(\pi_6)^0(\pi_1^*)^2$	0.001	4.42	0.32 $(\pi_6)^0(\pi_1^*)^2$
		0.21 $(\pi_4)^1(\pi_1^*)^1$		0.19 $(\pi_4)^1(\pi_1^*)^1$			0.19 $(\pi_6)^1(\pi_2^*)^1$
		0.19 $(\pi_6)^1(\pi_2^*)^1$		0.17 $(\pi_6)^1(\pi_2^*)^1$			0.18 $(\pi_4)^1(\pi_1^*)^1$
S_3			4.84	0.55 $(\pi_6)^1(\pi_1^*)^1$	1.595	4.87	0.58 $(\pi_6)^1(\pi_1^*)^1$
				0.21 $(\pi_6)^2$			0.17 $(\pi_6)^2$
S_4						5.18	0.36 $(\pi_6)^1(\pi_3^*)^1$

Close inspection of Table 4.2 reveals that with the SA3-CASSCF level of theory the electronic ground state S_0 is pure, as it is composed of mainly the closed-shell CSF, that we label with $(\pi_6)^2$. In contrast, with the SA4-CASSCF and SA5-CASSCF the S_0 has two main CSFs, $(\pi_6)^2$ and $(\pi_6)^1(\pi_1^*)^1$, which are then also the two major CSFs of S_3. These two CSFs are consistent with the push-pull property of CCD, i.e. the competing quinoid and zwitter-ionic, aromatic, structure of CCD in S_0 state. Both the S_0 and S_3 states are sharing the same two main CSFs, $(\pi_6)^2$ and

$(\pi_6)^1(\pi_1^*)^1$, pointing to a mixing between these two states. This mixing nominates the S_3 state to be the bright spectroscopic state, as it can be confirmed by the oscillator strengths. The oscillator strengths using SA4-CASSCF(12,10) level of theory for the states S_1, S_2 and S_3 are then found to be 0.002, 0.001 and 1.595, respectively, as in Table 4.2. Accordingly, S_1 and S_2 states are spectroscopically dark, while S_3 is a very bright spectroscopic state, in agreement with the fact that the S_0 and S_3 mixes, as mentioned above.

Accordingly, the SA3-CASSCF level of theory does not give a good description of S_0, so using this level of theory was avoided. Instead, one should use either the SA4-CASSCF or SA5-CASSCF level of theory. Since the relative energy of each of the states S_0, S_1, S_2 and S_3 is almost the same in both cases and the type and number of the CSFs that describe each state are also the same, both levels of theory give almost the same qualitative picture. The advantage of the SA4-CASSCF level of theory is that it is computationally less demanding. Therefore, the SA4-CASSCF level of theory was selected.

Using the equilibrium geometry and the SA4-CASSCF(12,10) level of theory, the torsional angle Φ_1 was varied from -90° to 90° and the torsional angle Φ_2 from 0° to 90°, both with a step size of 5°, to provide a scan of the two-dimensional PESs of the four lowest singlet electronic states using C_1 symmetry. All other degrees of freedom are kept frozen at the equilibrium geometry. To ensure the consistency of the active space, we used the fully converged CASSCF wavefunction of the previous step as an initial guess for the next step and we carefully checked several one electron properties like the NACTs, transition dipole moments and permanent dipole moments. MOLPRO2012 program package [71] was employed for all of these calculations. We performed 703 calculations, which result from 37 points along Φ_1 and 19 points along Φ_2. Using the symmetry generators explained in the next section the full PES along the two torsional angles running from -90° to 270° was generated.

4.1.1. Generation of all equivalent equilibrium structures and of the PESs of CCD

The "first" equilibrium structure of CCD has a C_{2v} point group, i.e. it has a C_2 symmetry axis and it is planar. This C_2-axis is assumed to be oriented along the laboratory Z-axis, see Section 3.5.

The PESs for the lowest four singlet electronic states were calculated using quantum chemistry, as explained earlier in this section. Molecular symmetry plays an important role in the reduction of the computational costs, due to the sufficiency of carrying out those rather expensive evaluations of the PESs of the lowest four singlet electronic states in a domain which is as small as possible, close to the

"first" equilibrium structure, and to generate the rest of the PESs for those states in complementary domains by employing the operations of molecular symmetry. To do so, the following domains (in $^\circ$ units) shown in Figure 4.2 are defined:

- domain Ia: $-90 \leq \Phi_1 < 90$, $0 \leq \Phi_2 < 90$.
- domain Ib: $-90 \leq \Phi_1 < 90$, $-90 \leq \Phi_2 < 0$.
- domain I: $-90 \leq \Phi_1 < 90$, $-90 \leq \Phi_2 < 90$.
- domain II: $90 \leq \Phi_1 < 270$, $-90 \leq \Phi_2 < 90$.
- domain III: $90 \leq \Phi_1 < 270$, $90 \leq \Phi_2 < 270$.
- domain IV: $-90 \leq \Phi_1 < 90$, $90 \leq \Phi_2 < 270$.

The domain Ia is added to the domain Ib to compose the domain I, surrounding the "first" equilibrium structure. Practically the domain Ia, neighboring to the "first" equilibrium structure located at the point $(0, 0)$ is the only domain that is calculated by quantum chemistry.

Applying the molecular symmetry operators $\mathcal{E}, (12), (34), \ldots, (12)(34)(56)^*$ of the molecular symmetry group G_{16}^A to the "first" equilibrium structure (G_{eq_1}), see equations (3.11) and (3.12), generates the complete set of all equivalent equilibrium structures of CCD. The transformation properties of the two torsional angles, see equation (3.46), afford four equivalent equilibrium structures, which are characterized by the torsional angles $(\Phi_{1,G_{eq_l}}, \Phi_{2,G_{eq_l}}) = (0, 0), (180, 0), (180, 180)$ and $(0, 180)$ for $l = 1, 2, 3, 4$, respectively, see Figure 4.2. Applying the generators (12), (34) and (56) of G_{16}^A to (0,0) generates then the set of equilibrium structures $(180, 0), (180, 180)$ and $(0, 180)$.

In the same way, the application of the inversion $\mathcal{E}^*$ on the PES of the S_0 state ($V_0(\Phi_1, \Phi_2)$) in the domain Ia produces $V_0(\Phi_1, \Phi_2)$ in the domain Ib, leading to get $V_0(\Phi_1, \Phi_2)$ in the domain I, as shown in Figure 4.2, which surrounds the G_{eq_1}. In order to get $V_0(\Phi_1, \Phi_2)$ in the domains II, III and IV, that surrounds the equilibrium structures $(180, 0), (180, 180)$ and $(0, 180)$, the generators (12), (34) and (56) of G_{16}^A are applied on $V_0(\Phi_1, \Phi_2)$ in the domain I, see Figure 4.2. Following these symmetry rules, the full $V(\Phi_1, \Phi_2)$, i.e. from -90° to 270°, for the four lowest singlet electronic states S_0, S_1, S_2 and S_3 are obtained, as shown in Figures 4.3 - 4.6, respectively.

For example, Figure 4.3 shows the resulting $V_0(\Phi_1, \Phi_2)$ for arbitrary torsional angle with four equivalent potential wells, which are centered at the equilibrium structures (0,0) - $(0, 180)$. These potential wells are separated from each other by potential barriers. The potential barriers for torsions along Φ_1 are higher than those for torsions along Φ_2. The $V_0(\Phi_1, \Phi_2)$ has cyclic boundaries for the torsions

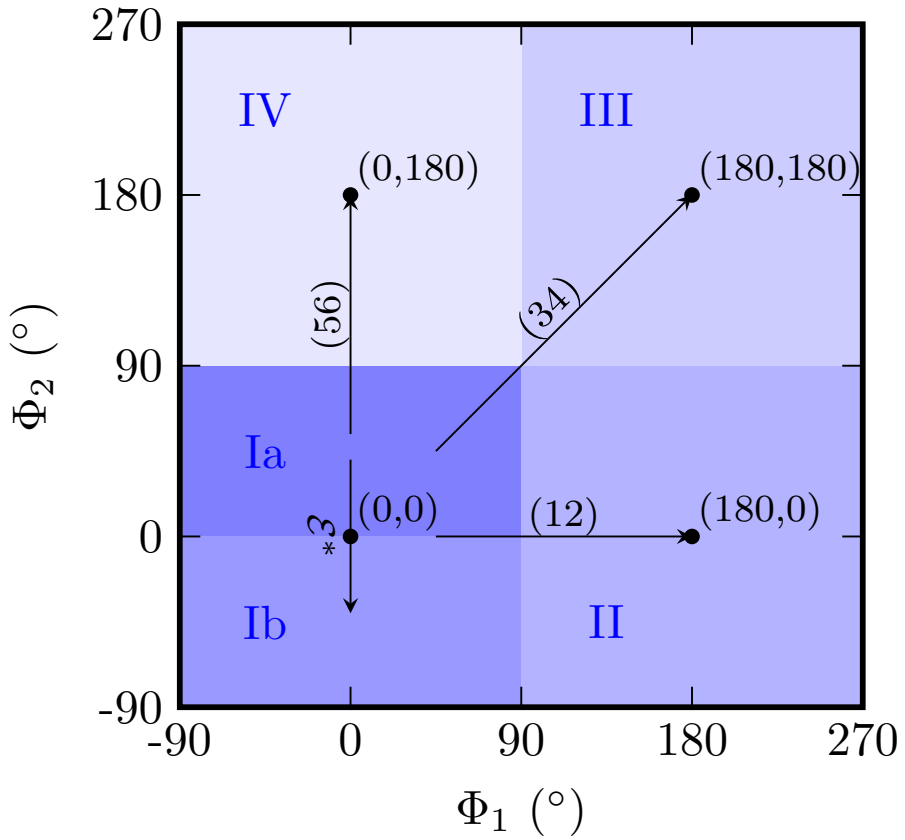

Figure 4.2.: A scheme for generating three equivalent equilibrium structures located at $(180, 0)$, $(180, 180)$ and $(0, 180)$ of CCD by application of the generators (12), (34) and (56) of the molecular symmetry group G_{16}^{A} to the "first" equilibrium structure located at (0, 0). Moreover, a scheme for generating $V_0(\Phi_1, \Phi_2)$ in the domain Ib by application of the generator $\mathcal{E}^*$ in the domain Ia. Subsequently, application of the generators (12), (34) and (56) to $V_0(\Phi_1, \Phi_2)$ in the domain I to get it in the domains II, III and IV, respectively.

along Φ_1 or Φ_2, allowing cyclic extensions of $V_0(\Phi_1, \Phi_2)$ to arbitrary torsional angles, even beyond the domain shown in Figure 4.3. Based on the molecular symmetry group G_{16}^{A}, $V_0(\Phi_1, \Phi_2)$ is invariant with respect to the application of the generators (12), (34), (56) and $\mathcal{E}^*$, corresponding to the mappings $V_0(\Phi_1, \Phi_2) \rightarrow V_0(\Phi_1+180, \Phi_2), V_0(\Phi_1+180, \Phi_2+180), V_0(\Phi_1, \Phi_2+180)$ and $V_0(-\Phi_1, -\Phi_2)$, respectively. One may think when looking at Figure 4.3 that there is additional symmetries, e.g. the abscissa and ordinates ($\Phi_2 = 0$ and $\Phi_1 = 0$) appear as symmetry lines for reflection, but close inspection reveals that $V_0(\Phi_1, \Phi_2) \neq V_0(-\Phi_1, \Phi_2)$ and $V_0(\Phi_1, \Phi_2) \neq V_0(\Phi_1, -\Phi_2)$. The reason is that the mappings $(\Phi_1, \Phi_2) \rightarrow (-\Phi_1, \Phi_2)$ or $(\Phi_1, \Phi_2) \rightarrow (\Phi_1, -\Phi_2)$ are not included in any of the molecular symmetry group operators of G_{16}^{A}.

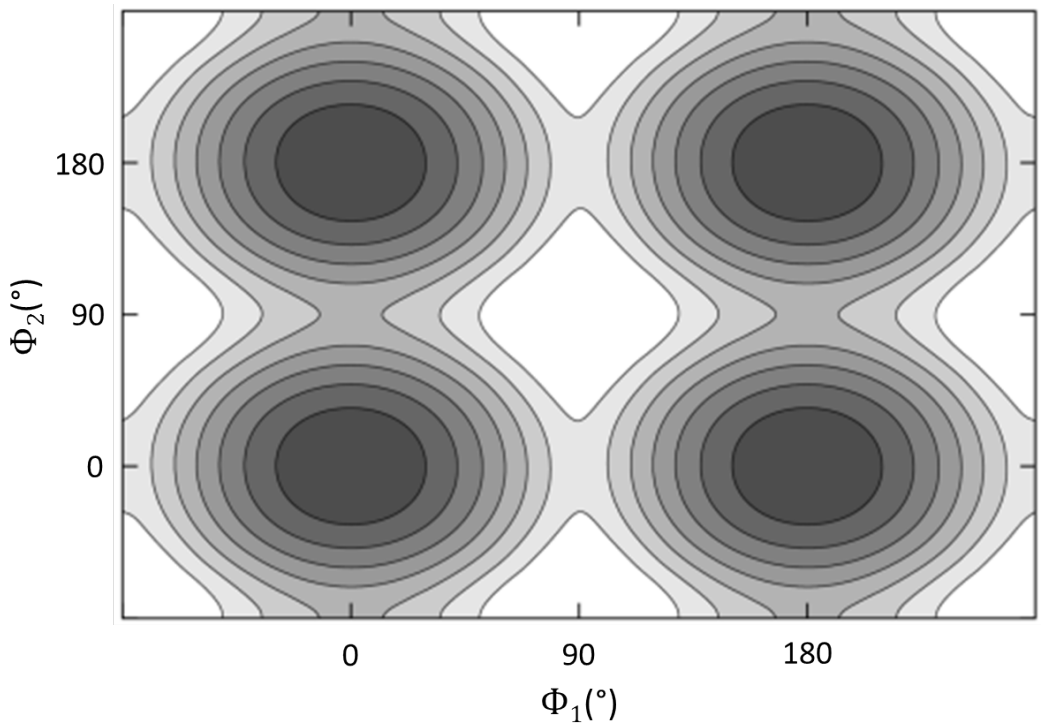

Figure 4.3.: A contour plot of the PES of the S_0 state ($V_0(\Phi_1, \Phi_2)$). The contours are drawn for $V_0(\Phi_1, \Phi_2)$ = (0.4, 0.8, 1.2, 1.6, 2.0, 2.4 and 2.8) eV

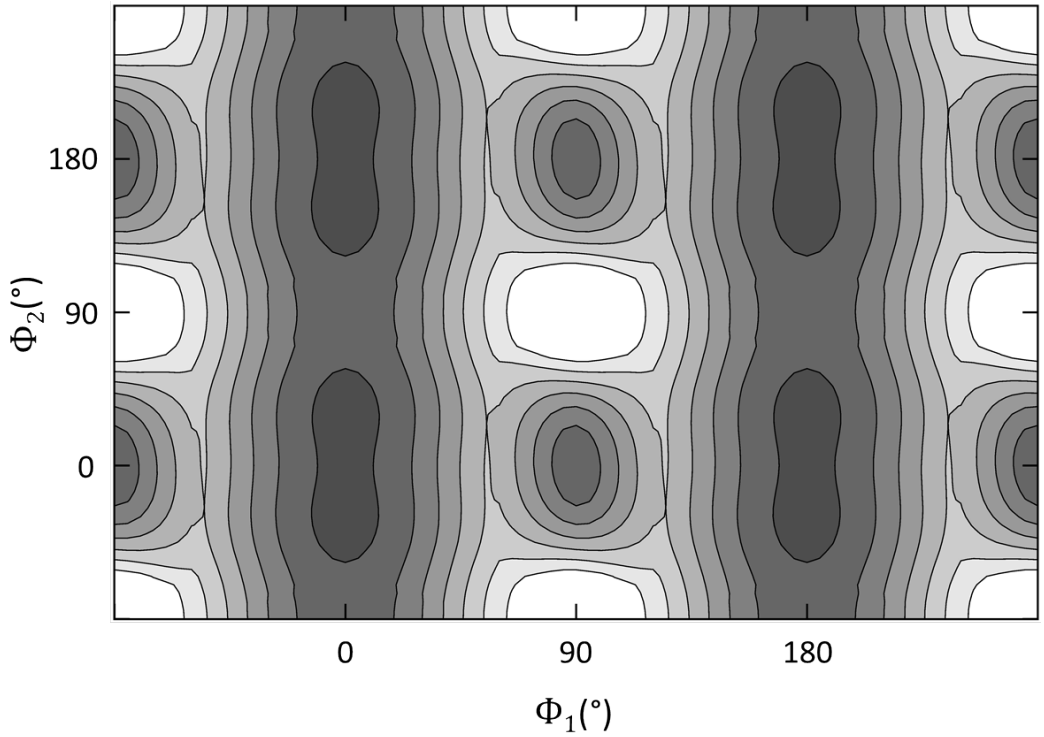

Figure 4.4.: A contour plot of the PES of the S_1 state ($V_1(\Phi_1, \Phi_2)$). The contours are drawn for $V_1(\Phi_1, \Phi_2)$ = (3.4, 3.6, 3.8, 4.0, 4.2, 4.4 and 4.6) eV

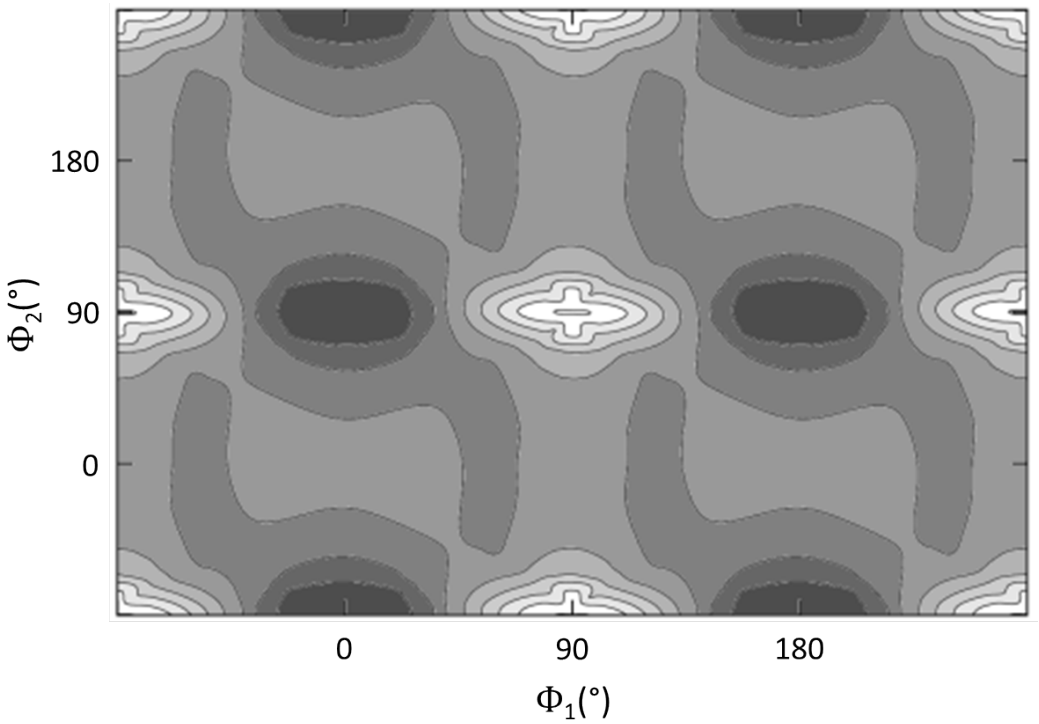

Figure 4.5.: A contour plot of the PES of the S_2 state ($V_2(\Phi_1, \Phi_2)$). The contours are drawn for $V_2(\Phi_1, \Phi_2)$ = (4.0, 4.2, 4.4, 4.6, 4.8, 5.0, 5.2 and 5.4) eV

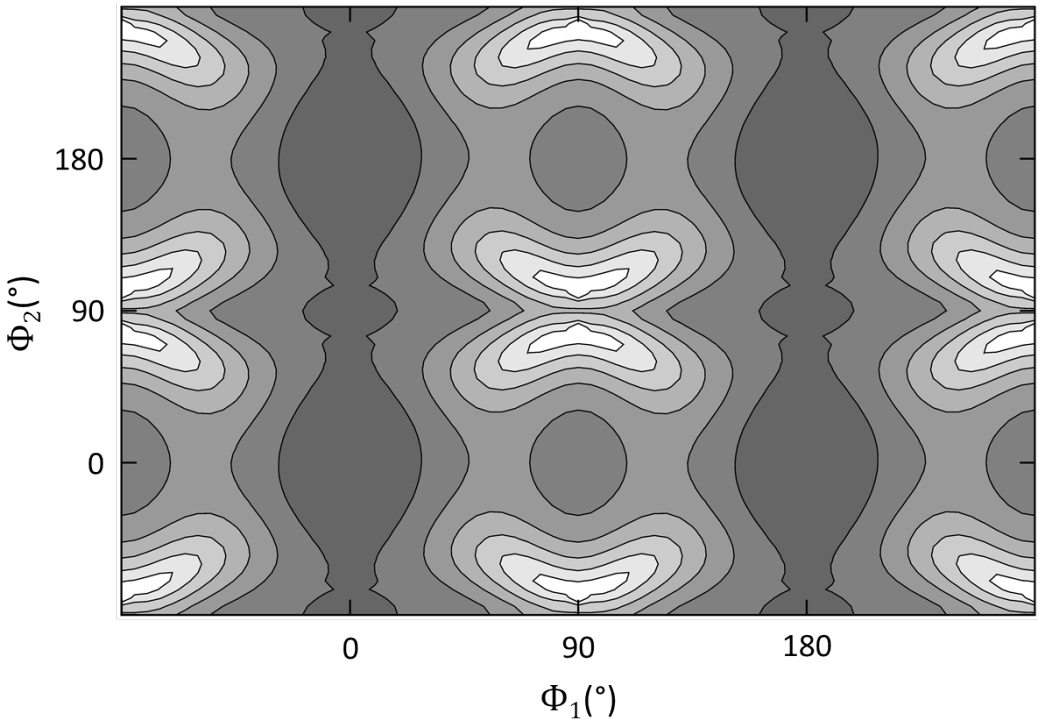

Figure 4.6.: A contour plot of the PES of the S_3 state ($V_3(\Phi_1, \Phi_2)$). The contours are drawn for $V_3(\Phi_1, \Phi_2)$ = (5.0, 5.2, 5.4, 5.6, 5.8 and 6.0) eV

4.1.2. Topology of the PESs and one-electron properties of CCD

Two cuts of the adiabatic unrelaxed two-dimensional PESs along Φ_1 with $\Phi_2 = 0°$ and Φ_2 with $\Phi_1 = 0°$, respectively, together with their corresponding permanent dipole moments and kinetic coupling elements, are shown in Figure 4.7(a-f). The two cuts are symmetric with respect to the 90° axis and periodic with a period of 360°, due to the symmetry of the molecule. Hence, the ground state S_0 has four equivalent minima. Two of them are located at $\Phi_1 = 0°$ and 180°, with $\Phi_2 = 0°$, while the other two equivalent minima are located at $\Phi_1 = 0°$ and 180° with $\Phi_2 = 180°$. The four equivalent minima are separated by a potential barrier of 2.68 eV along Φ_1 and by a barrier of 1.94 eV along Φ_2, see Figure 4.7(a-b).

A close inspection of Figure 4.7(a), which shows the first one dimensional cut along Φ_1 reveals that the states S_1 and S_2 come very close to each other at four positions, $\Phi_1 = -55°, 55°, 125°$ and 235°, while $\Phi_2 = 0°$ for each. This indicates an avoided crossing between these two states at these four positions. If a crossing between these two states takes place then the character of each of these two states should change along Φ_1. To check whether the character of any of these four states changes, we calculated the permanent dipole moments for the lowest four states (d_{00}, d_{11}, d_{22} and d_{33}). Since CCD is oriented along the Z-axis and it has two oxygen atoms on the upper five-membered ring, recall Figure 1.4, the highest permanent dipole moment component is along its Z-component, which is shown in Figure 4.7(c). The $d_{00,z}$ and $d_{33,z}$ curves are smooth, see Figure 4.7(c). This means that the character of the relevant states does not change i.e. neither S_0 nor S_3 crosses with any of the other three states. The $d_{11,z}$ and $d_{22,z}$ curves contrary to $d_{00,z}$ and $d_{33,z}$ curves are not smooth, see Figure 4.7(c); a sudden jump is seen in these two curves at the Φ_1 values mentioned above. This means that both S_1 and S_2 change their characters, indicating a crossing between S_1 and S_2 along this one dimensional cut of the PESs along Φ_1, see Figure 4.7(a). This change of the character of these two states is also seen in the transition dipole moments $d_{01,z}$ and $d_{02,z}$, as shown in Figure 4.7(g). A sudden jump at these crossing points takes place in the $d_{01,z}$ and $d_{02,z}$ curves, emphasizing the crossing between these two states.

Along the other one-dimensional cut along Φ_2, with $\Phi_1 = 0°$ in Figure 4.7(b), the states S_1 and S_2 come close to each other at Φ_2 values of $-90°, 90°$ and 270°, but their curves do not touch each other implying no avoided crossing at these points. We calculated the permanent dipoles along Φ_2, as we did along Φ_1, to check whether the character of any of the four states changes. The curves for $d_{00,z}$, $d_{11,z}$, $d_{22,z}$ and $d_{33,z}$ are all smooth, see Figure 4.7(d), i.e. the character of each of the four states does not change, pointing to no crossing between the states. The transition

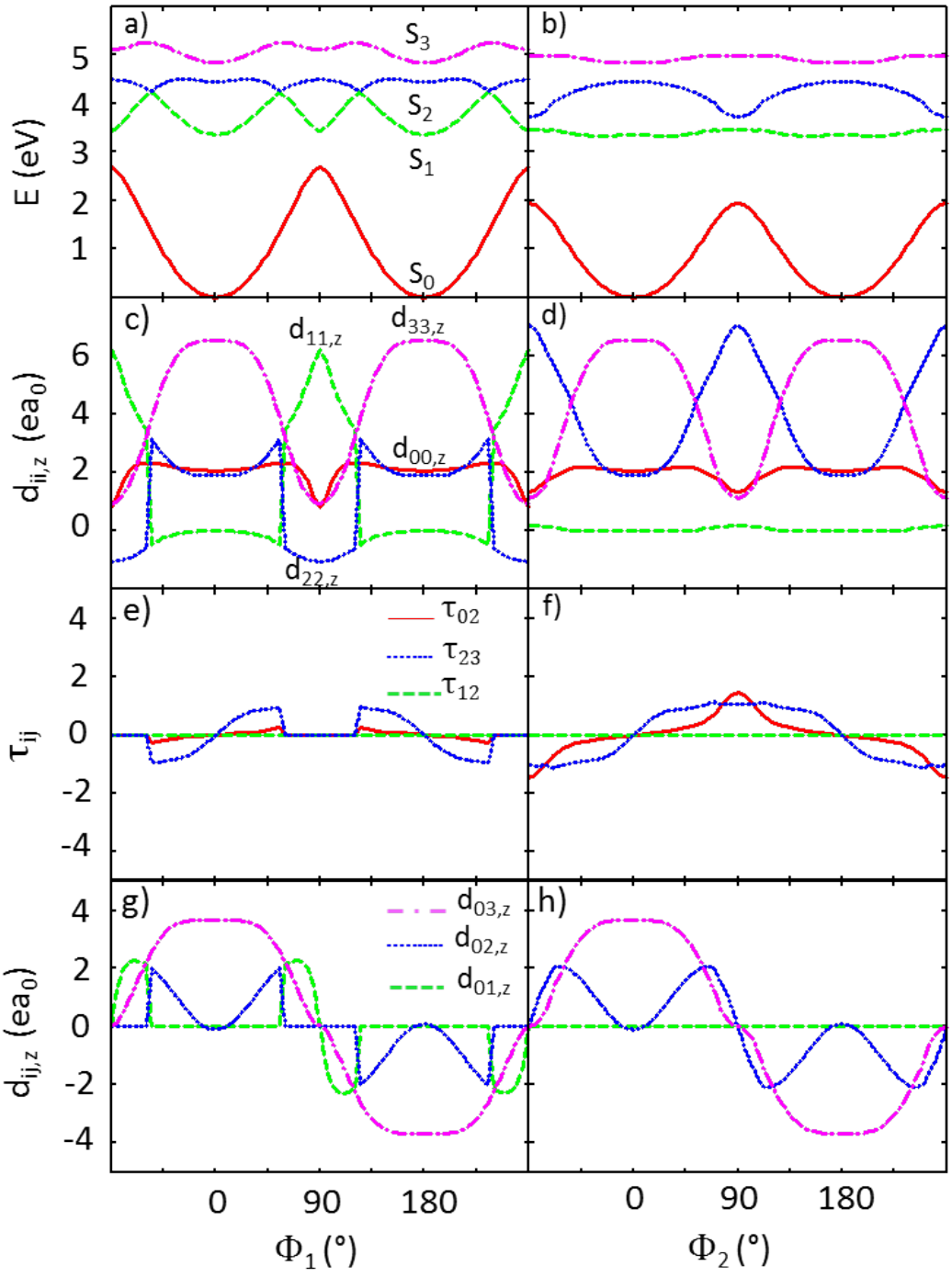

Figure 4.7.: Two one-dimensional cuts of the two-dimensional potential energy surfaces along Φ_1 and Φ_2, respectively, with the corresponding permanent and transition dipole moments and kinetic couplings calculated at the SA4-CASSCF(12,10)/cc-pVDZ level of theory. a) Unrelaxed adiabatic singlet electronic ground state (S_0 in solid), first excited state (S_1 in dashed), second excited state (S_2 in dotted) and third excited state (S_3 in dotted and dashed) along Φ_1 for $\Phi_2 = 0°$. b) Dito along Φ_2 for $\Phi_1 = 0°$. c-d) Permanent dipole moments along Φ_1 and Φ_2, respectively, for the one-dimensional cuts shown in (a) and (b), respectively. e-f) Kinetic couplings between: S_0 and S_2 (τ_{02} solid), S_1 and S_2 (τ_{12} dashed) and S_2 and S_3 (τ_{23} dotted). g-h) Transition dipole moments between the states S_0 and S_1, S_2 and S_3, denoted as $d_{01,z}$, $d_{02,z}$ and $d_{03,z}$ respectively.

dipole moments $d_{01,z}$ and $d_{02,z}$ along Φ_2 are shown in Figure 4.7(h). Their curves are smooth showing that no crossing takes place between the states S_1 and S_2.

The permanent and transition dipole moments shown in Figure 4.7(g-h) were calculated only in the domain Ia, recall subsection 4.1.1. In order to generate the values of the permanent and transition dipole moments in the full range, i.e. from $-90°$ to $270°$ along Φ_1 and Φ_2, molecular symmetry generators were employed as explained in subsection 4.1.1.

Later in this thesis, for the quantum dynamics simulations, we need to know to which state the wavepacket should be excited, as elucidated below. Once we determine this state, the couplings between this state and the other three states should be calculated to define the deactivation path of the excited wavepacket.

Looking at the topology of the excited states (see Figure 4.7(a)), we see that all three states show a local minimum along the Φ_1 coordinate for $\Phi_2 = 0°$ at the Franck-Condon region around $\Phi_1 = 0°$ and $180°$. The same is true along Φ_2 (with constant $\Phi_1 = 0°$) for the states S_1 and S_3, while S_2 shows a local maximum along the Φ_2 coordinate at the Franck-Condon region around $\Phi_2 = 0°$ and $180°$. This makes the latter state to be the state of choice for the electronic excitation to trigger the torsional dynamics, since an excitation into one of the other two states (S_1 or S_3) would trap the wavepacket in the local minimum.

Figure 4.7(e-f) shows the kinetic (non-adiabatic) couplings terms (NACTs) τ_{02}, τ_{12} and τ_{23} as a function of the two torsional angles Φ_1 and Φ_2. These NACTs couple S_2 to the electronically excited states S_1 and S_3, as well as to the electronic ground state S_0. They might induce a possible deactivation pathway for the torsional dynamics of the excited wavepacket and should, in principle, be considered within the quantum dynamical simulations. The one-dimensional cuts along Φ_1 and Φ_2 show that τ_{12} is exactly zero along both angles due to symmetry restrictions (S_1 and S_2 belonging to different symmetry classes), and the other two quantities τ_{02} and τ_{23} have low values, especially at the Franck-Condon region, which is not strong enough for a significant deactivation from S_2, into one of the other states, see Figure 4.7(e-f). We therefore neglected the NACTs in the quantum dynamical simulations described in the following section and for simplicity we shall propagate on the purely adiabatic PES.

4.2. Quantum dynamics

Our objective now is to show the selective torsional dynamics for the four "surviving" nuclear spin isomers in the $T \to 0$ K limit, labeled with the IREPs Γ_i, with $i = 1, 4, 6$ and 7 (see section 3.7). This is done by following the expectation values of

selected operators (subsections 4.2.1 and 4.2.2) and using ultra-short laser pulses to simulate pump-dump processes (subsection 4.2.3).

One can write the torsional ground state wavefunction $\Psi^{S_0}_{\mathrm{tor}_{\Gamma_i}}$ of the different isomers as a linear combination of a wavefunction localized within one potential well $\Psi^{S_0}_l$ (the normalization constant will be ignored for simplicity)

$$\Psi^{S_0}_{\mathrm{tor}_{\Gamma_i}} = \sum_{l=1}^{4} c_l \cdot \Psi^{S_0}_l, \tag{4.1}$$

where the 4 coefficients c_l can have the values of either +1 or -1, respectively, according to Figure 4.8.

Our target is to show that using $\Psi^{S_0}_{\mathrm{tor}_{\Gamma_i}}$ as a starting wavefunction for any kind of laser-induced dynamics on any of the excited state potentials S_1 to S_3, we can expect different dynamics depending on the relative phase c_l of the different localized wavefunctions $\Psi^{S_0}_l$. Here, we illustrate the mathematical derivation for $\Psi^{S_0}_{\mathrm{tor}_{\Gamma_1}}$ and $\Psi^{S_0}_{\mathrm{tor}_{\Gamma_4}}$, as a representative of constructive and destructive interferences along Φ_2. For the sake of simplicity, we assume that $\Psi^{S_0}_{\mathrm{tor}_{\Gamma_1}}$ and $\Psi^{S_0}_{\mathrm{tor}_{\Gamma_4}}$ are made out only of two localized wavefunctions $\Psi^{S_0}_l$, with $l = 1, 2$. The extension of the derivation to the case of more than 2 localized wavefunctions is straightforward.

In this simplified case, the starting wavefunction $\Psi^{S_0}_{\mathrm{tor}_{\Gamma_i}}$, can be expressed as:

$$\Psi^{S_0}_{\mathrm{tor}_{\Gamma_1}} = \Psi^{S_0}_1 + \Psi^{S_0}_2 \tag{4.2}$$

and

$$\Psi^{S_0}_{\mathrm{tor}_{\Gamma_4}} = \Psi^{S_0}_1 - \Psi^{S_0}_2 \tag{4.3}$$

To prove that we can discriminate the torsional dynamics for these two different torsional wavefunctions, we follow the expectation value of an operator $\hat{O}$, describing the time evolution of these wavefunctions $\Psi^{S_k}_{\mathrm{tor}_{\Gamma_i}}$ in the electronically excited state S_k, for IREP Γ_i expressed as:

$$\langle \Psi^{S_k}_{\mathrm{tor}_{\Gamma_i}}(t) \mid \hat{O} \mid \Psi^{S_k}_{\mathrm{tor}_{\Gamma_i}}(t) \rangle = \langle \Psi^{S_0}_1(t) \pm \Psi^{S_0}_2(t) \mid \hat{O} \mid \Psi^{S_0}_1(t) \pm \Psi^{S_0}_2(t) \rangle \,. \tag{4.4}$$

This can be written as:

$$\begin{aligned} \langle \Psi^{S_k}_{\mathrm{tor}_{\Gamma_1}}(t) \mid \hat{O} \mid \Psi^{S_k}_{\mathrm{tor}_{\Gamma_1}}(t) \rangle = {} & \langle \Psi^{S_0}_1(t) \mid \hat{O} \mid \Psi^{S_0}_1(t) \rangle + \langle \Psi^{S_0}_2(t) \mid \hat{O} \mid \Psi^{S_0}_2(t) \rangle \\ & + \langle \Psi^{S_0}_1(t) \mid \hat{O} \mid \Psi^{S_0}_2(t) \rangle + \langle \Psi^{S_0}_2(t) \mid \hat{O} \mid \Psi^{S_0}_1(t) \rangle \end{aligned} \tag{4.5}$$

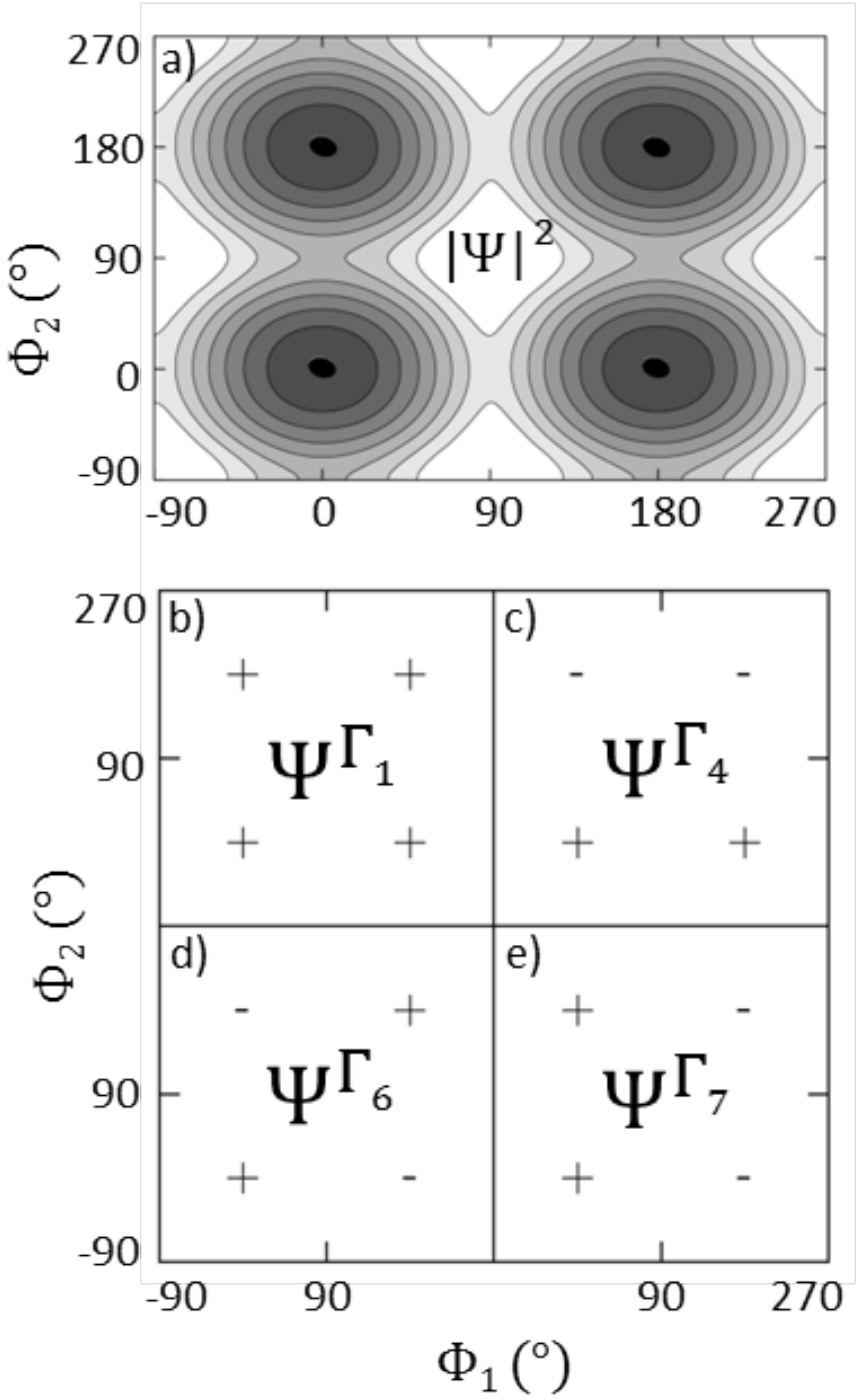

Figure 4.8.: The lowest torsional eigenfunctions in the electronic ground state (S_0) a) A contour plot of S_0 with the torsional eigenfunction labelled with the irreducible representation (IREP) Γ_1 is embedded in. The contours were drawn for S_0 = (0.4, 0.8, 1.2, 1.6, 2.0, 2.4 and 2.8) eV. b-e) A sketch of the four lowest torsional eigenfunctions with their sign patterns for the IREPs Γ_1, Γ_4, Γ_6 and Γ_7.

and

$$\begin{aligned}\langle \Psi^{S_k}_{\mathrm{tor}\Gamma_4}(t) \mid \hat{O} \mid \Psi^{S_k}_{\mathrm{tor}\Gamma_4}(t)\rangle &= \langle \Psi^{S_0}_1(t) \mid \hat{O} \mid \Psi^{S_0}_1(t)\rangle + \langle \Psi^{S_0}_2(t) \mid \hat{O} \mid \Psi^{S_0}_2(t)\rangle \\ &- \langle \Psi^{S_0}_1(t) \mid \hat{O} \mid \Psi^{S_0}_2(t)\rangle - \langle \Psi^{S_0}_2(t) \mid \hat{O} \mid \Psi^{S_0}_1(t)\rangle \\ &= \langle \Psi^{S_0}_1(t) \mid \hat{O} \mid \Psi^{S_0}_1(t)\rangle + \langle \Psi^{S_0}_2(t) \mid \hat{O} \mid \Psi^{S_0}_2(t)\rangle \\ &- (\langle \Psi^{S_0}_1(t) \mid \hat{O} \mid \Psi^{S_0}_2(t)\rangle + \langle \Psi^{S_0}_2(t) \mid \hat{O} \mid \Psi^{S_0}_1(t)\rangle). \quad (4.6)\end{aligned}$$

A close inspection of equations 4.5 and 4.6, shows that they differ only in the sign in front of the interference term $\mathcal{I}$:

$$\mathcal{I} = \langle \Psi^{S_0}_1(t) \mid \hat{O} \mid \Psi^{S_0}_2(t)\rangle + \langle \Psi^{S_0}_2(t) \mid \hat{O} \mid \Psi^{S_0}_1(t)\rangle \,. \quad (4.7)$$

This difference in the sign is a result of having different patterns of constructive and/or destructive interferences during the propagation for the different nuclear spin isomers. These different patterns should lead to differences in the expectation values of the operator, which could be used experimentally to discriminate the different nuclear spin isomers.

For the case of CCD, we started calculating the torsional wavefunction localized in only one potential well using the Fourier Grid Hamiltonian method [72]. Then the localized torsional wavefunctions in the other three wells were constructed according to the sign pattern shown in figure 4.3, i.e. following the symmetry rules explained in section 3.7, as we did for the PESs (Section 4.1.1).

To trigger the torsional dynamics on the electronic excited states, a delta pulse was used, i.e. we assumed an instantaneous electronic excitation of the electronic ground state wavefunction ($\Psi^{S_0}_{\mathrm{tor}}$) to the electronic excited state S_2. Moreover, we assumed that the transition dipole moment is equal to one everywhere (unless specified otherwise, e.g. as in the dump simulations shown in subsection 4.2.3). Therefore,

$$\Psi^{S_2}_{\mathrm{tor}}(t=0) = \Psi^{S_0}_{\mathrm{tor}} \quad (4.8)$$

The propagation was done by solving the nuclear TDSE, equation (2.35), using the split operator ansatz for the propagator, see equation (2.38). The propagation was carried out on an equidistant spatial grid, i.e. $\Delta\Phi_1 = \Delta\Phi_2$ with equal minima for both Φ_1 and Φ_2, which is equal to $-90°$ and with equal maxima for both Φ_1 and Φ_2, equal to 270°. We started with using different even numbers of grid points; 128, 256 and 512 in each coordinate. Using these grid sizes of even number

of grid points results in having one point less for the wavefunction than for the PES. As a consequence, we got a shift in the center of the wavepacket (the torsional eigenfunction) in the S_2 state at t = 0 fs, which is reflected in the expectation value of the position operator of Φ_1 and Φ_2 at t = 0 fs, see Figures 4.9 and 4.10. This shift in the expectation value of the position operator of Φ_1 and Φ_2 at t = 0 fs, decreases with increasing the grid size. However, the corresponding dynamics was incorrect since we got different dynamical behaviour for the same nuclear spin isomer depending on the number of grid points employed in the simulations. This is illustrated in Figures 4.9 and 4.10.

A possible solution to this problem would be to use an odd number of grid points in each coordinate, but this is computationally not efficient, due to the FFT involved in the propagation.

To overcome the two problems, the complete torsional eigenfunctions of the S_0 state were constructed, i.e. without constructing the localized torsional wavefunctions in the wells from the torsional wavefunction localized in the first well of the PES of the S_0 state. For this purpose we have to use a grid with at least 512 points along both coordinates, in order to guarantee that the wavepacket will not hit the boundaries of the momentum grid during the propagation.

Since the Fourier Grid Hamiltonian method gets computationally too much demanding for such a large grid size, we used the relaxation method, i.e. propagating in imaginary time, as explained in section 2.7. The propagation was done by solving the nuclear TDSE (equation (2.35)) using the split operator ansatz for the propagator (equation (2.38)). We did the propagation on an equidistant spatial grid with 512 grid points in each coordinate. Consequently, $\Delta\Phi_1 = \Delta\Phi_2 = 0.7049°$, with equal minima for both of Φ_1 and Φ_2, which is equal to $-90°$ and with equal maxima for both of Φ_1 and Φ_2, equal to 270°.

The reduced moments of inertia are $I_1 = 2.21 \cdot 10^5\ m_e \cdot a_0^2$ and $I_2 = 2.36 \cdot 10^5\ m_e \cdot a_0^2$, respectively. These are obtained from the moments of inertia at the "first" equilibrium structure, $I_\mathrm{A} = 3.47 \cdot 10^5\ m_e \cdot a_0^2$, $I_\mathrm{B} = 6.07 \cdot 10^5\ m_e \cdot a_0^2$ and $I_\mathrm{C} = 3.86 \cdot 10^5\ m_e \cdot a_0^2$ for intramolecular rotations of the segments A, B and C around the C_2-axis, respectively, using equation (2.28).

Figure 4.8(a) shows the nuclear eigenfunction of IREP Γ_1, as an example for these four lowest torsional eigenfunctions, embedded in the ab initio PES of the electronic ground S_0. In order to force the system to converge into one of the four desired IREPs, the initial wavefunctions were created such that they fulfill the restrictions for the corresponding representation, i.e. the starting wavefunction and thus the converged torsional eigenfunctions follow the sign pattern for the IREPs Γ_1, Γ_4, Γ_6 and Γ_7, which are shown in Figure 4.8(b-e).

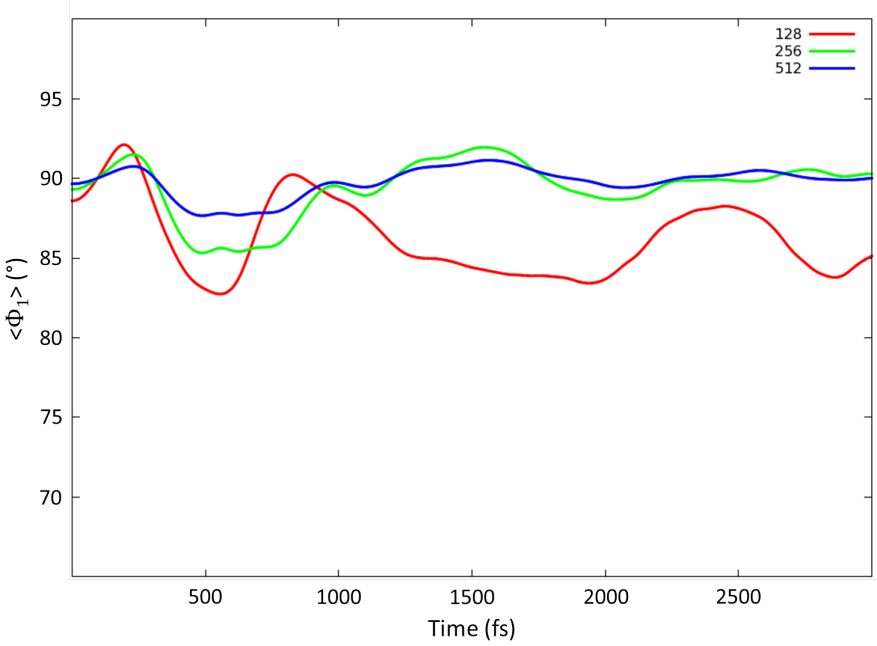

Figure 4.9.: The expectation value of the position operator of Φ_1 for the nuclear spin isomer labelled with Γ_1, using different even number of grid points; 128, 256 and 512 along each of Φ_1 and Φ_2. It can be seen from the figure that the torsional dynamics of this nuclear spin isomer is sensitive to the number of grid points.

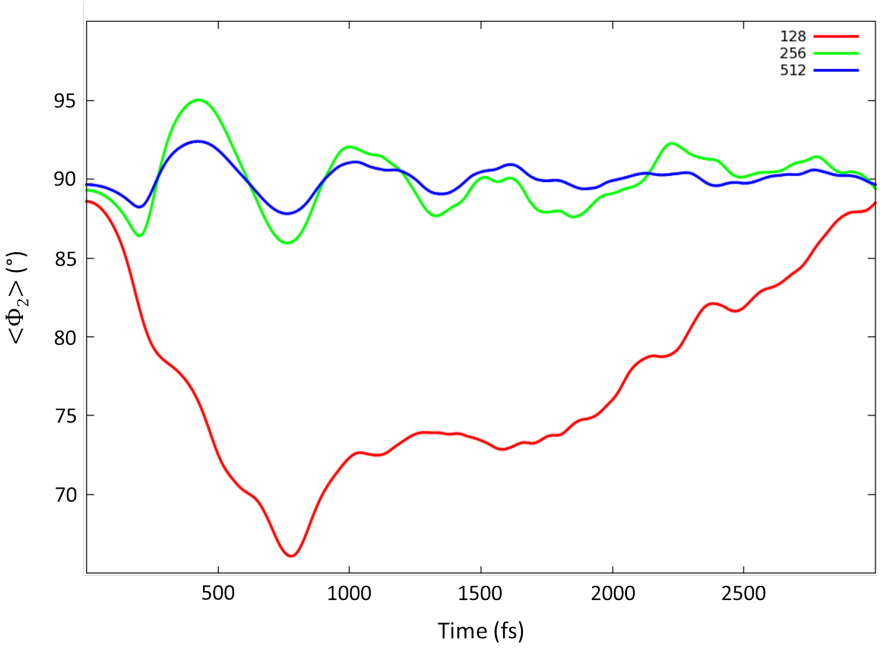

Figure 4.10.: The expectation value of the position operator of Φ_2 for the nuclear spin isomer labelled with Γ_1, using different even number of grid points; 128, 256 and 512 along each of Φ_1 and Φ_2. The figure shows the sensitivity of the torsional dynamics of this nuclear spin isomer to the number of grid points.

For the investigation of the torsional dynamics on the excited state for these torsional eigenfunctions, a delta pulse is used to pump each of these four resulting nuclear spin isomers from S_0 to S_2. The density of the wavepacket Ψ^{Γ_1} at t = 0 fs in the S_2 potential, is shown in Figure 4.11(a) as a representative for these four nuclear spin isomers.

The obtained dynamics is depicted, for the same wavepacket Ψ^{Γ_1}, for different time frames in Figures 4.11(b-f). At the beginning (t = 0 fs), the wavepacket is trapped in the Φ_1 coordinate, since we have two local minima in the S_2 potential at $\Phi_1 = 0°$ and 180°, recall Figure 4.7(a). At time t = 150 fs, we see that the wavepacket starts to move mainly along Φ_2, recall Figure 4.7(b). Following the dynamics until t = 230 fs, we see a spread of the wavepacket along the Φ_2 coordinate until the different parts of the initial wavepacket meet at the central region around $\Phi_2 = 90°$ at t = 300 fs. From this moment on, the different parts of the initial wavepacket are interfering. At the same time, we see a pronounced motion along the Φ_1 coordinate (which is due to the different topology of the PES of S_2 state along Φ_1 at $\Phi_2 = 90°$).

The investigation of the dynamics on a longer time scale (t $\geq$ 300 fs) shows that the interference is more pronounced along Φ_2 than along Φ_1, with a noticeable spread of the wavepacket along the Φ_1 coordinate. Due to the topology of the S_2 potential, the different parts of the wavepackets never cross the barrier along Φ_1 (at least within the simulated time scale). Therefore, the four nuclear spin isomers are classified into two groups. This classification is based on the type of interference whether it is constructive or destructive along Φ_2, no matter what type of interference they have along Φ_1. Thus, the first group contains Ψ^{Γ_1} and Ψ^{Γ_7}, both showing constructive interference along Φ_2 (Figure 4.8(b) and (e)), and the other group contains Ψ^{Γ_4} and Ψ^{Γ_6}, both showing destructive interference along Φ_2 (Figure 4.8(c) and (d)).

To show the ability of distinguishing between the torsional dynamics of these two groups of nuclear spin isomers, we analyzed the expectation values of different operators $\hat{O}$ in subsection 4.2.1, the dispersion (variance) of some of these operators for the nuclear spin isomers in subsection 4.2.2 and finally perform pump-dump simulations, shown in subsection 4.2.3.

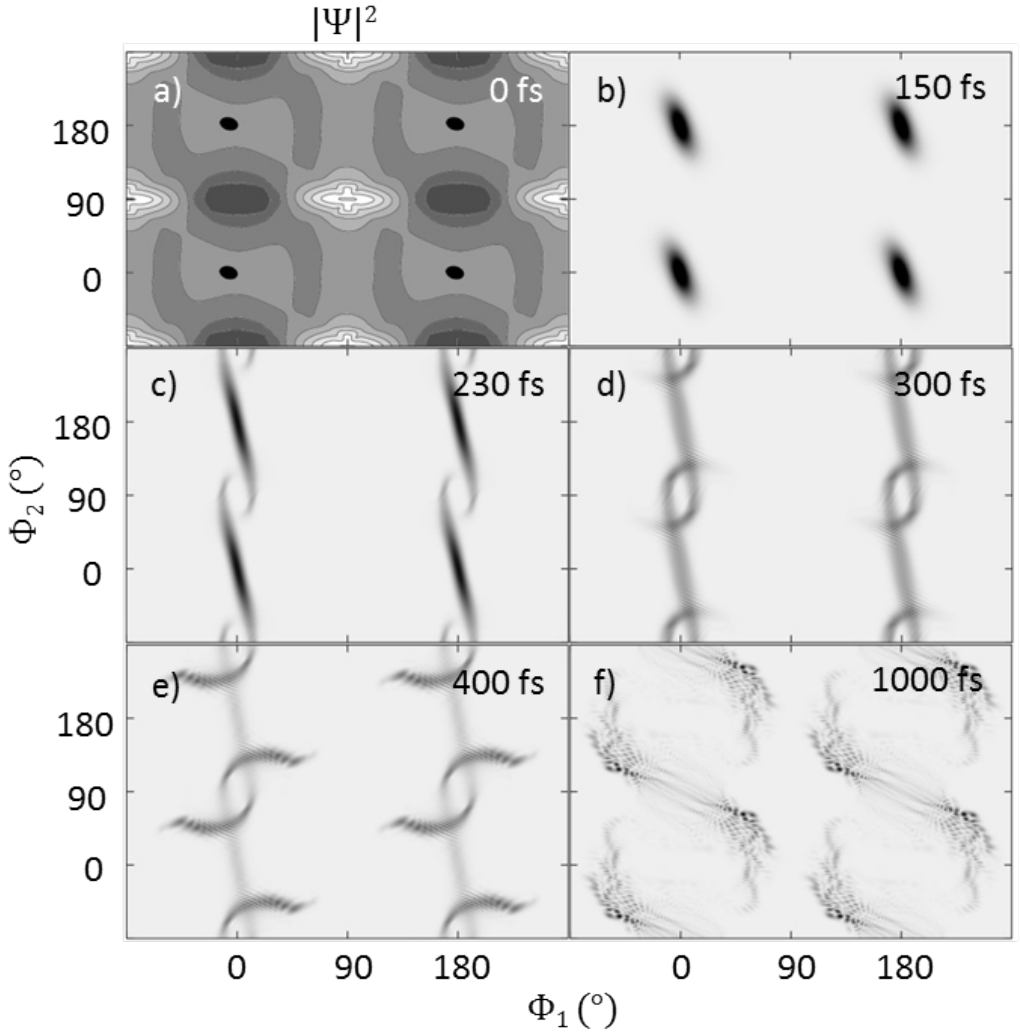

Figure 4.11.: Snapshots of the probability density of Ψ^{Γ_1}, as an example for the constructive interference along Φ_2, in the S_2 potential a) A contour plot for S_2 with embedded Ψ^{Γ_1}. The contours are drawn for S_2 = (4.0, 4.2, 4.4, 4.6, 4.8, 5.0, 5.2 and 5.4) eV. b-c) The wavepacket movement is pronounced along Φ_2. d) The four components of the wavepacket meet. e) The wavepacket finally moves along Φ_1. f) The wavepacket is spread along both Φ_1 and Φ_2 except that it does not overcome the barrier in the S_2 potential around 90° along Φ_1.

4.2.1. Expectation values

Discriminating the torsional dynamics of the two groups of nuclear spin isomers through following the expectation value of selected operators is the aim of this subsection. Due to the symmetry of the PES of the S_2 state, we found out that following the expectation value of the angles $\langle\Phi_1\rangle$ and $\langle\Phi_2\rangle$, does not help, as these values are always equal to 90° during the simulated time. This is due to the symmetric movement of the wavepacket along Φ_1 and Φ_2. The same behavior is encountered for the angular momentum $\langle\hat{L}_1\rangle$ and $\langle\hat{L}_2\rangle$, see Figure 4.12. This figure shows that following the $\langle\hat{L}_1\rangle$ and $\langle\hat{L}_2\rangle$ that are associated to Φ_1 and Φ_2 in the whole domain, i.e. from −90° to 270°, no discrimination can be seen for the two groups of nuclear spin isomers, as we always get zero.

Therefore, we follow the directed angular momentum in the positive $\langle\hat{L}^+_{1/2}\rangle$ and the negative $\langle\hat{L}^-_{1/2}\rangle$ ranges that are defined as:

$$\langle\hat{L}^+_{1/2}\rangle = \int_0^{\aleph_{\max}} \Psi^*_{\text{tor}}\hat{L}_{1/2}\Psi_{\text{tor}}d\aleph \tag{4.9}$$

and

$$\langle\hat{L}^-_{1/2}\rangle = \int_{\aleph_{\min}}^{0} \Psi^*_{\text{tor}}\hat{L}_{1/2}\Psi_{\text{tor}}d\aleph, \tag{4.10}$$

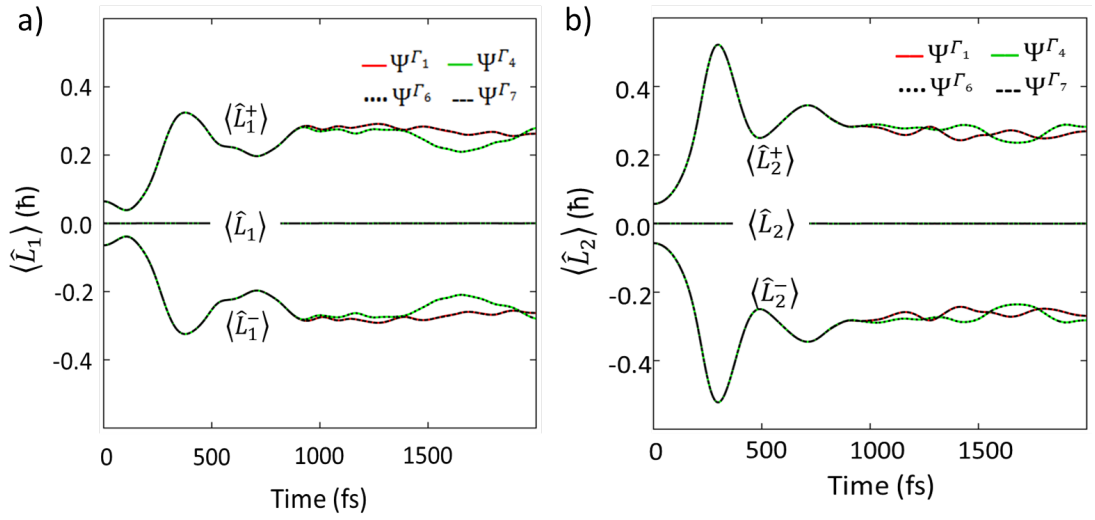

Figure 4.12.: The expectation value of the angular momentum $\langle\hat{L}_1\rangle$ and $\langle\hat{L}_2\rangle$ that are associated to Φ_1 (a) and Φ_2 (b), respectively, for the four nuclear spin isomers Ψ^{Γ_1}, Ψ^{Γ_4}, Ψ^{Γ_6} and Ψ^{Γ_7} . The figure also shows the expectation value for the directed angular momentum in the positive $\langle\hat{L}_1^+\rangle$ and the negative $\langle\hat{L}_1^-\rangle$ range, where a discrimination for two groups of the four nuclear spin isomers (Ψ^{Γ_1} and Ψ^{Γ_7}) and (Ψ^{Γ_4} and Ψ^{Γ_6}) can be achieved.

in the momentum $\mathfrak{K}$ space. Figure 4.12 shows that a discrimination for the two groups of nuclear spin isomers can be seen in both $\langle \hat{L}^{+}_{1/2} \rangle$ and $\langle \hat{L}^{-}_{1/2} \rangle$, starting shortly before 1000 fs.

4.2.2. Dispersion

We now monitor the spread of the wavepacket by following the dispersion (variance) of the position (associated to Φ_1 and Φ_2) and the momentum operator for the two groups of nuclear spin isomers.

The dispersion $D_{\hat{O}}$ of the operator $\hat{O}$ for the wavepacket $\Psi^{S_k}_{\mathrm{tor}\Gamma_i}$ (i= 1 or 4 or 6 or 7) is defined as:

$$D_{\hat{O}} = \langle \Psi^{S_k}_{\mathrm{tor}\Gamma_i}(t) \mid \hat{O}^2 \mid \Psi^{S_k}_{\mathrm{tor}\Gamma_i}(t) \rangle - \langle \Psi^{S_k}_{\mathrm{tor}\Gamma_i}(t) \mid \hat{O} \mid \Psi^{S_k}_{\mathrm{tor}\Gamma_i}(t) \rangle^2 . \tag{4.11}$$

Following the dispersion of either the position or the momentum operator shows that indeed we can discriminate these two groups of nuclear spin isomers, see Figures 4.13 and 4.14. These two figures show the dispersion of the angular momentum along both directions ($D_{\hat{L}_1}$ and $D_{\hat{L}_2}$) and of the two torsional angles ($D_{\hat{\Phi}_1}$ and $D_{\hat{\Phi}_2}$), respectively. One can see that in all cases a difference in the dispersion starts shortly before 1000 fs.

Comparing Figure 4.13(b) with Figure 4.13(a) shows that the dispersion of the wavepacket of any of the four nuclear spin isomers along Φ_2 that is associated to $\hat{L}_2$ is more pronounced than along Φ_1 that is associated to $\hat{L}_1$. The same can be seen when comparing Figure 4.14(b) with Figure 4.14(a).

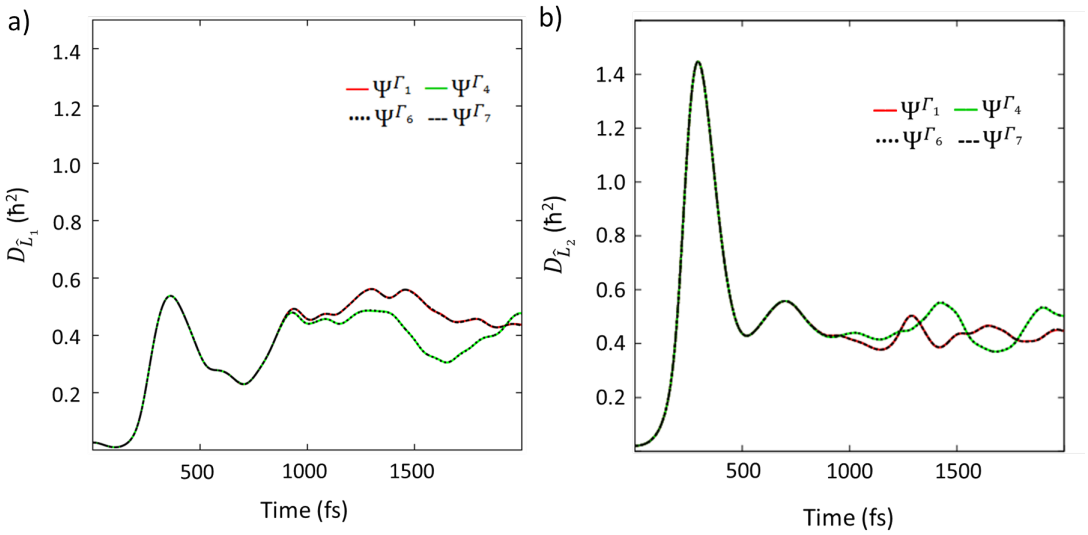

Figure 4.13.: The dispersion $D_{\hat{L}_1}$ and $D_{\hat{L}_2}$ of the angular momentum $\hat{L}_1$ (a) and $\hat{L}_2$ (b) for the four nuclear spin isomers Ψ^{Γ_1}, Ψ^{Γ_4}, Ψ^{Γ_6} and Ψ^{Γ_7}. A discrimination between two groups (Ψ^{Γ_1} and Ψ^{Γ_7}) and (Ψ^{Γ_4} and Ψ^{Γ_6}) of the nuclear spin isomers can be seen shortly before 1000 fs.

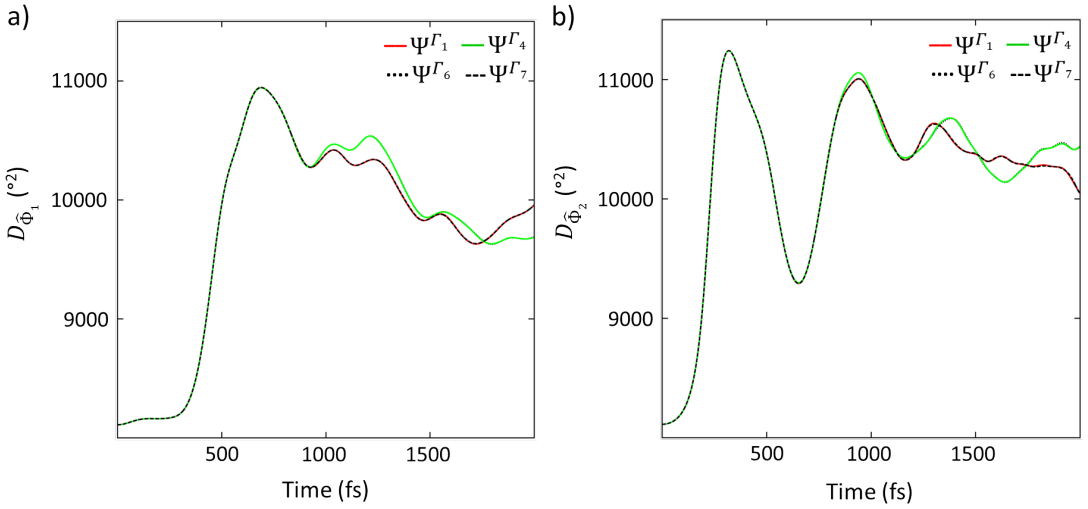

Figure 4.14.: The dispersion $D_{\hat{\Phi}_1}$ and $D_{\hat{\Phi}_2}$ of the position operator $\hat{\Phi}_1$ and $\hat{\Phi}_2$ of the torsional angle Φ_1 (a) and Φ_2 (b), respectively, for the four nuclear spin isomers Ψ^{Γ_1}, Ψ^{Γ_4}, Ψ^{Γ_6} and Ψ^{Γ_7}. Two groups (Ψ^{Γ_1} and Ψ^{Γ_7}) and (Ψ^{Γ_4} and Ψ^{Γ_6}) of the nuclear spin isomers are discriminated through their $D_{\hat{\Phi}_1}$ and $D_{\hat{\Phi}_2}$ shortly before 1000 fs.

4.2.3. Pump-dump simulations

Within this subsection we simulated ultra-short laser pulses in a pump-dump like fashion to separate the two groups of nuclear spin isomers. Here, separation means enhancing the ratio of one of these two groups of nuclear spin isomers beyond its high temperature equilibrium values. The total electric field $\epsilon^{tot}(t)$ induced by the pump and the dump laser pulses can be written as:

$$\epsilon^{tot}(t) = \epsilon^{p}(t) + \epsilon^{d}(t). \tag{4.12}$$

Here and henceforth, the superscript p is for pump and the superscript d is for dump, where

$$\epsilon^{p}(t) = \begin{cases} F_0^p \sin^2\left(\frac{\pi t}{t_p^p}\right)\cos(\omega^p t), & \text{if} \quad t \leq t_p^p \\ 0, & \text{otherwise} \end{cases}, \tag{4.13}$$

like in equations 2.31 and 2.32. A Z-polarized pulse is assumed to be used, F_0 is the field amplitude, ω is the frequency and t_p is the pulse duration. The pump pulse starts at $t_s = 0$ fs. Likewise $\epsilon^{d}(t)$ is:

$$\epsilon^{d}(t) = \begin{cases} F_0^d \sin^2\left(\frac{\pi t}{t_p^d}\right)\cos(\omega^d t), & \text{if} \quad t_d + t_p^p < t \leq t_d + t_p^p + t_p^d \\ 0, & \text{otherwise} \end{cases}, \tag{4.14}$$

where t_d is the delay time between the two pulses.

We optimized the fs laser pulses that are used in these pump-dump simulations to get the best enhancement for one of these two groups of nuclear spin isomers. The optimization for the two pulses was done by varying their frequency ω, their amplitude F_0 and their duration t_p. Furthermore, the time delay between the two pulses t_d was used as an additional variable.

Due to the topology of the PESs of the lowest three excited states as illustrated in subsection 4.1.2, the proposed state for pumping is the S_2 state. Our purpose now is to specify the parameters for the pumping and the dumping lasers with the criterion to maximize the population difference between the two different groups of nuclear spin isomers that are dumped to the electronic ground state S_0.

For pumping, we need the transition dipole moment $\mathrm{d}_{02,z}$, recall Figure 4.7(g-h), to couple between the S_0 and the S_2 states. Since $\mathrm{d}_{02,z}$ is low as the oscillator strength for the S_2 state is equal to 0.001, we need a very long pulse for pumping the system from the S_0 to the S_2 state. We found that for a resonant pulse of $t_p^p = 1500$ fs and $F_0 = 1.5$ GV/m only 27% of the system are pumped from the

S_0 to the S_2 state as shown in Figure 4.15. In this figure we see that the norm is $|\langle\Psi|\Psi\rangle| = 1$ for S_0 and zero for the other three states at the beginning. Then, the norm decreases for S_0 and increases for S_2 state with time till the S_2 norm converges to 0.27. The norm for the S_1 state also increases shortly before 400 fs, even though the pulse is non-resonant. The total norm for all the four states is constant and equal to one throughout the pump simulations, as it should be.

For optimizing the dump pulse, we start a new simulation where we assumed that the wavepacket is already on the S_2 state, i.e. we used a delta pulse to pump the system from the S_0 to the S_2 state. Moreover, we assumed that the transition dipole moment between the S_0 and the S_2 state is equal to one, as in equation 4.8.

To start the optimization of the dump pulse, we first need to determine the time delay t_d between the delta pulse (pump laser) and the dump pulse. Thus, we scanned t_d to specify t_d that gives the largest difference in the population of the dumped Ψ^{Γ_1} and Ψ^{Γ_6} (representing the two groups of nuclear spin isomers) to the S_0 state, as shown in Figure 4.16. This figure shows the change of the population (expressed as the norm, i.e. $|\langle\Psi|\Psi\rangle|$) of the dumped Ψ^{Γ_1} and Ψ^{Γ_6} with different t_d. The scan for t_d was done with a step size of 100 fs, except in the domain between 700-850 fs, where the step size is 10 fs. This step size was chosen becuase the population difference between the dumped Ψ^{Γ_1} and Ψ^{Γ_6} increases in the t_d domain 700-850 fs. Thus to get more insight in the dump process in this domain we used a small step size. Analyzing the data of the t_d scan, we found that at $t_d = 760$ fs the largest population difference between the dumped Ψ^{Γ_1} and Ψ^{Γ_6} equal to 0.014 is obtained. The optimal pulse duration for the dump laser is $t_p^d = 200$ fs. This duration was found to be the best compromise between having a discrimination in the population of the dumped Ψ^{Γ_1} and Ψ^{Γ_6}, while still having an efficient dumping.

Subsequently, we proceeded to scan F_0^d and ω^d for the dumping laser using $t_d = 760$ fs and $t_p^d = 200$ fs. Firstly, we started with the F_0^d scan as shown in Figure 4.17 and used $\hbar\omega^d = 2.2764$ eV for this scan. Figure 4.17 shows that the population difference between the dumped Ψ^{Γ_1} and Ψ^{Γ_6} increases with increasing F_0^d. The scan of F_0^d was run from 0.8-1.2 GV/m with a step size of 0.1 GV/m. We stopped the F_0^d scan till 1.2 GV/m because going to higher values causes non-resonant dumping, i.e. the system will not be dumped only to the S_0 state but also to the S_3 state, which we are not interested in.

Afterwards, we scanned ω^d for the dump laser utilizing $t_p^d = 200$ fs, $F_0^d = 1.2$ GV/m and $t_d = 760$ fs, see Table 4.3. This table shows the difference in the population (Δ_{norm}) between the dumped Ψ^{Γ_1} and Ψ^{Γ_6} from the S_2 to the S_0 state for different $\hbar\omega^d$ in the domain 2.1764 - 2.7764 eV. It is found that $\hbar\omega^d = 2.2764$ eV leads to the highest $\Delta_{\text{norm}} = 17.12 \cdot 10^{-3}$.

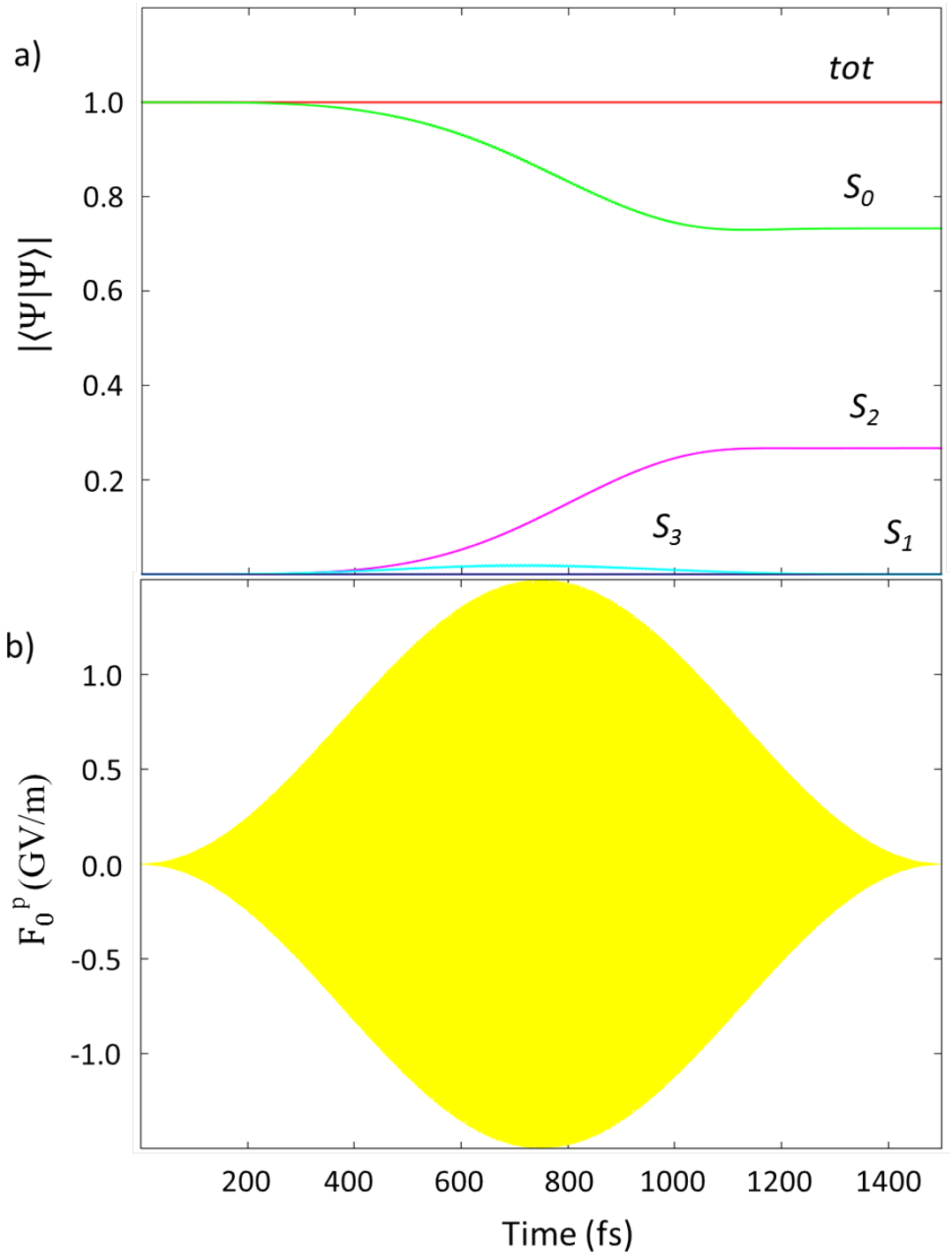

Figure 4.15.: (a) The change of the norm ($|\langle\Psi|\Psi\rangle|$) of the S_0, S_1, S_2 and S_3 states with time and the total norm (green, dark blue, pink, light blue and red solid lines, respectively) for Ψ^{Γ_1}. (b) The employed pump laser of amplitude = 1.5 GV/m, $\hbar\omega^p = 4.4493$ eV and a pulse duration $t_p^p = 1500$ fs.

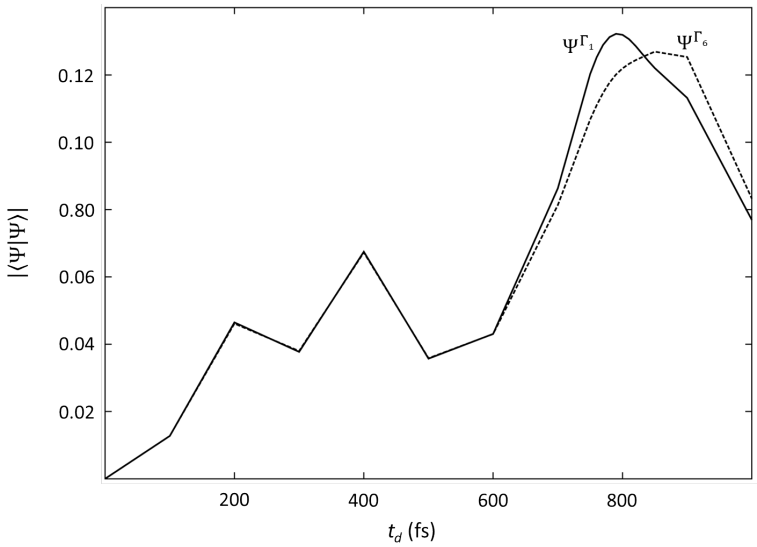

Figure 4.16.: The change of the population expressed as the norm ($|\langle\Psi|\Psi\rangle|$) of Ψ^{Γ_1} and Ψ^{Γ_6} (solid and dashed lines, respectively) in the electronic ground state S_0 with different time delay t_d for a dumping pulse of amplitude = 1.0 GV/m, $\hbar\omega$ = 2.2764 eV and a pulse duration = 200 fs to dump the system from the S_2 to the S_0 state. The scan for t_d was done with a step size of 100 fs except in the domain between 700-850 fs, where the step size was 10 fs. The system was pumped to the S_2 state by a delta pulse.

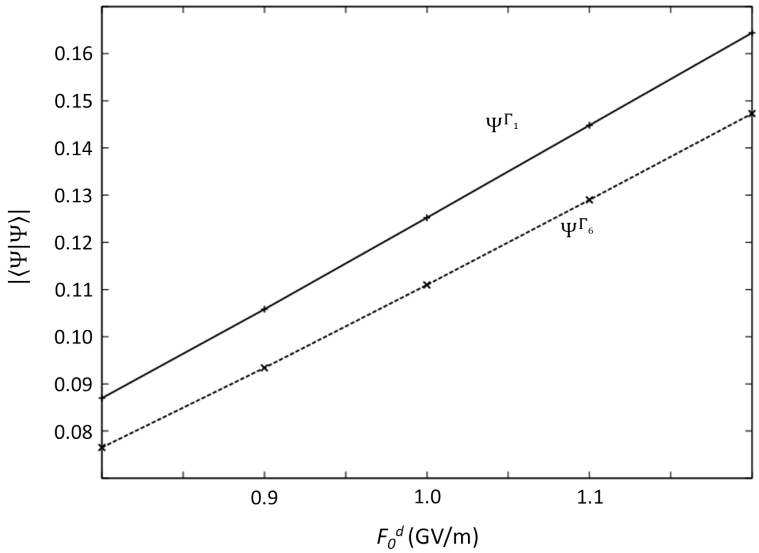

Figure 4.17.: The change of the population expressed as the norm ($|\langle\Psi|\Psi\rangle|$) of the dumped Ψ^{Γ_1} and Ψ^{Γ_6} (solid and dashed lines, respectively) to the electronic ground state S_0 with the field amplitude F_0^d. This scan was perfomed for F_0^d in the range 0.8-1.2 GV/m with a step size of 0.1 GV/m, utilizing delay time t_d = 760 fs, dump pulse duration t_p^d = 200 fs and dump pulse frequency $\hbar\omega^d$ = 2.2764 eV. The system was pumped to the S_2 state by a delta pulse.

Table 4.3.: The population difference (Δ_{norm}) between the dumped Ψ^{Γ_1} and Ψ^{Γ_6} to the S_0 state for different frequencies for the dumping laser ω^d. The dump laser parameters are $t_p^d = 200$ fs for its duration and its amplitude $F_0^d = 1.2$ GV/m. The system was pumped to the S_2 state by a delta pulse and the time delay $t_d = 760$ fs.

$\hbar\omega^d$ (eV)	$\Delta_{\text{norm}} \cdot 10^{-3}$
2.1764	-5.83
2.2764	17.12
2.3764	-14.27
2.4764	3.75
2.5764	-3.82
2.6764	1.00
2.7764	-1.76

Consequently, the optimizing parameters for the dumping laser are $\hbar\omega^d = 2.2764$ eV, $F_0^d = 1.2$ GV/m and $t_p^d = 200$ fs in addition to $t_d = 760$ fs that result in having the largest difference in the population of the dumped Ψ^{Γ_1} and Ψ^{Γ_6} (from the S_2 to the S_0 state) equal to $17.12 \cdot 10^{-3}$, as summarized in Table 4.4. This difference in the population is very small. Repeating this pump-dump like experiment for several times would enhance this difference till we get a value which can be efficient for separating these two groups of nuclear spin isomers. However, we should wait for equilibration before repeating the pump-dump scheme to make sure that the dumped wavepacket has relaxed to the vibrational ground state in order to guarantee that this wavefunction which will be used for the next pump-dump scheme has always the same initial conditions.

Table 4.4.: The optimized parameters for the dump laser that leads to have the largest difference in the population between the dumped Ψ^{Γ_1} and Ψ^{Γ_6}, which is equal to $17.12 \cdot 10^{-3}$.

Parameter	Value
$\hbar\omega^d$	2.2764 eV
F_0^d	1.2 GV/m
t_p^d	200 fs
t_d	760 fs

In this section, we explained how we optimized the pump and the dump pulses separately. However, this is not how it would work in potential experiment, where the pumping process takes place and subsequently, in the same experiment, the dumping process. To simulate these two processes in one simulation, further investigations should be carried out. Our goal within this thesis is to show that in principle we can use the pump-dump simulations to push the ratio of these two

groups of nuclear spin isomers away from their high temperature equilibrium value, pointing to the possibility of separating them. Even though the highest obtained $\Delta_{\text{norm}} = 17.12 \cdot 10^{-3}$ is low, repeating this pump-dump process in an experiment fashion again and again would lead to increase the value of Δ_{norm} so that it can be efficiently detected.

5. Conclusion and outlook

We were able to discriminate two groups of nuclear spin isomers of CCD through the investigation of their torsional dynamics on electronic excited states. These two groups are classified according to their constructive or destructive interference along Φ_2, no matter what type of interference they have along Φ_1. This classification of these two groups of nuclear spin isomers is due to the topology of the PES of the S_2 state, which has a maximum in the Franck-Condon region in the Φ_2 coordinate.

In order to investigate the torsional dynamics of the nuclear spin isomers, we need a proper symmetry tool to label them. This symmetry tool should be able to describe large amplitude motions such as torsion. This symmetry tool is called molecular symmetry, contrary to the well known molecular point group that can describe only local molecular properties.

We found out that the molecular symmetry group of CCD, as a model for a certain class of molecules that have a C_2 symmetry axis and three segments A, B, C which can rotate independently about that axis (fulfills items (i) and (ii) of the Introduction), is G_{16}^{A}. We provide its multiplication, character and product tables, which are of general use when dealing with this molecular symmetry group.

It turned out that CCD, or any molecule that belong to this class of molecules, has at most eight nuclear spin isomers. For CCD, only four out of these eight nuclear spin isomers "survive" as $T \to 0$. Each NSI is characterized by a specific tandem of two (out of eight) IREPs for the nuclear spin and the torsional wavefunctions.

The discrimination between the two groups of nuclear spin isomers was achieved by the expectation value of selected operators like the directed angular momentum in either the positive or the negative direction along the two torsional angles Φ_1 and Φ_2. Moreover, this discrimination was also seen in the dispersion of the wavepacket in the position and momentum spaces.

We performed pump-dump simulations for these nuclear spin isomers as we pumped the system from the S_0 to the S_2 state and dumped the wavepacket from the S_2 back to the S_0 state. These simulations showed that we can increase the population of the dumped nuclear spin isomer that belong to one of the two groups relative to the other nuclear spin isomer that belong to the other group. Thus, we can shift the ratio of the nuclear spin isomers of these two groups

away from its high temperature equilibrium value. This gives rise to the possibility of separating these two groups of nuclear spin isomers in a femtosecond experiment.

Several further extensions are possible for this work: Application of the dynamical simulations to other systems that have the same molecular symmetry group, i.e. G_{16}^{A}, and to different isotopomers of CCD. Including additional degrees of freedom and introducing the non-adiabatic coupling terms can also be other possible extensions for this work. The latter would lead to a more realistic description of the system. This would answer the question if the discovered mechanism for discriminating the nuclear spin isomers can still be seen using a more complex model.

A. Appendix

A.1. Hamiltonian

The Hamiltonian of difloro-quinodimethane shown in Figure A.1 (which is a derivative of quinodimethanes that belongs to the ABC-system, i.e. fulfills items (i) and (ii) in the Introduction) without making use of the equivalent fragments is:

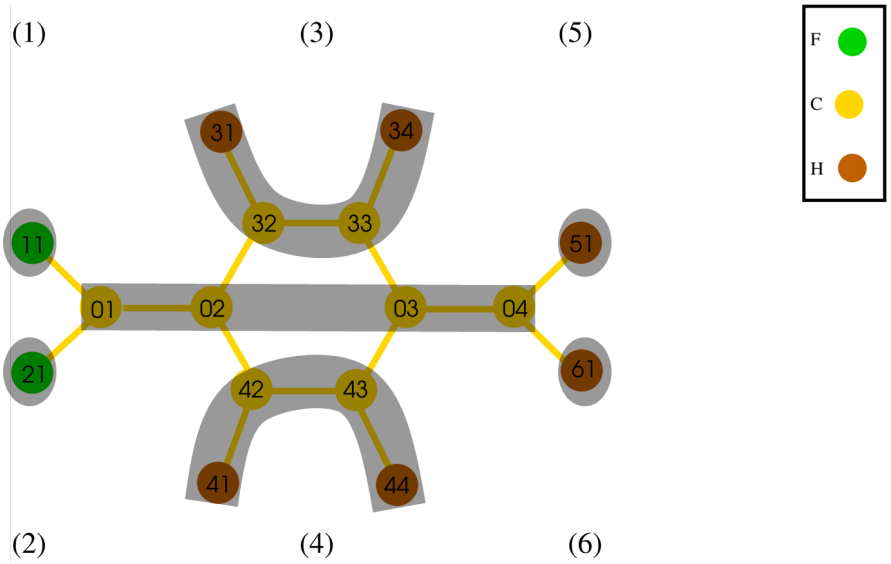

Figure A.1.: The difloro-quinodimethane structure with equivalent fragments (1) & (2), (3) & (4) and (5) & (6). The fragments are marked in shaded gray. The first label for each nucleus determines the fragment and the second label specifies the nucleus within the fragment. The fragment labelled 0 includes the nuclei located along the C_2 symmetry axis of the system.

$$
\begin{aligned}
\hat{H} \;=\; & -\frac{\hbar^2\nabla_{11}^2}{2M_{11}} - \frac{\hbar^2\nabla_{21}^2}{2M_{21}} - \frac{\hbar^2\nabla_{01}^2}{2M_{01}} - \frac{\hbar^2\nabla_{02}^2}{2M_{02}} - \frac{\hbar^2\nabla_{31}^2}{2M_{31}} - \frac{\hbar^2\nabla_{32}^2}{2M_{32}} - \frac{\hbar^2\nabla_{33}^2}{2M_{33}} - \frac{\hbar^2\nabla_{34}^2}{2M_{34}} \\
& - \frac{\hbar^2\nabla_{41}^2}{2M_{41}} - \frac{\hbar^2\nabla_{42}^2}{2M_{42}} - \frac{\hbar^2\nabla_{43}^2}{2M_{43}} - \frac{\hbar^2\nabla_{44}^2}{2M_{44}} - \frac{\hbar^2\nabla_{03}^2}{2M_{03}} - \frac{\hbar^2\nabla_{04}^2}{2M_{04}} - \frac{\hbar^2\nabla_{51}^2}{2M_{51}} - \frac{\hbar^2\nabla_{61}^2}{2M_{61}} \\
& - \sum_{i=1}^{72} \frac{\hbar^2\nabla^2}{2m_e} + \sum_{i=1}^{71}\sum_{j>i}^{72} \frac{e^2}{4\pi\epsilon_\circ \mid \vec{r_i} - \vec{r_j} \mid} \\
& - \sum_{i=1}^{72} \frac{Z_{11}e^2}{4\pi\epsilon_\circ \mid \vec{R_{11}} - \vec{r_i} \mid} - \sum_{i=1}^{72} \frac{Z_{21}e^2}{4\pi\epsilon_\circ \mid \vec{R_{21}} - \vec{r_i} \mid} - \sum_{i=1}^{72} \frac{Z_{01}e^2}{4\pi\epsilon_\circ \mid \vec{R_{01}} - \vec{r_i} \mid} \\
& - \sum_{i=1}^{72} \frac{Z_{02}e^2}{4\pi\epsilon_\circ \mid \vec{R_{02}} - \vec{r_i} \mid} - \sum_{i=1}^{72} \frac{Z_{31}e^2}{4\pi\epsilon_\circ \mid \vec{R_{31}} - \vec{r_i} \mid} - \sum_{i=1}^{72} \frac{Z_{32}e^2}{4\pi\epsilon_\circ \mid \vec{R_{32}} - \vec{r_i} \mid} \\
& - \sum_{i=1}^{72} \frac{Z_{33}e^2}{4\pi\epsilon_\circ \mid \vec{R_{33}} - \vec{r_i} \mid} - \sum_{i=1}^{72} \frac{Z_{34}e^2}{4\pi\epsilon_\circ \mid \vec{R_{34}} - \vec{r_i} \mid} - \sum_{i=1}^{72} \frac{Z_{41}e^2}{4\pi\epsilon_\circ \mid \vec{R_{41}} - \vec{r_i} \mid} \\
& - \sum_{i=1}^{72} \frac{Z_{42}e^2}{4\pi\epsilon_\circ \mid \vec{R_{42}} - \vec{r_i} \mid} - \sum_{i=1}^{72} \frac{Z_{43}e^2}{4\pi\epsilon_\circ \mid \vec{R_{43}} - \vec{r_i} \mid} - \sum_{i=1}^{72} \frac{Z_{44}e^2}{4\pi\epsilon_\circ \mid \vec{R_{44}} - \vec{r_i} \mid} \\
& - \sum_{i=1}^{72} \frac{Z_{03}e^2}{4\pi\epsilon_\circ \mid \vec{R_{03}} - \vec{r_i} \mid} - \sum_{i=1}^{72} \frac{Z_{04}e^2}{4\pi\epsilon_\circ \mid \vec{R_{04}} - \vec{r_i} \mid} - \sum_{i=1}^{72} \frac{Z_{51}e^2}{4\pi\epsilon_\circ \mid \vec{R_{51}} - \vec{r_i} \mid} \\
& - \sum_{i=1}^{72} \frac{Z_{61}e^2}{4\pi\epsilon_\circ \mid \vec{R_{61}} - \vec{r_i} \mid} + \frac{Z_{11}Z_{21}e^2}{4\pi\epsilon_\circ \mid \vec{R_{11}} - \vec{R_{21}} \mid} + \frac{Z_{11}Z_{01}e^2}{4\pi\epsilon_\circ \mid \vec{R_{11}} - \vec{R_{01}} \mid} \\
& + \frac{Z_{11}Z_{02}e^2}{4\pi\epsilon_\circ \mid \vec{R_{11}} - \vec{R_{02}} \mid} + \left\{ \frac{Z_{11}Z_{31}e^2}{4\pi\epsilon_\circ \mid \vec{R_{11}} - \vec{R_{31}} \mid} + \frac{Z_{11}Z_{32}e^2}{4\pi\epsilon_\circ \mid \vec{R_{11}} - \vec{R_{32}} \mid} \right. \\
& \left. + \frac{Z_{11}Z_{33}e^2}{4\pi\epsilon_\circ \mid \vec{R_{11}} - \vec{R_{33}} \mid} + \frac{Z_{11}Z_{34}e^2}{4\pi\epsilon_\circ \mid \vec{R_{11}} - \vec{R_{34}} \mid} \right\} + \left\{ \frac{Z_{11}Z_{41}e^2}{4\pi\epsilon_\circ \mid \vec{R_{11}} - \vec{R_{41}} \mid} \right. \\
& \left. + \frac{Z_{11}Z_{42}e^2}{4\pi\epsilon_\circ \mid \vec{R_{11}} - \vec{R_{42}} \mid} + \frac{Z_{11}Z_{43}e^2}{4\pi\epsilon_\circ \mid \vec{R_{11}} - \vec{R_{43}} \mid} + \frac{Z_{11}Z_{44}e^2}{4\pi\epsilon_\circ \mid \vec{R_{11}} - \vec{R_{44}} \mid} \right\} \\
& + \frac{Z_{11}Z_{03}e^2}{4\pi\epsilon_\circ \mid \vec{R_{11}} - \vec{R_{03}} \mid} + \frac{Z_{11}Z_{04}e^2}{4\pi\epsilon_\circ \mid \vec{R_{11}} - \vec{R_{04}} \mid} + \frac{Z_{11}Z_{51}e^2}{4\pi\epsilon_\circ \mid \vec{R_{11}} - \vec{R_{51}} \mid} \\
& + \frac{Z_{11}Z_{61}e^2}{4\pi\epsilon_\circ \mid \vec{R_{11}} - \vec{R_{61}} \mid} + \frac{Z_{21}Z_{01}e^2}{4\pi\epsilon_\circ \mid \vec{R_{21}} - \vec{R_{01}} \mid} + \frac{Z_{21}Z_{02}e^2}{4\pi\epsilon_\circ \mid \vec{R_{21}} - \vec{R_{02}} \mid} \\
& + \left\{ \frac{Z_{21}Z_{31}e^2}{4\pi\epsilon_\circ \mid \vec{R_{21}} - \vec{R_{31}} \mid} + \frac{Z_{21}Z_{32}e^2}{4\pi\epsilon_\circ \mid \vec{R_{21}} - \vec{R_{32}} \mid} + \frac{Z_{21}Z_{33}e^2}{4\pi\epsilon_\circ \mid \vec{R_{21}} - \vec{R_{33}} \mid} \right. \\
& \left. + \frac{Z_{21}Z_{34}e^2}{4\pi\epsilon_\circ \mid \vec{R_{21}} - \vec{R_{34}} \mid} \right\} + \left\{ \frac{Z_{21}Z_{41}e^2}{4\pi\epsilon_\circ \mid \vec{R_{21}} - \vec{R_{41}} \mid} + \frac{Z_{21}Z_{42}e^2}{4\pi\epsilon_\circ \mid \vec{R_{21}} - \vec{R_{42}} \mid} \right.
\end{aligned}
$$

$$+\frac{Z_{21}Z_{43}e^2}{4\pi\epsilon_\circ \mid \vec{R_{21}}-\vec{R_{43}} \mid}+\frac{Z_{21}Z_{44}e^2}{4\pi\epsilon_\circ \mid \vec{R_{21}}-\vec{R_{44}} \mid}\Bigg\}+\frac{Z_{21}Z_{03}e^2}{4\pi\epsilon_\circ \mid \vec{R_{21}}-\vec{R_{03}} \mid}$$
$$+\frac{Z_{21}Z_{04}e^2}{4\pi\epsilon_\circ \mid \vec{R_{21}}-\vec{R_{04}} \mid}+\frac{Z_{21}Z_{51}e^2}{4\pi\epsilon_\circ \mid \vec{R_{21}}-\vec{R_{51}} \mid}+\frac{Z_{21}Z_{61}e^2}{4\pi\epsilon_\circ \mid \vec{R_{21}}-\vec{R_{61}} \mid}$$
$$+\frac{Z_{01}Z_{02}e^2}{4\pi\epsilon_\circ \mid \vec{R_{01}}-\vec{R_{02}} \mid}+\Bigg\{\frac{Z_{01}Z_{31}e^2}{4\pi\epsilon_\circ \mid \vec{R_{01}}-\vec{R_{31}} \mid}+\frac{Z_{01}Z_{32}e^2}{4\pi\epsilon_\circ \mid \vec{R_{01}}-\vec{R_{32}} \mid}$$
$$+\frac{Z_{01}Z_{33}e^2}{4\pi\epsilon_\circ \mid \vec{R_{01}}-\vec{R_{33}} \mid}+\frac{Z_{01}Z_{34}e^2}{4\pi\epsilon_\circ \mid \vec{R_{01}}-\vec{R_{34}} \mid}\Bigg\}+\Bigg\{\frac{Z_{01}Z_{41}e^2}{4\pi\epsilon_\circ \mid \vec{R_{01}}-\vec{R_{41}} \mid}$$
$$+\frac{Z_{01}Z_{42}e^2}{4\pi\epsilon_\circ \mid \vec{R_{01}}-\vec{R_{42}} \mid}+\frac{Z_{01}Z_{43}e^2}{4\pi\epsilon_\circ \mid \vec{R_{01}}-\vec{R_{43}} \mid}+\frac{Z_{01}Z_{44}e^2}{4\pi\epsilon_\circ \mid \vec{R_{01}}-\vec{R_{44}} \mid}\Bigg\}$$
$$+\frac{Z_{01}Z_{03}e^2}{4\pi\epsilon_\circ \mid \vec{R_{01}}-\vec{R_{03}} \mid}+\frac{Z_{01}Z_{04}e^2}{4\pi\epsilon_\circ \mid \vec{R_{01}}-\vec{R_{04}} \mid}+\frac{Z_{01}Z_{51}e^2}{4\pi\epsilon_\circ \mid \vec{R_{01}}-\vec{R_{51}} \mid}$$
$$+\frac{Z_{01}Z_{61}e^2}{4\pi\epsilon_\circ \mid \vec{R_{01}}-\vec{R_{61}} \mid}+\Bigg\{\frac{Z_{02}Z_{31}e^2}{4\pi\epsilon_\circ \mid \vec{R_{02}}-\vec{R_{31}} \mid}+\frac{Z_{02}Z_{32}e^2}{4\pi\epsilon_\circ \mid \vec{R_{02}}-\vec{R_{32}} \mid}$$
$$+\frac{Z_{02}Z_{33}e^2}{4\pi\epsilon_\circ \mid \vec{R_{02}}-\vec{R_{33}} \mid}+\frac{Z_{02}Z_{34}e^2}{4\pi\epsilon_\circ \mid \vec{R_{02}}-\vec{R_{34}} \mid}\Bigg\}+\Bigg\{\frac{Z_{02}Z_{41}e^2}{4\pi\epsilon_\circ \mid \vec{R_{02}}-\vec{R_{41}} \mid}$$
$$+\frac{Z_{02}Z_{42}e^2}{4\pi\epsilon_\circ \mid \vec{R_{02}}-\vec{R_{42}} \mid}+\frac{Z_{02}Z_{43}e^2}{4\pi\epsilon_\circ \mid \vec{R_{02}}-\vec{R_{43}} \mid}+\frac{Z_{02}Z_{44}e^2}{4\pi\epsilon_\circ \mid \vec{R_{02}}-\vec{R_{44}} \mid}\Bigg\}$$
$$+\frac{Z_{02}Z_{03}e^2}{4\pi\epsilon_\circ \mid \vec{R_{02}}-\vec{R_{03}} \mid}+\frac{Z_{02}Z_{04}e^2}{4\pi\epsilon_\circ \mid \vec{R_{02}}-\vec{R_{04}} \mid}+\frac{Z_{02}Z_{51}e^2}{4\pi\epsilon_\circ \mid \vec{R_{02}}-\vec{R_{51}} \mid}$$
$$+\frac{Z_{02}Z_{61}e^2}{4\pi\epsilon_\circ \mid \vec{R_{02}}-\vec{R_{61}} \mid}+\frac{Z_{31}Z_{32}e^2}{4\pi\epsilon_\circ \mid \vec{R_{31}}-\vec{R_{32}} \mid}+\frac{Z_{31}Z_{33}e^2}{4\pi\epsilon_\circ \mid \vec{R_{31}}-\vec{R_{33}} \mid}$$
$$+\frac{Z_{31}Z_{34}e^2}{4\pi\epsilon_\circ \mid \vec{R_{31}}-\vec{R_{34}} \mid}+\Bigg\{\frac{Z_{31}Z_{41}e^2}{4\pi\epsilon_\circ \mid \vec{R_{31}}-\vec{R_{41}} \mid}+\frac{Z_{31}Z_{42}e^2}{4\pi\epsilon_\circ \mid \vec{R_{31}}-\vec{R_{42}} \mid}$$
$$+\frac{Z_{31}Z_{43}e^2}{4\pi\epsilon_\circ \mid \vec{R_{31}}-\vec{R_{43}} \mid}+\frac{Z_{31}Z_{44}e^2}{4\pi\epsilon_\circ \mid \vec{R_{31}}-\vec{R_{44}} \mid}\Bigg\}+\frac{Z_{31}Z_{03}e^2}{4\pi\epsilon_\circ \mid \vec{R_{31}}-\vec{R_{03}} \mid}$$
$$+\frac{Z_{31}Z_{04}e^2}{4\pi\epsilon_\circ \mid \vec{R_{31}}-\vec{R_{04}} \mid}+\frac{Z_{31}Z_{51}e^2}{4\pi\epsilon_\circ \mid \vec{R_{31}}-\vec{R_{51}} \mid}+\frac{Z_{31}Z_{61}e^2}{4\pi\epsilon_\circ \mid \vec{R_{31}}-\vec{R_{61}} \mid}$$
$$+\frac{Z_{32}Z_{33}e^2}{4\pi\epsilon_\circ \mid \vec{R_{32}}-\vec{R_{33}} \mid}+\frac{Z_{32}Z_{34}e^2}{4\pi\epsilon_\circ \mid \vec{R_{32}}-\vec{R_{34}} \mid}+\Bigg\{\frac{Z_{32}Z_{41}e^2}{4\pi\epsilon_\circ \mid \vec{R_{32}}-\vec{R_{41}} \mid}$$
$$+\frac{Z_{32}Z_{42}e^2}{4\pi\epsilon_\circ \mid \vec{R_{32}}-\vec{R_{42}} \mid}+\frac{Z_{32}Z_{43}e^2}{4\pi\epsilon_\circ \mid \vec{R_{32}}-\vec{R_{43}} \mid}+\frac{Z_{32}Z_{44}e^2}{4\pi\epsilon_\circ \mid \vec{R_{32}}-\vec{R_{44}} \mid}\Bigg\}$$

$$
\begin{aligned}
&+\frac{Z_{32}Z_{03}e^2}{4\pi\epsilon_\circ \mid \vec{R_{32}}-\vec{R_{03}} \mid}+\frac{Z_{32}Z_{04}e^2}{4\pi\epsilon_\circ \mid \vec{R_{32}}-\vec{R_{04}} \mid}+\frac{Z_{32}Z_{51}e^2}{4\pi\epsilon_\circ \mid \vec{R_{32}}-\overrightarrow{R_{51}} \mid}\\
&+\frac{Z_{32}Z_{61}e^2}{4\pi\epsilon_\circ \mid \vec{R_{32}}-\vec{R_{61}} \mid}+\frac{Z_{33}Z_{34}e^2}{4\pi\epsilon_\circ \mid \vec{R_{33}}-\vec{R_{34}} \mid}+\left\{\frac{Z_{33}Z_{41}e^2}{4\pi\epsilon_\circ \mid \vec{R_{33}}-\vec{R_{41}} \mid}\right.\\
&\left.+\frac{Z_{33}Z_{42}e^2}{4\pi\epsilon_\circ \mid \vec{R_{33}}-\vec{R_{42}} \mid}+\frac{Z_{33}Z_{43}e^2}{4\pi\epsilon_\circ \mid \vec{R_{33}}-\vec{R_{43}} \mid}+\frac{Z_{33}Z_{44}e^2}{4\pi\epsilon_\circ \mid \vec{R_{33}}-\vec{R_{44}} \mid}\right\}\\
&+\frac{Z_{33}Z_{03}e^2}{4\pi\epsilon_\circ \mid \vec{R_{33}}-\vec{R_{03}} \mid}+\frac{Z_{33}Z_{04}e^2}{4\pi\epsilon_\circ \mid \vec{R_{33}}-\vec{R_{04}} \mid}+\frac{Z_{33}Z_{51}e^2}{4\pi\epsilon_\circ \mid \vec{R_{33}}-\vec{R_{51}} \mid}\\
&+\frac{Z_{33}Z_{61}e^2}{4\pi\epsilon_\circ \mid \vec{R_{33}}-\vec{R_{61}} \mid}+\left\{\frac{Z_{34}Z_{41}e^2}{4\pi\epsilon_\circ \mid \vec{R_{34}}-\vec{R_{41}} \mid}+\frac{Z_{34}Z_{42}e^2}{4\pi\epsilon_\circ \mid \vec{R_{34}}-\vec{R_{42}} \mid}\right.\\
&\left.+\frac{Z_{34}Z_{43}e^2}{4\pi\epsilon_\circ \mid \vec{R_{34}}-\vec{R_{43}} \mid}+\frac{Z_{34}Z_{44}e^2}{4\pi\epsilon_\circ \mid \vec{R_{34}}-\vec{R_{44}} \mid}\right\}+\frac{Z_{34}Z_{03}e^2}{4\pi\epsilon_\circ \mid \vec{R_{34}}-\vec{R_{03}} \mid}\\
&+\frac{Z_{34}Z_{04}e^2}{4\pi\epsilon_\circ \mid \vec{R_{34}}-\vec{R_{04}} \mid}+\frac{Z_{34}Z_{51}e^2}{4\pi\epsilon_\circ \mid \vec{R_{34}}-\vec{R_{51}} \mid}+\frac{Z_{34}Z_{61}e^2}{4\pi\epsilon_\circ \mid \vec{R_{34}}-\vec{R_{61}} \mid}\\
&+\frac{Z_{41}Z_{42}e^2}{4\pi\epsilon_\circ \mid \vec{R_{41}}-\vec{R_{42}} \mid}+\frac{Z_{41}Z_{43}e^2}{4\pi\epsilon_\circ \mid \vec{R_{41}}-\vec{R_{43}} \mid}+\frac{Z_{41}Z_{44}e^2}{4\pi\epsilon_\circ \mid \vec{R_{41}}-\vec{R_{44}} \mid}\\
&+\frac{Z_{41}Z_{03}e^2}{4\pi\epsilon_\circ \mid \vec{R_{41}}-\vec{R_{03}} \mid}+\frac{Z_{41}Z_{04}e^2}{4\pi\epsilon_\circ \mid \vec{R_{41}}-\vec{R_{04}} \mid}+\frac{Z_{41}Z_{51}e^2}{4\pi\epsilon_\circ \mid \vec{R_{41}}-\vec{R_{51}} \mid}\\
&+\frac{Z_{41}Z_{61}e^2}{4\pi\epsilon_\circ \mid \vec{R_{41}}-\vec{R_{61}} \mid}+\frac{Z_{42}Z_{43}e^2}{4\pi\epsilon_\circ \mid \vec{R_{42}}-\vec{R_{43}} \mid}+\frac{Z_{42}Z_{44}e^2}{4\pi\epsilon_\circ \mid \vec{R_{42}}-\vec{R_{44}} \mid}\\
&+\frac{Z_{42}Z_{03}e^2}{4\pi\epsilon_\circ \mid \vec{R_{42}}-\vec{R_{03}} \mid}+\frac{Z_{42}Z_{04}e^2}{4\pi\epsilon_\circ \mid \vec{R_{42}}-\vec{R_{04}} \mid}+\frac{Z_{42}Z_{51}e^2}{4\pi\epsilon_\circ \mid \vec{R_{42}}-\vec{R_{51}} \mid}\\
&+\frac{Z_{42}Z_{61}e^2}{4\pi\epsilon_\circ \mid \vec{R_{42}}-\vec{R_{61}} \mid}+\frac{Z_{43}Z_{44}e^2}{4\pi\epsilon_\circ \mid \vec{R_{43}}-\vec{R_{44}} \mid}+\frac{Z_{43}Z_{03}e^2}{4\pi\epsilon_\circ \mid \vec{R_{43}}-\vec{R_{03}} \mid}\\
&+\frac{Z_{43}Z_{04}e^2}{4\pi\epsilon_\circ \mid \vec{R_{43}}-\vec{R_{04}} \mid}+\frac{Z_{43}Z_{51}e^2}{4\pi\epsilon_\circ \mid \vec{R_{43}}-\vec{R_{51}} \mid}+\frac{Z_{43}Z_{61}e^2}{4\pi\epsilon_\circ \mid \vec{R_{43}}-\vec{R_{61}} \mid}\\
&+\frac{Z_{44}Z_{03}e^2}{4\pi\epsilon_\circ \mid \vec{R_{44}}-\vec{R_{03}} \mid}+\frac{Z_{44}Z_{04}e^2}{4\pi\epsilon_\circ \mid \vec{R_{44}}-\vec{R_{04}} \mid}+\frac{Z_{44}Z_{51}e^2}{4\pi\epsilon_\circ \mid \vec{R_{44}}-\vec{R_{51}} \mid}\\
&+\frac{Z_{44}Z_{61}e^2}{4\pi\epsilon_\circ \mid \vec{R_{44}}-\vec{R_{61}} \mid}+\frac{Z_{03}Z_{04}e^2}{4\pi\epsilon_\circ \mid \vec{R_{03}}-\vec{R_{04}} \mid}+\frac{Z_{03}Z_{51}e^2}{4\pi\epsilon_\circ \mid \vec{R_{03}}-\vec{R_{51}} \mid}\\
&+\frac{Z_{03}Z_{61}e^2}{4\pi\epsilon_\circ \mid \vec{R_{03}}-\vec{R_{61}} \mid}+\frac{Z_{04}Z_{51}e^2}{4\pi\epsilon_\circ \mid \vec{R_{04}}-\vec{R_{51}} \mid}+\frac{Z_{04}Z_{61}e^2}{4\pi\epsilon_\circ \mid \vec{R_{04}}-\vec{R_{61}} \mid}\\
&+\frac{Z_{51}Z_{61}e^2}{4\pi\epsilon_\circ \mid \vec{R_{51}}-\vec{R_{61}} \mid} \qquad . \qquad \text{(A.1)}
\end{aligned}
$$

The following step will reduce the above equation (A.1) by gathering the terms of the Hamiltonian that belong to a certain fragment,

$$\begin{aligned}
\hat{H} \;=\; & \{\hat{T}_{01}+\hat{T}_{02}+\hat{T}_{03}+\hat{T}_{04}\}+\hat{T}_{11}+\hat{T}_{21}+\{\hat{T}_{31}+\hat{T}_{32}+\hat{T}_{33}+\hat{T}_{34}\}+\{\hat{T}_{41}+\hat{T}_{42} \\
& +\hat{T}_{43}+\hat{T}_{44}\}+\hat{T}_{51}+\hat{T}_{61}+\hat{T}_{e}+\hat{V}_{ee}+\{\hat{V}_{01e}+\hat{V}_{02e}+\hat{V}_{03e}+\hat{V}_{04e}\}+\hat{V}_{11e}+\hat{V}_{21e} \\
& +\{\hat{V}_{31e}+\hat{V}_{32e}+\hat{V}_{33e}+\hat{V}_{34e}\}+\{\hat{V}_{41e}+\hat{V}_{42e}+\hat{V}_{43e}+\hat{V}_{44e}\}+\hat{V}_{51e}+\hat{V}_{61e} \\
& +\{\hat{V}_{0102}+\hat{V}_{0103}+\hat{V}_{0104}+\hat{V}_{0203}+\hat{V}_{0204}+\hat{V}_{0304}\} \\
& +\{\hat{V}_{0111}+\hat{V}_{0211}+\hat{V}_{0311}+\hat{V}_{0411}\}+\{\hat{V}_{0121}+\hat{V}_{0221}+\hat{V}_{0321}+\hat{V}_{0421}\} \\
& +\{\hat{V}_{0131}+\hat{V}_{0231}+\hat{V}_{0331}+\hat{V}_{0431}\}+\{\hat{V}_{0132}+\hat{V}_{0232}+\hat{V}_{0332}+\hat{V}_{0432}\} \\
& +\{\hat{V}_{0133}+\hat{V}_{0233}+\hat{V}_{0333}+\hat{V}_{0433}\}+\{\hat{V}_{0134}+\hat{V}_{0234}+\hat{V}_{0334}+\hat{V}_{0434}\} \\
& +\{\hat{V}_{0141}+\hat{V}_{0241}+\hat{V}_{0341}+\hat{V}_{0441}\}+\{\hat{V}_{0142}+\hat{V}_{0242}+\hat{V}_{0342}+\hat{V}_{0442}\} \\
& +\{\hat{V}_{0143}+\hat{V}_{0243}+\hat{V}_{0343}+\hat{V}_{0443}\}+\{\hat{V}_{0144}+\hat{V}_{0244}+\hat{V}_{0344}+\hat{V}_{0444}\} \\
& +\{\hat{V}_{0151}+\hat{V}_{0251}+\hat{V}_{0351}+\hat{V}_{0451}\}+\{\hat{V}_{0161}+\hat{V}_{0261}+\hat{V}_{0361}+\hat{V}_{0461}\} \\
& +\hat{V}_{1121}+\{\hat{V}_{1131}+\hat{V}_{1132}+\hat{V}_{1133}+\hat{V}_{1134}\}+\{\hat{V}_{1141}+\hat{V}_{1142}+\hat{V}_{1143}+\hat{V}_{1144}\} \\
& +\hat{V}_{1151}+\hat{V}_{1161}+\{\hat{V}_{2131}+\hat{V}_{2132}+\hat{V}_{2133}+\hat{V}_{2134}\}+\{\hat{V}_{2141}+\hat{V}_{2142}+\hat{V}_{2143} \\
& +\hat{V}_{2144}\}+\hat{V}_{2151}+\hat{V}_{2161}+\{\hat{V}_{3132}+\hat{V}_{3133}+\hat{V}_{3134}+\hat{V}_{3233}+\hat{V}_{3234}+\hat{V}_{3334}\} \\
& +\{\hat{V}_{3141}+\hat{V}_{3142}+\hat{V}_{3143}+\hat{V}_{3144}+\hat{V}_{3241}+\hat{V}_{3242}+\hat{V}_{3243}+\hat{V}_{3244}+\hat{V}_{3341} \\
& +\hat{V}_{3342}+\hat{V}_{3343}+\hat{V}_{3344}+\hat{V}_{3441}+\hat{V}_{3442}+\hat{V}_{3443}+\hat{V}_{3444}\} \\
& +\{\hat{V}_{3151}+\hat{V}_{3251}+\hat{V}_{3351}+\hat{V}_{3451}\}+\{\hat{V}_{3161}+\hat{V}_{3261}+\hat{V}_{3361}+\hat{V}_{3461}\} \\
& +\{\hat{V}_{4142}+\hat{V}_{4143}+\hat{V}_{4144}+\hat{V}_{4243}+\hat{V}_{4244}+\hat{V}_{4344}\} \\
& +\{\hat{V}_{4151}+\hat{V}_{4251}+\hat{V}_{4351}+\hat{V}_{4451}\}+\{\hat{V}_{4161}+\hat{V}_{4261}+\hat{V}_{4361}+\hat{V}_{4461}\} \\
& +\hat{V}_{5161} \qquad . \qquad \text{(A.2)}
\end{aligned}$$

In equation A.2, the kinetic energy operator of all the electrons is written as $\hat{T}_e$ and the sum of the electron-electron potential energy operator is written as $\hat{V}_{ee}$. Some terms can be surrounded by brackets, like the sum of the kinetic energy operators for nuclei 1, 2, 3 and 4 in the 0 fragment $\{\hat{T_{01}}+\hat{T_{02}}+\hat{T_{03}}+\hat{T_{04}}\}$. This sum can be replaced by the term $\hat{T}_0$. The same can be done for the other fragments. The same also can be done for the potential energy operator. For example, the potential energy operators between the nuclei in the 0 fragment itself which is written as $\{\hat{V}_{0102}+\hat{V}_{0103}+\hat{V}_{0104}+\hat{V}_{0203}+\hat{V}_{0204}+\hat{V}_{0304}\}$ (where $\hat{V}_{0102}$ is the nuclear nuclear potential between nuclei 01 and 02) can be replaced by the term $\hat{V}_{00}$. The same can be done for the other fragments. This yields the following much simpler expression for the Hamiltonian:

$$\begin{aligned}\hat{H} \;=\; & \hat{T}_0+\hat{T}_1+\hat{T}_2+\hat{T}_3+\hat{T}_4+\hat{T}_5+\hat{T}_6+\hat{T}_e+\hat{V}_{ee}+\hat{V}_{0e}+\hat{V}_{1e}+\hat{V}_{2e}+\hat{V}_{3e}+\hat{V}_{4e}\\ & +\hat{V}_{5e}+\hat{V}_{6e}+\hat{V}_{00}+\hat{V}_{01}+\hat{V}_{02}+\hat{V}_{03}+\hat{V}_{04}+\hat{V}_{05}+\hat{V}_{06}+\hat{V}_{12}+\hat{V}_{13}+\hat{V}_{14}\\ & +\hat{V}_{15}+\hat{V}_{16}+\hat{V}_{23}+\hat{V}_{24}+\hat{V}_{25}+\hat{V}_{26}+\hat{V}_{33}+\hat{V}_{34}+\hat{V}_{35}+\hat{V}_{36}+\hat{V}_{44}+\hat{V}_{45}\\ & +\hat{V}_{46}+\hat{V}_{56} \qquad . \end{aligned} \tag{A.3}$$

The Hamiltonian of equation A.3 can be written as a sum of one-fragment Hamiltonians $\hat{H}^{(1)}$ (which include the operators of the kinetic energy of the nuclei of one fragment, of the potential energy of the intra-nuclear-nuclear interaction, and of the potential energy of the intra-nuclear-electron interaction) and two-fragment Hamiltonians $\hat{H}^{(2)}$ (which include the nuclear-nuclear potential energy operator between these two fragments) as shown below:

$$\begin{aligned}\hat{H} = & \hat{H}_0^{(1)}+\hat{H}_1^{(1)}+\hat{H}_2^{(1)}+\hat{H}_3^{(1)}+\hat{H}_4^{(1)}+\hat{H}_5^{(1)}+\hat{H}_6^{(1)}\\ & +\hat{H}_{01}^{(2)}+\hat{H}_{02}^{(2)}+\hat{H}_{03}^{(2)}+\hat{H}_{04}^{(2)}+\hat{H}_{05}^{(2)}+\hat{H}_{06}^{(2)}\\ & +\hat{H}_{12}^{(2)}+\hat{H}_{13}^{(2)}+\hat{H}_{14}^{(2)}+\hat{H}_{15}^{(2)}+\hat{H}_{16}^{(2)}\\ & +\hat{H}_{23}^{(2)}+\hat{H}_{24}^{(2)}+\hat{H}_{25}^{(2)}+\hat{H}_{26}^{(2)}\\ & +\hat{H}_{34}^{(2)}+\hat{H}_{35}^{(2)}+\hat{H}_{36}^{(2)}\\ & +\hat{H}_{45}^{(2)}+\hat{H}_{46}^{(2)}\\ & +\hat{H}_{56}^{(2)}\\ & +\hat{T}_e+\hat{V}_{ee} \end{aligned} \tag{A.4}$$

Equation A.4 shows that using fragments, which is suggested by molecular symmetry, helps to reduce the Hamiltonian in a way that facilitates reading. If the fragments 1, 2, 5 or 6 consist of more than one nuclei like for the CCD molecule (as in Figure 1.4), then the following Hamiltonians $\hat{H}_1^{(1)}, \hat{H}_2^{(1)}, \hat{H}_5^{(1)}, \hat{H}_6^{(1)}$ contain analogous intra-nuclear-nuclear interactions.

A.2. Symmetry projection operator

The idempotence property of the symmetry projection operator $\hat{P}^{\Gamma_i}$ of equation 3.17 is shown in this study for Γ_7^+, as an example,

$$\begin{aligned}\hat{P}^{\Gamma_7^+} &= \frac{1}{16}\sum_{\hat{R}=1}^{16}\chi^{\Gamma_7^+}(\hat{R})\hat{R} \\ &= \frac{1}{16}(\mathcal{E} - (12) - (34) + (12)(34) + (56) - (12)(56) - (34)(56) + (12)(34)(56) + \mathcal{E}^* \\ &- (12)^* - (34)^* + (12)(34)^* + (56)^* - (12)(56)^* - (34)(56)^* + (12)(34)(56)^*).\end{aligned} \tag{A.5}$$

Therefore,

$$\begin{aligned}\hat{P}^{\Gamma_7^+}\hat{P}^{\Gamma_7^+} = \frac{1}{16}\frac{1}{16}(&\mathcal{E} - (12) - (34) + (12)(34) + (56) - (12)(56) - (34)(56) + (12)(34)(56) \\ &+ \mathcal{E}^* - (12)^* - (34)^* + (12)(34)^* + (56)^* - (12)(56)^* - (34)(56)^* + (12)(34)(56)^* \\ &- (12) + \mathcal{E} + (12)(34) - (34) - (12)(56) + (56) + (12)(34)(56) - (34)(56) - (12)^* \\ &+ \mathcal{E}^* + (12)(34)^* - (34)^* - (12)(56)^* + (56)^* + (12)(34)(56)^* - (34)(56)^* \\ &- (34) + (34)(12) + \mathcal{E} - (12) - (34)(56) + (34)(12)(56) + (56) - (12)(56) - (34)^* \\ &+ (34)(12)^* + \mathcal{E}^* - (12)^* - (34)(56)^* + (34)(12)(56)^* + (56)^* - (12)(56)^* \\ &+ (12)(34) - (34) - (12) + \mathcal{E} + (12)(34)(56) - (34)(56) - (12)(56) + (56) + (12) \\ &(34)^* - (34)^* - (12)^* + \mathcal{E}^* + (12)(34)(56)^* - (34)(56)^* - (12)(56)^* + (56)^* \\ &+ (56) - (12)(56) - (34)(56) + (12)(34)(56) + \mathcal{E} - (12) - (34) + (12)(34) + (56)^* \\ &- (56)(12)^* - (56)(34)^* + (56)(12)(34)^* + \mathcal{E}^* - (12)^* - (34)^* + (12)(34)^* \\ &- (12)(56) + (56) + (34)(12)(56) - (34)(56) - (12) + \mathcal{E} + (12)(34) - (34) - (12) \\ &(56)^* + (56)^* + (12)(56)(34)^* - (56)(34)^* - (12)^* + \mathcal{E}^* + (12)(34)^* - (34)^* \\ &- (34)(56) + (12)(34)(56) + (56) - (12)(56) - (34) + (12)(34) + \mathcal{E} - (12) - (34) \\ &(56)^* + (34)(56)(12)^* + (56)^* - (56)(12)^* - (34)^* + (34)(12)^* + \mathcal{E}^* - (12)^* \\ &+ (12)(34)(56) - (34)(56) - (12)(56) + (56) + (12)(34) - (34) - (12) + \mathcal{E} + (12) \\ &(34)(56)^* - (34)(56)^* - (12)(56)^* + (56)^* + (12)(34)^* - (34)^* - (12)^* + \mathcal{E}^* \\ &+ \mathcal{E}^* - (12)^* - (34)^* + (12)(34)^* + (56)^* - (12)(56)^* - (34)(56)^* + (12)(34)(56)^* \\ &+ \mathcal{E} - (12) - (34) + (12)(34) + (56) - (12)(56) - (34)(56) + (12)(34)(56) \\ &- (12)^* + \mathcal{E}^* + (34)(12)^* - (34)^* - (12)(56)^* + (56)^* + (12)(34)(56)^* - (34)(56)^* \\ &- (12) + \mathcal{E} + (12)(34) - (34) - (12)(56) + (56) + (12)(34)(56) - (34)(56) \\ &- (34)^* + (12)(34)^* + \mathcal{E}^* - (12)^* - (56)(34)^* + (12)(56)(34)^* + (56)^* - (12)(56)^* \\ &- (34) + (12)(34) + \mathcal{E} - (12) - (34)(56) + (12)(34)(56) + (56) - (12)(56) \\ &+ (12)(34)^* - (34)^* - (12)^* + \mathcal{E}^* + (12)(34)(56)^* - (56)(34)^* - (12)(56)^* + (56)^* \\ &+ (12)(34) - (34) - (12) + \mathcal{E} + (12)(34)(56) - (34)(56) - (12)(56) + (56)\end{aligned} \tag{A.6}$$

$$
\begin{aligned}
&+ (56)^* - (56)(12)^* - (56)(34)^* + (12)(34)(56)^* + \mathcal{E}^* - (12)^* - (34)^* + (12)(34)^* \\
&+ (56) - (56)(12) - (56)(34) + (56)(12)(34) + \mathcal{E} - (12) - (34) + (12)(34) \\
&- (12)(56)^* + (56)^* + (34)(12)(56)^* - (34)(56)^* - (12)^* + \mathcal{E}^* + (34)(12)^* - (34)^* \\
&- (12)(56) + (56) + (34)(12)(56) - (34)(56) - (12) + \mathcal{E} + (12)(34) - (34) \\
&- (34)(56)^* + (12)(34)(56)^* + (56)^* - (12)(56)^* - (34)^* + (12)(34)^* + \mathcal{E}^* - (12)^* \\
&- (34)(56) + (12)(34)(56) + (56) - (12)(56) - (34) + (12)(34) + \mathcal{E} - (12) \\
&+ (12)(34)(56)^* - (34)(56)^* - (12)(56)^* + (56)^* + (12)(34)^* - (34)^* - (12)^* + \mathcal{E}^* \\
&+ (12)(34)(56) - (34)(56) - (12)(56) + (56) + (12)(34) - (34) - (12) + \mathcal{E} \\
&= \frac{1}{16}\frac{1}{16}\{16\mathcal{E} - 16(12) - 16(34) + 16(12)(34) + 16(56) - 16(12)(56) - 16(34)(56) \\
&+ 16(12)(34)(56) + 16\mathcal{E}^* - 16(12)^* - 16(34)^* + 16(12)(34)^* + 16(56)^* - 16(12)(56)^* \\
&- 16(34)(56)^* + 16(12)(34)(56)^*\} \\
&= \frac{1}{16}(\mathcal{E} - (12) - (34) + (12)(34) + (56) - (12)(56) - (34)(56) + (12)(34)(56) + \mathcal{E}^* \\
&- (12)^* - (34)^* + (12)(34)^* + (56)^* - (12)(56)^* - (34)(56)^* + (12)(34)(56)^*) \\
&= \hat{P}^{\Gamma_7^+}. \qquad \text{(A.7)}
\end{aligned}
$$

Equation A.7 proves that applying the projection operator $\hat{P}^{\Gamma_7^+}$ twice gives the same result as applying it once. Equivalent proofs of the idempotence property can be shown for all the other 15 other IREPs of the G_{16}^A listed in Table 3.7.

The orthogonality property of the symmetry projection operator of equation (3.21) is given in this study for $\hat{P}^{\Gamma_7^+}\hat{P}^{\Gamma_6^-}$, as an example,

$$
\begin{aligned}
\hat{P}^{\Gamma_6^-} = \frac{1}{16}(&\mathcal{E} - (12) + (34) - (12)(34) - (56) + (12)(56) - (34)(56) + (12)(34) \\
&(56) - \mathcal{E}^* + (12)^* - (34)^* + (12)(34)^* + (56)^* - (12)(56)^* + (34)(56)^* \\
&- (12)(34)(56)^*). \qquad \text{(A.8)}
\end{aligned}
$$

The result of $\hat{P}^{\Gamma_7^+}\hat{P}^{\Gamma_6^-}$, using equations (A.5) and (A.8), is:

$$
\begin{aligned}
\hat{P}^{\Gamma_7^+}\hat{P}^{\Gamma_6^-} = \frac{1}{16}\frac{1}{16}(&\mathcal{E} - (12) - (34) + (12)(34) + (56) - (12)(56) - (34)(56) + (12)\\
&(34)(56) + \mathcal{E}^* - (12)^* - (34)^* + (12)(34)^* + (56)^* - (12)(56)^* - (34)\\
&(56)^* + (12)(34)(56)^* - (12) + \mathcal{E} + (12)(34) - (34) - (12)(56) + (56)\\
&+ (12)(34)(56) - (34)(56) - (12)^* + \mathcal{E}^* + (12)(34)^* - (34)^* - (12)(56)^*\\
&+ (56)^* + (12)(34)(56)^* - (34)(56)^* + (34) - (34)(12) - \mathcal{E} + (12) + (34)\\
&(56) - (34)(12)(56) - (56) + (12)(56) + (34)^* - (34)(12)^* - \mathcal{E}^* + (12)^*\\
&+ (34)(56)^* - (34)(12)(56)^* - (56)^* + (12)(56)^* - (12)(34) + (34) + (12)\\
&- \mathcal{E} - (12)(34)(56) + (34)(56) + (12)(56) - (56) - (12)(34)^* + (34)^* +\\
&(12)^* - \mathcal{E}^* - (12)(34)(56)^* + (34)(56)^* + (12)(56)^* - (56)^* - (56) + (56)\\
&(12) + (56)(34) - (12)(34)(56) - \mathcal{E} + (12) + (34) - (12)(34) - (56)^* +\\
&(56)(12)^* + (56)(34)^* - (12)(34)(56)^* - \mathcal{E}^* + (12)^* + (34)^* - (12)(34)^*\\
&+ (12)(56) - (56) - (12)(56)(34) + (56)(34) + (12) - \mathcal{E} - (12)(34) + (34)\\
&+ (12)(56)^* - (56)^* - (12)(56)(34)^* + (56)(34)^* + (12)^* - \mathcal{E}^* - (12)(34)^*\\
&+ (34)^* - (34)(56) + (34)(56)(12) + (56) - (56)(12) - (34) + (34)(12) +\\
&\mathcal{E} - (12) - (34)(56)^* + (12)(34)(56)^* + (56)^* - (56)(12)^* - (34)^* + (34)\\
&(12)^* + \mathcal{E}^* - (12)^* + (12)(34)(56) - (34)(56) - (12)(56) + (56) + (12)(34)\\
&- (34) - (12) + \mathcal{E} + (12)(34)(56)^* - (34)(56)^* - (12)(56)^* + (56)^* + (12)\\
&(34)^* - (34)^* - (12)^* + \mathcal{E}^* - \mathcal{E}^* + (12)^* + (34)^* - (12)(34)^* - (56)^* +\\
&(12)(56)^* + (34)(56)^* - (12)(34)(56)^*\\
&- \mathcal{E} + (12) + (34) - (12)(34) - (56) + (12)(56) + (34)(56) - (12)(34)(56)\\
&+ (12)^* - \mathcal{E}^* - (12)(34)^* + (34)^* + (12)(56)^* - (56)^* - (12)(34)(56)^* + (34)(56)^*\\
&+ (12) - \mathcal{E} - (12)(34) + (34) + (12)(56) - (56) - (12)(34)(56) + (34)(56)\\
&- (34)^* + (34)(12)^* + \mathcal{E}^* - (12)^* - (34)(56)^* + (34)(12)(56)^* + (56)^* - (12)(56)^*\\
&- (34) + (34)(12) + \mathcal{E} - (12) - (34)(56) + (34)(12)(56) + (56) - (12)(56)\\
&+ (12)(34)^* - (34)^* - (12)^* + \mathcal{E}^* + (12)(34)(56)^* - (34)(56)^* - (12)(56)^* + (56)^*\\
&+ (12)(34) - (34) - (12) + \mathcal{E} + (12)(34)(56) - (34)(56) - (12)(56) + (56)\\
&+ (56)^* - (56)(12)^* - (56)(34)^* + (56)(12)(34)^* + \mathcal{E}^* - (12)^* - (34)^* + (12)(34)^*\\
&+ (56) - (56)(12) - (56)(34) + (56)(12)(34) + \mathcal{E} - (12) - (34) + (12)(34)\\
&- (12)(56)^* + (56)^* + (12)(56)(34)^* - (56)(34)^* - (12)^* + \mathcal{E}^* + (12)(34)^* - (34)^*\\
&- (12)(56) + (56) + (12)(56)(34) - (56)(34) - (12) + \mathcal{E} + (12)(34) - (34)\\
&+ (34)(56)^* - (34)(56)(12)^* - (56)^* + (56)(12)^* + (34)^* - (34)(12)^* - \mathcal{E}^* + (12)^*\\
&+ (34)(56) - (34)(56)(12) - (56) + (56)(12) + (34) - (34)(12) - \mathcal{E} + (12)\\
&- (12)(34)(56)^* + (34)(56)^* + (12)(56)^* - (56)^* - (12)(34)^* + (34)^* + (12)^* - \mathcal{E}^*\\
&- (12)(34)(56) + (34)(56) + (12)(56) - (56) - (12)(34) + (34) + (12) - \mathcal{E}\\
&= 0. \qquad \text{(A.9)}
\end{aligned}
$$

Equivalent proofs of the orthogonality can be given for all other pairs of symmetry projection operators. This provides another test of self-consistency of the character table of the G_{16}^{A} (Table 3.7).

A.3. Labelling the electronic and nuclear coordinates and their derivatives

Assigning the IREPs for the electronic and nuclear coordinates with their derivatives is the goal of this section. This is important for assigning the IREPs of the transition dipole moments and the non-adiabatic coupling elements as in [73]. Starting with the nuclear coordinates, it is found that the radii $\mathcal{R}_1$ and $\mathcal{R}_2$ are not affected by the eight equivalent molecular symmetry operations, see Table 3.10, so they transform according to the totally symmetric IREP Γ_1^+, as shown in Table A.1. The assignment of the IREP for X_1 is shown as an example for the assignment of the Cartesian nuclear coordinates. X_1 is labelled with the IREP Γ_7^+. This labelling is done by studying the effects of performing the symmetry operations of G_{16}^{A} on X_1. Applying the eight equivalent molecular symmetry operations (of Table 3.10) $\mathcal{E}, (12), \ldots, (12)(34)^*$ on X_1 gives $X_1, -X_1, -X_1, X_1, X_1, -X_1, -X_1, X_1$, respectively, as shown in Table 3.10. Thus, X_1 transforms according to the IREP Γ_7^+, see Table A.1. This is consistent with applying the symmetry projection operator $\hat{P}^{\Gamma_7^+}$ on X_1:

$$
\begin{aligned}
\hat{P}^{\Gamma_7^+} X_1 &= \frac{1}{16} \sum_{\mathcal{R}=1}^{16} \mathcal{X}^{\Gamma_7^+}(\mathcal{R}) \mathcal{R} X_1 \\
&= \frac{1}{16} \{ \mathcal{E} X_1 - (12) X_1 - (34) X_1 + (12)(34) X_1 + (56) X_1 \\
&- (12)(56) X_1 - (34)(56) X_1 + (12)(34)(56) X_1 + \mathcal{E}^* X_1 \\
&- (12)^* X_1 - (34)^* X_1 + (12)(34)^* X_1 + (56)^* X_1 - (12)(56)^* X_1 \\
&- (34)(56)^* X_1 + (12)(34)(56)^* X_1 \} \\
&= \frac{1}{16} \{ X_1 + X_1 + X_1 + X_1 + X_1 + X_1 + X_1 + X_1 + X_1 + X_1 + X_1 + X_1 \\
&+ X_1 + X_1 + X_1 + X_1 \} \\
&= \frac{1}{16} \{ 16 X_1 \} \\
&= X_1 .
\end{aligned}
\tag{A.10}
$$

Analogous considerations can be done for the other nuclear Cartesian coordinates (X_2, Y_1, Y_2), as summarized in Table A.1. It is found that the Cartesian derivatives

transform as their corresponding Cartesian coordinates, e.g. $\frac{\partial}{\partial X_1}$ transforms as X_1, see Table A.1.

The transformation between polar and Cartesian coordinates is done by making use of equations (3.33) and (3.34), hence,

$$\frac{\partial}{\partial \Phi} = -Y \frac{\partial}{\partial X} + X \frac{\partial}{\partial Y}. \tag{A.11}$$

Each of X_1 and $\frac{\partial}{\partial X_1}$ transforms as Γ_7^+ and each of Y_1 and $\frac{\partial}{\partial Y_1}$ transforms as Γ_7^-, as shown in Table A.1. Therefore, substituting these in equation (A.11) and using the product table of G_{16}^A (Table 3.9), yields the IREP for $\frac{\partial}{\partial \Phi_1}$,

$$\begin{aligned} \Gamma(\frac{\partial}{\partial \Phi_1}) &= \Gamma_7^- \otimes \Gamma_7^+ \\ &= \Gamma_1^-. \end{aligned} \tag{A.12}$$

Consequently, $\frac{\partial}{\partial \Phi_1}$ transforms as Γ_1^-, similarly, $\frac{\partial}{\partial \Phi_2}$ has the IREP Γ_1^-, see Table A.1. The IREPs of the molecular symmetry adapted nuclear coordinates, expressed in terms of Cartesian coordinates with their derivatives and their associated polar coordinates with their derivatives are summarized in Table A.1.

After the assignment of the IREPs for the nuclear coordinates of CCD, we will proceed to do the same for the electronic coordinates. The effects of the symmetry operations on the Cartesian electronic coordinates are shown in Figure A.2. Small letters are used for electronic coordinates to distinguish them from nuclear coordinates. The Cartesian electronic coordinate z is not affected by the symmetry operations as in Figure A.2, so it transforms according to the totally symmetric IREP Γ_1^+. The Cartesian electronic coordinates x and y are labelled with the IREP Γ_3^+ and Γ_3^-, respectively. This labelling is done using the same way used for labelling the IREPs of the nuclear coordinates, see Figure A.2.

It is noticed from Figure A.2 that permutation of identical fragments changes the electronic coordinates. Due to using molecule-fixed-coordinate-system.

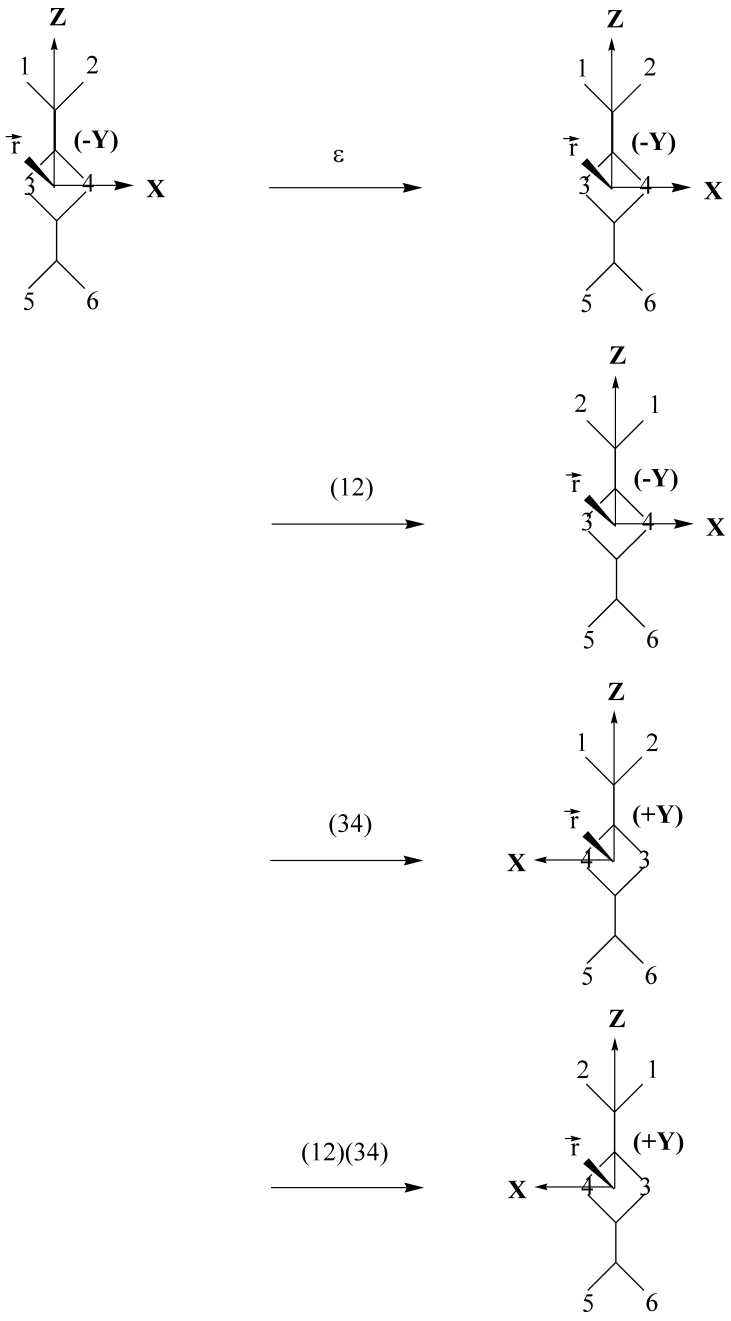
Z
1
2
(-Y)
r
3
4
X
5
6
ε
(12)
(34)
(12)(34)
(+Y)

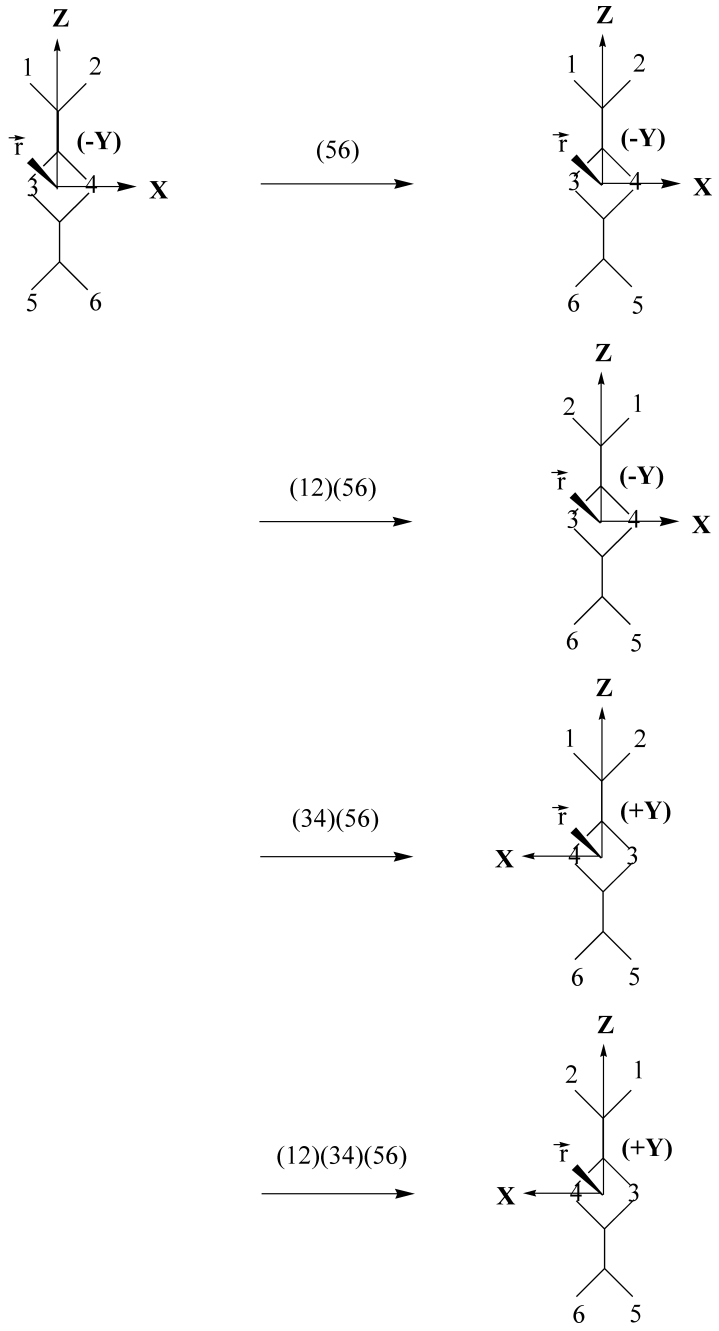
Z
1
2
(-Y)
r
3
4
X
5
6
(56)
Z
1
2
(-Y)
r
3
4
X
6
5
(12)(56)
Z
2
1
(-Y)
r
3
4
X
6
5
(34)(56)
Z
1
2
(+Y)
r
X
4
3
6
5
(12)(34)(56)
Z
2
1
(+Y)
r
X
4
3
6
5

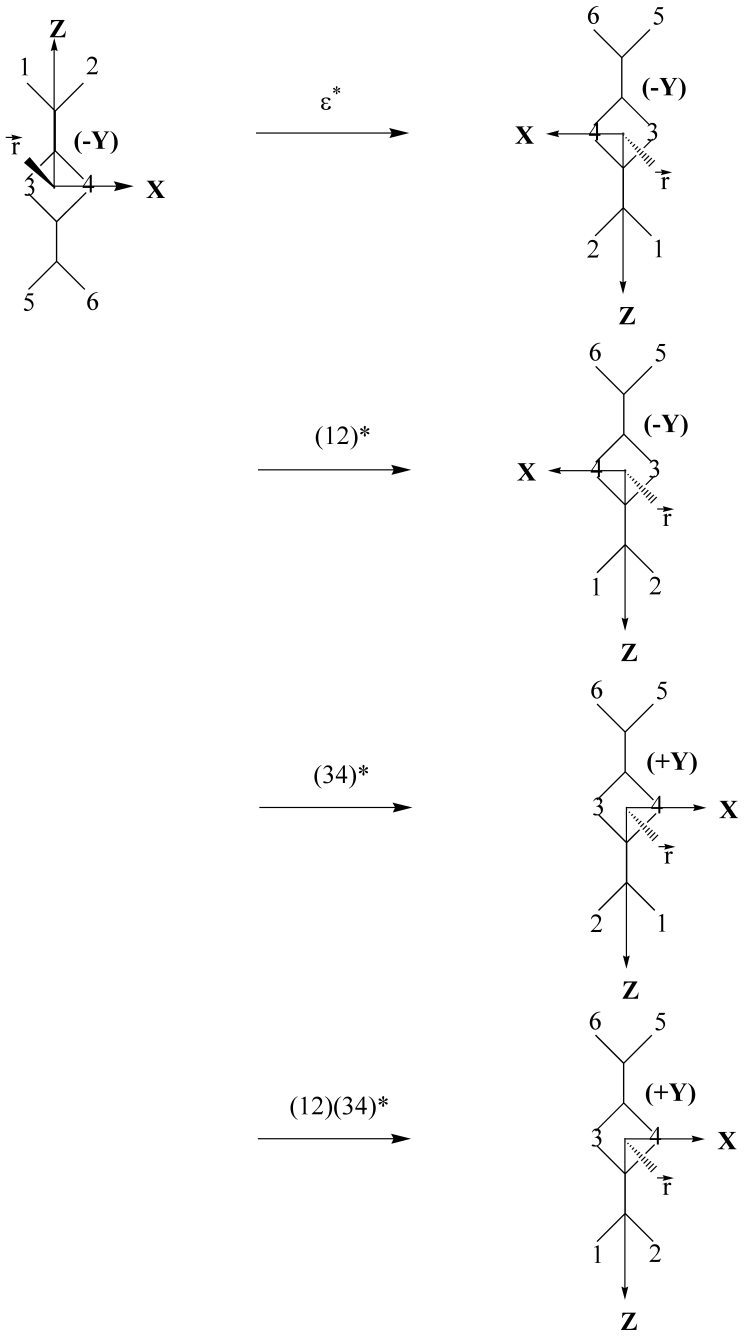
Z
1
2
r
(-Y)
3
4
X
5
6
ε*
6
5
(-Y)
X
4
3
r
2
1
Z
(12)*
6
5
(-Y)
X
4
3
r
1
2
Z
(34)*
6
5
(+Y)
3
4
X
r
2
1
Z
(12)(34)*
6
5
(+Y)
3
4
X
r
1
2
Z

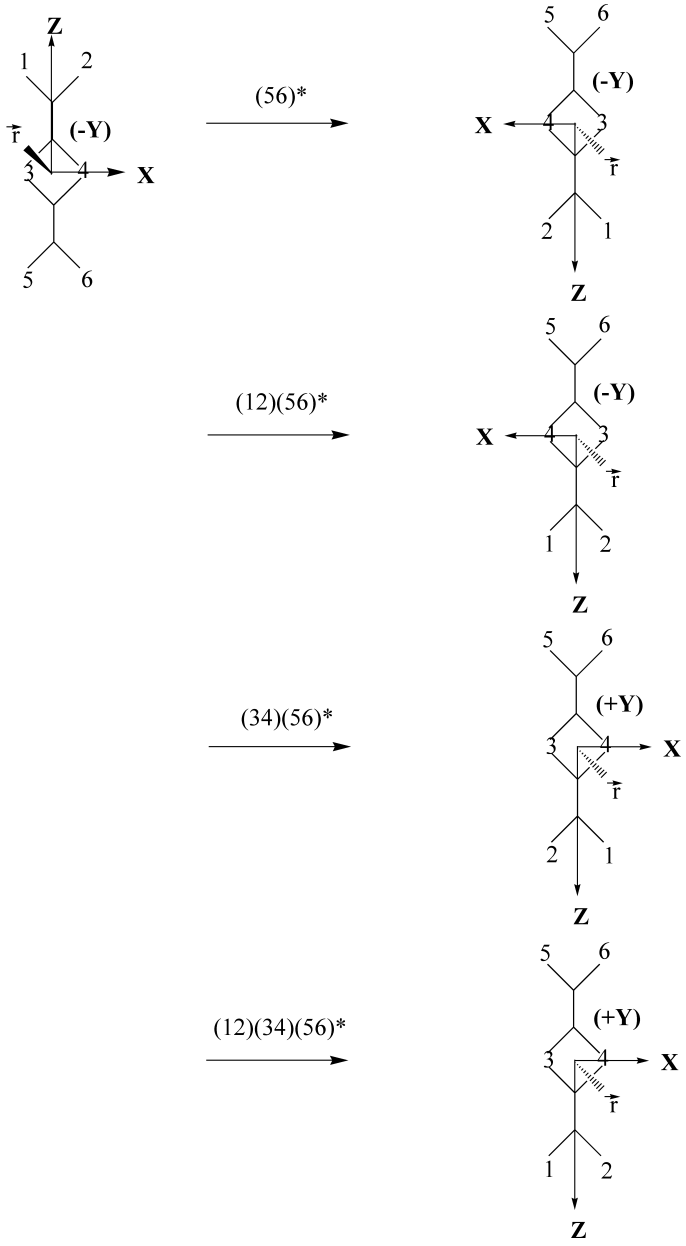

Figure A.2.: Effects of the molecular symmetry operators of G_{16}^{A} on the electronic coordinates. The right-handed-molecule-fixed-coordinate system is used. The molecule-fixed-coordinate Y points perpendicularly into the paper plane.

Table A.1.: The IREPs of the molecular symmetry adapted nuclear coordinates of CCD and their derivatives

G_{16}^{A}	$\mathcal{E}$ (12)(34)(56)	(12) (34)(56)	(34) (12)(56)	(12)(34) (56)	$\mathcal{E}^*$ (12)(34)(56)*	(12)* (34)(56)*	(34)* (12)(56)*	(12)(34)* (56)*	coordinate	derivative
Γ_1^+	1	1	1	1	1	1	1	1	R_1, R_2, Z_1, Z_2	$\frac{\partial}{\partial R_1}$, $\frac{\partial}{\partial R_2}$, $\frac{\partial}{\partial Z_1}$, $\frac{\partial}{\partial Z_2}$
Γ_4^+	1	1	-1	-1	1	1	-1	-1	X_2	$\frac{\partial}{\partial X_2}$
Γ_6^+	1	-1	1	-1	1	-1	1	-1		
Γ_7^+	1	-1	-1	1	1	-1	-1	1	X_1	$\frac{\partial}{\partial X_1}$
Γ_1^-	1	1	1	1	-1	-1	-1	-1		$\frac{\partial}{\partial \Phi_1}$, $\frac{\partial}{\partial \Phi_2}$
Γ_4^-	1	1	-1	-1	-1	-1	1	1	Y_2	$\frac{\partial}{\partial Y_2}$
Γ_6^-	1	-1	1	-1	-1	1	-1	1		
Γ_7^-	1	-1	-1	1	-1	1	1	-1	Y_1	$\frac{\partial}{\partial Y_1}$

This table summarizes the IREPs of the molecular symmetry adapted nuclear coordinates, expressed in terms of Cartesian coordinates with their derivatives and their associated polar coordinates with their derivatives.

Bibliography

[1] W. Heisenberg, *Z. Physik*, **41**, 239 (1927).

[2] F. Hund, *Z. Physik*, **42**, 93 (1927).

[3] R. J. Silbey, R. A. Alberty, *Physical Chemistry*. John Wiley & Sons, Inc., New York (2001).

[4] R. Mecke, *Z. Physik*, **31**, 709 (1925).

[5] T. L. Hill, *An Introduction to Statistical Thermodynamics*. Dover, New York (1986).

[6] S. Tomonaga, *The Story of Spin*. The University of Chicago Press, Chicago/London (1997).

[7] K. F. Bonhoeffer, P. Harteck, *Z. Phys. Chem.*, **B4**, 113 (1929).

[8] A. Eucken, Sitzber. Preuss. Akad. Wiss. 41 (1912).

[9] R. Berman, A. H. Cooke, R. W. Hill, *Annu. Rev. Phys. Chem.*, **7**, 1 (1956).

[10] P. R. Bunker, P. Jensen, *Spectroscopy and Broken Symmetry, in: Frontiers of Molecular Spectroscopy*. Elsevier, Amsterdam (2009).

[11] S. Belz, O. Deeb, L. González, T. Grohmann, D. Kinzel, M. Leibscher, J. Manz, R. Obaid, M. Oppel, G. D. Xavier, S. Zilberg, *Z. Phys. Chem.*, **227**, 1021 (2013).

[12] P. L. Chapovsky, L. J. F. Hermans, *Annu. Rev. Phys. Chem.*, **50**, 315 (1999).

[13] S. Fleischer, I. S. Averbukh, Y. Prior, *Phys. Rev. Lett.*, **99**, 093002 (2007).

[14] S. Fleischer, I. S. Averbukh, Y. Prior, *J. Phys. B*, **41**, 074018 (2008).

[15] S. Fleischer, Y. Khodorkovsky, Y. Prior, I. S. Averbukh, *New J. Phys.*, **11**, 105039 (2009).

[16] O. Deeb, M. Leibscher, J. Manz, W. von Muellern, T. Seideman, *ChemPhysChem*, **8**, 322 (2007).

[17] T. Grohmann, O. Deeb, M. Leibscher, *Chem. Phys.*, **338**, 252 (2007).

[18] S. Belz, T. Grohmann, M. Leibscher, *J. Chem. Phys.*, **131**, 034305 (2009).

[19] S. Belz, *Laser Control of Torsional Nuclear Wave Packet Dynamics Via Conical Intersections*. Dissertation, Freie Universität, Berlin (2011).

[20] S. Al-Jabour, *Molecular Symmetry, Quantum Chemistry and Dynamics: Simulation of Laser Driven Molecular Torsion in the Presence of a Conical Intersection*. Dissertation, Freie Universität, Berlin (2011).

[21] F. A. Cotton, *Chemical Applications of Group Theory*. Wiley, New York (1971).

[22] H. C. Longuet-Higgins, *Mol. Phys.*, **6**, 445 (1963).

[23] J. T. Hougen, *J. Chem. Phys.*, **37**, 1433 (1962).

[24] J. T. Hougen, *J. Chem. Phys.*, **39**, 358 (1963).

[25] P. R. Bunker, P. Jensen, *Molecular Symmetry and Spectroscopy*. NRC Research Press, Ottawa (1998).

[26] A. J. Merer, J. K. G. Watson, *J. Mol. Spec.*, **47**, 499 (1973).

[27] B. Lasorne, M. A. Robb, H. Meyer, F. Gatti, *Chem. Phys.*, **377**, 30 (2010).

[28] A. Szabo, N. S. Ostlund, *Modern Quantum Chemistry: Introduction to Advanced Electronic Structure Theory*. Dover, New York (1996).

[29] I. N. Levine, *Quantum Chemistry*. Prentice Hall, Upper Saddle River (2008).

[30] F. Jensen, *Introduction to Computational Chemistry*. John Wiley & Sons, Hoboken (2006).

[31] M. Born, R. Oppenheimer, *Ann. Phys.*, **389**, 457 (1927).

[32] D. Tannor, *Introduction to Quantum Mechanics: A Time-Dependent Perspective*. University Science Books, Sausalito (2006).

[33] M. Baer, *Beyond Born-Oppenheimer: Electronic Nonadiabatic Coupling Terms and Conical Intersections*. Wiley-Interscience, Hoboken (2006).

[34] D. R. Hartree, *Rev. Mod. Phys.*, **24**, 89 (1928).

[35] J. C. Slater, *Phys. Rev.*, **34**, 1293 (1929).

[36] D. Kinzel, *Photoisomerization versus Photodissociation of a Chiral Fluoroethylene Derivative. Quantum Chemistry, Dynamics and Control*. Dissertation, Friedrich-Schiller-Universität, Jena (2013).

[37] B. O. Roos, P. Widmark, *European Summerschool in Quantum Chemistry*. BookII. Lund University, Lund (2005).

[38] B. O. Roos, P. R. Taylor, P. E. Siegbahn, *Chem. Phys.*, **48**, 157 (1980).

[39] P. J. Knowles, H. Werner, *Chem. Phys. Lett.*, **115**, 259 (1985).

[40] P. J. Knowles, H. Werner, *J. Chem. Phys.*, **82**, 5053 (1985).

[41] B. O. Roos, *Adv. Chem. Phys.*, **69**, 399 (1987).

[42] W. Domcke, D. R. Yarkony, H. Köppel, *Conical Intersections: Electronic Structure, Dynamics and Spectroscopy*. World Scientific, Singapore (2004).

[43] D. R. Yarkony, *J. Phys. Chem. A*, **105**, 277 (2001).

[44] J. von Neumann, E. Wigner, *Phys. Z.*, **30**, 467 (1997).

[45] S. Alfalah, S. Belz, O. Deeb, M. Leibscher, J. Manz, S. Zilberg, *J. Chem. Phys.*, **130**, 124318 (2009).

[46] E. Thiele, D. J. Wilson, *J. Chem. Phys.*, **35**, 1256 (1961).

[47] H. Tal-Ezer, R. Kosloff, *J. Chem. Phys.*, **81**, 3967 (1984).

[48] T. J. Park, J. C. Light, *J. Chem. Phys.*, **85**, 5870 (1986).

[49] M. D. Feit, J. A. Fleck, A. Steiger, *J. Comput. Phys.*, **47**, 412 (1982).

[50] M. D. Feit, J. A. Fleck, *J. Chem. Phys.*, **78**, 301 (1983).

[51] M. D. Feit, J. A. Fleck, *J. Chem. Phys.*, **80**, 2578 (1984).

[52] R. Kosloff, *Ann. Rev. Phys. Chem.*, **45**, 145 (1994).

[53] K. Varga, J. A. Driscoll, *Computational Nanoscience: Applications for molecules, clusters and solids*. Cambridge University Press, Cambridge (2011).

[54] R. E. Wyatt, J. Z. H. Zhang, *Dynamics of Molecules and Chemical Reactions*. Chapter 5. Mercel Dekker, New York (1996).

[55] D. M. Bishop, *Group Theory and Chemistry*. Dover Publications, New York (1973).

[56] V. Heine, *Group Theory in Quantum Mechanics*. Pergamon Press, New York (1960).

[57] R. Mirman, *Group Theory: an Intuitive Approach*. World Scientific, Singapore (2007).

[58] P. H. E. Meijer, E. Bauer, *Group Theory The Application to Quantum Mechanics*. North-Holland Publishing Company, Amsterdam (1962).

[59] E. W. Weisstein, "rearrangement theorem" from MathWorld-A Wolfram Web Resource. http://mathworld.wolfram.com/RearrangementTheorem.html (17.01.2014).

[60] T. Grohmann, *Theoretische Untersuchungen zur Quantendynamik der Kernspinisomere nicht-linearer Moleküle*. Dissertation, Freie Universität Berlin (2012).

[61] J. K. G. Watson, *J. Mol. Spectrosc.*, **50**, 281 (1974).

[62] J. K. G. Watson, *Can. J. Phys.*, **53**, 75 (1975).

[63] B. Friedrich, D. R. Herschbach, *Nature*, **353**, 412 (1991).

[64] T. Grohmann, private communication (2012).

[65] J. Laane, *Frontiers of Molecular Spectroscopy*. Chapter 11, Elsevier, Amsterdam (2009).

[66] H. C. Longuet-Higgins, *Mol. Phys.*, **6**, 445 (1963).

[67] M. H. Levitt, *Spin Dynamics: Basics of Nuclear Magnetic Resonance*. Wiley-VCH, Weinheim (2008).

[68] R. McWeeny, *Symmetry: an Introduction to Group Theory and its Applications*. Dover, New York (2002).

[69] T. H. Dunning, *J. Chem. Phys.*, **90**, 1007 (1989).

[70] George Densingh Xavier, private communication (2010).

[71] H.-J. Werner, P. J. Knowles, G. Knizia, F. R. Manby, M. Schütz, P. Celani, T. Korona, R. Lindh, A. Mitrushenkov, G. Rauhut, K. R. Shamasundar, T. B. Adler, R. D. Amos, A. Bernhardsson, A. Berning, D. L. Cooper, M. J. O. Deegan, A. J. Dobbyn, F. Eckert, E. Goll, C. Hampel, A. Hesselmann, G. Hetzer, T. Hrenar, G. Jansen, C. Köppl, Y. Liu, A. W. Lloyd, R. A. Mata, A. J. May, S. J. McNicholas, W. Meyer, M. E. Mura, A. Nicklass, D. P. O'Neill, P. Palmieri, D. Peng, K. Pflüger, R. Pitzer, M. Reiher, T. Shiozaki, H. Stoll, A. J. Stone, R. Tarroni, T. Thorsteinsson, M. Wang, Molpro, version 2012.1, a package of ab initio programs. http://www.molpro.net (2012).

[72] C. C. Martson, G. G. Balint-Kurti, *J. Chem. Phys.*, **91**, 3571 (1989).

[73] S. Al-Jabour, M. Baer, O. Deeb, M. Leibscher, J. Manz, X. Xu, S. Zilberg, *J. Phys. Chem. A*, **114**, 2991 (2010).

Acknowledgements

This thesis was prepared in the group of **Prof. Dr. Leticia González** at the University of Vienna. The underlying research of the present work has been performed in the frame of a trilateral cooperation between the Free University of Berlin in Germany, The Al-Quds University in Palestine and the Hebrew University in Israel. This trilateral project can be considered as a quadrilateral project since 2011, after the University of Vienna became involved in this project.

I would like to express my deep and sincere gratitude to **Prof. Dr. Leticia González** for giving me the opportunity to join her group during the last two years of my PhD study and for guiding, correcting and helping me throughout this work.

I am deeply grateful to **Prof. Dr. Jörn Manz** for his detailed and constructive comments, support and running this cooperation from the bottom of his heart.

I wish to express my earnest thanks to **Dr. Monika Leibscher**, who was ready to spend her time supervising parts of my research and providing useful comments and advices.

I would like very much to thank **Prof. Dr. Omar Deeb** for his contribution to the success of this project. My thanks also go to **Prof. Dr. Shmuel Zilberg** and **Prof. Dr. Yehuda Haas** for their help and cooperation.

I am very thankful for the generous supervision of **Dr. Daniel Kinzel** and **Dr. Markus Oppel** and their continuous willingness to help and support me.

I would like to express my special thanks to **Dr. Thomas Grohmann** for his never ending patience and his continuous encouragement for me, as well as to **Dr.**

Steffen Belz.

I would like to also thank my colleages from the AG González, especially **Sebastian Mai, Dr. Philipp Marquetand, Martin Richter, Dr. Mariana Aßmann, Leon Freitag** and **Federico Latorre** for the very nice working atmosphere and the fruitful scientific discussions.

My thanks go to the Deutsche Forschungsgemeinschaft for the financial support in the frame of the trilateral project MA 515/22-3 and GO 1059/7-3.

My warmest thanks go to my husband for overcoming every obstacle to help me to proceed and to achieve my dream of doing my PhD study, as well as to my parents, sisters, brothers, mother in law and friends: Dr. Nafisah Al-Rifai and Ms. Huda Al-Husseni.

Curriculum vitae

Working experience

2012-present	Doctoral studies in the group of Prof. Dr. Leticia González at the Institute of Theoretical Chemistry, University of Vienna, Vienna, Austria
2010-2012	Doctoral studies in the groups of Prof. Dr. Jörn Manz at the Institute for Chemistry and Biochemistry, Free University of Berlin, Berlin, Germany and of Prof. Dr. Omar Deeb at the Faculty of Pharmacy, Al-Quds University, Abu Dis, Palestine
2006-2010	Teaching in: 1) Barakat Secondary School, Hebron, Palestine 2) Al-Shar'ia Secondary School, Hebron, Palestine 3) Nahaleen Secondary School, Bethlehem, Palestine 4) Khalayel El-looze Elementary School, Bethlehem, Palestine

Degrees and education

2003-2006	Master studies in Chemistry. Thesis title: *Kinetics of Oxidation of Cysteine and Captopril via [$Mo(CN)_8$] and [$W(CN)_8$]*. University of Jordan, Jordan
1999-2002	Bachelor studies in Chemistry. Thesis title: *Anomalous properties of water molecule*. Hebron University, Palestine
1991-1999	Secondary school, Hebron, Palestine

Attended conferences	
September 2013	STC 2013, the 49th Symposium on Theoretical Chemistry, Erlangen, Germany. Poster title: *Determining the nuclear spin isomers of a derivative of quinodimethane in the $T \to 0$ limit using the molecular symmetry group*

IT skills	
Scientific	Quantum chemistry packages (e.g. MOLPRO), programming skills (FORTRAN90), molecular visualisation software
General	LaTeX, Windows and Linux based office suites

Language skills	
Arabic	Mother tongue
English	very good in writing and speaking

List of Publications

S. Belz, O. Deeb, L. González, T. Grohmann*, D. Kinzel, M. Leibscher, J. Manz, R. Obaid*, M. Oppel*, G. D. Xavier and S. Zilberg. **Nuclear Spin Selective Torsional States: Implications of Molecular Symmetry**. *Z. Phys. Chem.*, **227**, 1021 (2013).

R. Obaid, et. al. **Discriminating Nuclear Spin Isomers Exploiting the Excited State Dynamics of a Quinodimethane Derivative** (to be submitted).

R. Obaid, et. al. **Using Pump-Dump Control to Separate Nuclear Spin Isomers of a Quinodimethane Derivative** (in preparation).

Selbstständigkeitserklärung

Hiermit erkläre ich, dass ich die vorliegende Arbeit selbstständig und ohne Zuhilfenahme weiterer als der aufgeführten Quellen angefertigt habe. Alle wörtlich oder sinngemäß übernommenen Textstellen anderer Verfasser wurden als solche gekennzeichnet.

Rana Obaid